BULGARIAN CHEMICAL COMMUNICATIONS

2009 Volume 41 / Number 4

Journal of the Chemical Institutes
of the Bulgarian Academy of Sciences
and of the Union of Chemists in Bulgaria

IN MEMORIAM

To the memory of Prof. DIMITER G. ELENKOV

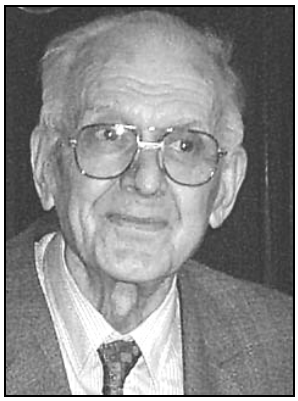

The team of the Institute of Chemical Engineering at the Bulgarian Academy of Sciences was prepared to celebrate the 90th anniversary of his former director and teacher Prof. Dimiter G. Elenkov. Unfortunately he passed away some days before - on October 18, 2009. Therefore, the words to be said will be *in memoriam* of his long and fruitful life.

He was born in Radomir, Bulgaria. He was graduated in St. Kliment Ohridski University of Sofia in 1943 and later – graduated as chemical engineer in industrial chemistry at the State Polytechnics of Sofia. Since 1947 he is consecutively an assistant professor in analytical chemistry at the Faculty of Mechanics, State University of Varna; in medical chemistry at the Medical Academy of Sofia and in physical chemistry at the State Polytechnics of Sofia.

He was elected as associate professor in "Processes and apparatuses in chemical industry" in 1956 and in 1965 – as full professor. During the period 1959–1966 he was Deputy-rector of the Higher Institute of Chemical Technology in Sofia, charged with the school scientific activity. In the period 1972–1980 he was Deputy director of the United Centre of Chemistry at the Bulgarian Academy of Sciences and in 1980–1988 – President of the Higher Testimonial Commission at the Bulgarian Government.

He was a Bulgarian representative and member of the Steering Board of the International Centre for Heat and Mass Transfer in Minsk, ex-USSR (now Belarus).

Prof. Dimiter G. Elenkov is the founder of chemical engineering in Bulgaria. He was Head of the chair "Processes and apparatuses with control and automation" at the Higher Institute of Chemical Technology in Sofia (now University of Chemical Technology and Metallurgy) until 1972. He had accomplished a substantial work on the establishing of Department of Chemical Engineering at Prof. Assen Zlatarov University of Burgas, Bulgaria. He was the first *Doctor of Sciences* in this area (since 1967); *Professor-in-Honour* (1978) and *Doctor Honoris Causa* of the Saint Petersburg State Institute of Technology (1982). He was awarded with numerous state awards. As recognition of his contribution to the development of Bulgarian chemical science and chemical engineering in particular, the academic body of the Bulgarian Academy of Sciences elected Prof. Dimiter G. Elenkov as its Corresponding Member in 1977.

Since 1961 Prof. Dimiter G. Elenkov was Head of the Department for Mass Transfer Processes at the Institute of General and Inorganic Chemistry at the Bulgarian Academy of Sciences, grown in 1972 in the Central Laboratory of Chemical Engineering. As a head of the latter, Prof. Dimiter Elenkov continuously concentrated his efforts for its development, either of the personnel and the research base. In 1986 the Central Laboratory was upgraded into the Institute of Chemical Engineering with total staff of over 80 persons. The research area of the institute included: heat and mass transfer in homogeneous and heterogeneous systems; chemical and biochemical reactors; methods of chemical engineering in environment protection; automation and computerization of the related processes. The development of all these scientific areas in Bulgaria is closely associated with the name of Prof. Dimiter Elenkov. He is author of more than 200 research papers, the majority of them being published abroad in well-known journals of chemical engineering.

He is an author and co-author of many patents, some of them, like the equipment for removal of sulphur dioxide and particulate matter from industrial gases, modern adsorbers and absorbers, unsteady-state reactors for sulphur dioxide oxidation, *etc*., were successfully applied and still operate in Bulgarian industry.

The contribution of Prof. Dimiter Elenkov in training and development of thousands of highly qualified chemists and chemical engineers is outstanding. His students, from their part, created, maintained and still maintain the chemical industry of Bulgaria that for many years is a basic profitable branch of Bulgarian economy.

It could be stated that there are no Bulgarian scientists and engineers working in the field of chemical engineering who is not feeling his strong impact – either through his textbooks and lectures, scientific supervision or practical advices.

There are dozens of doctors, promoted their theses in the field of technical chemistry under his supervision. All of the present professors working in this field have been his PhD students or co-researchers. Today they use to teach, to lead research and to run enterprises in Bulgaria and abroad.

With the death of Prof. Dimiter Elenkov our chemical engineering community lost an outstanding scientists, teacher and good friend.

Sofia, November 24, 2009

The colleagues from the
Institute of Chemical Engineering,
Bulgarian Academy of Sciences

Bulgarian Chemical Communications, Volume 41, Number 4 (pp. 343–354) 2009

Application of Bessel's functions in the modelling of chemical engineering processes

T. St. Petrova

Institute of Chemical Engineering, Bulgarian Academy of Sciences,
Acad. G. Bonchev St., Block 103, 1113 Sofia, Bulgaria

Received March 18, 2009

It is shown, that under given conditions the differential equations, describing some kind of transfer processes, allow an exact solution, expressed by Bessel's functions. For that purpose a wide range literature survey, covering the modelling of transfer processes in chemical engineering as well as in the related fields, is done. The typical examples from hydrodynamics, heat transfer, diffusion, bioprocesses and so on, are considered and discussed.

Keywords: chemical engineering, transfer processes, modelling, Bessel's functions.

INTRODUCTION

Modelling of transfer processes is based on the construction of some hypothesis for the process state and its growth in the space and time. The next step is to express that hypothesis by specific mathematical structure, *e.g*., to work out equations – ordinary (ODE) or partial differential (PDE), in which the unknown process function and variables are taking part. The sound reasoning to compose these equations follows from balance of transfer towards certain volume or boundaries. Finally, to "shut up" the resulting system of equations it is necessary to lay down the initial or/and boundary conditions for unknown functions and variables over the boundary domain and time interval, where the process occurred. When the initial time conditions are given and the domain for other independent variables (coordinates) is not fixed preliminary, the so called Cauchy's problem is obtained. If the unknown function(s) are determined on the domain boundaries, the boundary value problem exists. The most often used type of boundary conditions are those of Dirichlet (value of unknown function at the boundary) and Neumann's (the value of normal derivative of this function at the boundary) conditions.

The number of cases, where the so composed system of equations and initial and boundary conditions (model of process) admits solution (exact or numerical), is limited. The more complete account of all alterations of the unknown functions and values leads to a more complex and unsolvable model, especially when introducing physical or geometrical non-linearity. There are several approaches to obtain the exact solution, the common between them is to decrease the number of independent variables and reduce the above system to a simpler and solvable system, for example:

- introducing of additional assumptions to simplify the system (symmetry, isotropy, independence from temperature, time, *etc*.)
- applying of different integral transformations (Laplace, Fourier), method of separation of variables, method of eigenfunctions and eigenvalues;
- expansion of the unknown function in series (Taylor, Fourier), using special functions (Green, harmonic, *etc*.).

The above mentioned approaches to obtaining the solution are related mainly to systems containing linear PDE of second order and corresponding initial and boundary conditions. The various kinds of linear PDE, domain boundaries and boundary conditions, as well as methods for solving some linear PDE are well-known and these can be seen in a lot of mathematical textbooks like [1, Ch. 8].

In this work, the focus is centred only on those cases, where the linear PDE's describing various chemical transfer processes, allow the exact solution expressed in terms of one special kind of functions – Bessel's functions (BF). Modelling of different process cases from hydrodynamics, diffusion, heat transfer and other interdisciplinary topics, which illustrated the wide application of the BF, are considered. The theoretical conditions needed to obtain a solution in BF are briefly represented in next section.

* To whom all correspondence should be sent:
E-mail: tpetrova@ice.bas.bg

TYPES OF LINEAR PDES IN TRANSFER PROCESS MODELLING AND CONDITIONS FOR THEIR REDUCING TO BESSEL'S ODE. BESSEL'S ODE SOLUTIONS AND THEIR PROPERTIES

Some of the most used in transfer processes modelling linear PDE of second order are represented in Figure 1. For simplicity, the considered equations are written towards a function $f = f(x, t)$ of only two linearly independent variables, with constant coefficients. Generally speaking, the elliptical PDE describe stationary processes (distribution of temperature and electrostatic fields, elastic deformation). Parabolic and hyperbolic PDE describe time-dependent, transient processes (free fluctuations after a given initial disturbance), or processes of distribution of the disturbances (forced fluctuations, emitting waves) [2].

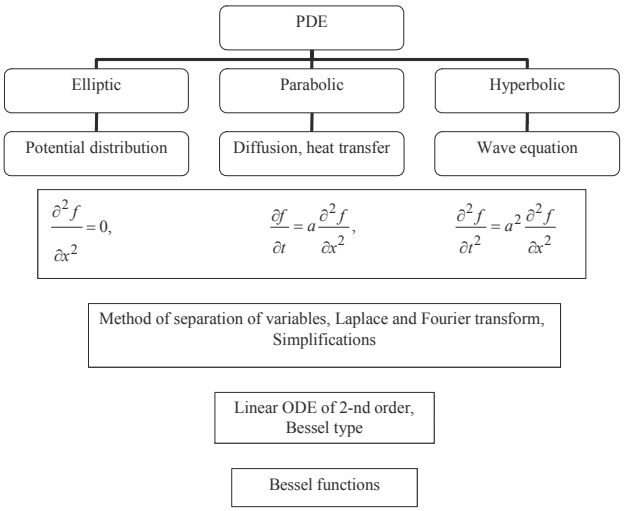

Fig. 1. Connection between linear PDE and Bessel's ODE.

The representatives of linear elliptical PDE are Laplace, Poisson and Helmholtz equations. The Laplace equation describes a potential field distribution. If the right hand side of this equation is not equal to zero, we have inhomogeneity and the so called Poisson equation. Here the inhomogeneity is a result of internal impact (force, heat, current and other sources) on the considered domain.

The parabolic PDE widespread representatives are heat transfer and diffusion equations. They can be reduced and solved by the method of separation of variables (MSV) and their solutions contain exponential functions of negative arguments, partial solutions of Helmholtz equation and arbitrary constants; the latter ones are determined from the problem boundary conditions.

The typical example of hyperbolic PDE is the wave equation. It can be solved with the D`Alambert formulae when two initial conditions for the unknown function and its derivative are given. The Laplace и Fourier transforms are used to convert a hyperbolic into the elliptic type PDE towards one of the spatial coordinates. Another way to reduce it is to apply the MSV both to hyperbolic and parabolic PDE in the cases of mixed problems. The Helmholtz equation represents time-independent form of wave equation, obtained by him after applying the MSV. This equation is used in problems of transmission and distribution of electro-magnetic, seismologic and other waves in space.

Commonly speaking when we try to solve some of the most familiar linear PDE we become aware of the fact that to apply one of several methods decreasing the number of independent variables, the Bessel ODE may appear as a result in certain cases. It is occurring most frequently when we search solutions of linear boundary problems consisting in Laplace or Helmholtz equation in cylindrical or spherical coordinates. One of the most popular ways to find it is to apply MSV, which turns the basic equation into a set of ODEs, each one of them is towards one independent variable only. Then non-trivial solutions of ODE must be detected such ones that satisfy the given boundary conditions only for the eigenvalues and respectively the searched solution is expressed by the corresponding set-up of orthogonal eigenfunctions and unknown coefficients. In problems with cylindrical or spherical symmetry, these orthogonal eigenfunctions are solutions of Laplace operator; in case of Cartesian coordinates the trigonometric functions appear [3]. The unknown coefficients are determined from the boundary conditions with the requirement that the solution must be physically reliable.

The MSV is a very simple and powerful instrument but its application is possible only if the following conditions are fulfilled [4]: "(i) the variables are separable out in the given coordinate system, (ii) the existence of an infinite set of eigenfunctions for the reduced, self-adjoint ordinary differential equation, (iii) the orthogonality of the eigenfunctions permitting the direct evaluation of the coefficients in the series expansion that represents the solution, and (iv) the boundary data are given on constant coordinate lines". The last restriction can be overcome successfully with newly discovered way [4], proposed recently for a heat conduction linear problems in domains with complex geometry. When the MSV is applicable and we have Bessel's type of ODE, the following solutions are well-known – these are the so called Bessel's functions (BF). They can be classified (Figs. 2−5) according to the coordinate system

considered and type of space – real or complex. Since Bessel's ODE is of second order, it has two linearly independent solutions. Each linear combination of these solutions is also a solution.

As it is seen from Fig. 3, 4 and 5 different types of BF have different behaviour. The cylindrical BF of 1-st kind is limited at point $x = 0$, but those of 2-nd kind here turned to infinity. The BF of 3-th kind are also limited at the same point, but for the case of too large complex argument. It can be seen from Figure 4 that the values of modified BF are real numbers at complex value of its argument. Unlike BF of 1-st and 2-nd kind, which are oscillating functions of real argument, the modified BF I_α and K_α are exponentially increasing/decreasing functions of complex arguments. In Figure 5 the spherical BF are represented.

The BF properties are described at some length [3, 5−10], but even nowadays they still continue to be a subject of learning and intrigue many researchers from various scientific fields [11−15]. The general properties of BF are: 1) they can be developed in asymptotic series, 2) they are orthogonal functions, 3) they satisfy various recurrent relations and 4) they permit various integral representations.

$$x^2\frac{d^2y}{dx^2}+x\frac{dy}{dx}+\left(x^2-\alpha^2\right)y=0$$

BF of first kind

$$J_\alpha(x)=\sum_{m=0}^{\infty}\frac{(-1)^m}{m!\,\Gamma(m+\alpha+1)}\left(\frac{x}{2}\right)^{2m+\alpha}$$

BF of second kind

$$Y_\alpha(x)=\frac{J_\alpha(x)\cos(\alpha\pi)-J_{-\alpha}(x)}{\sin(\alpha\pi)}$$

BF of 3-rd kind

$$H_\alpha^{(1)}(x)=J_\alpha(x)+iY_\alpha(x)\qquad H_\alpha^{(2)}(x)=J_\alpha(x)-iY_\alpha(x)$$

Fig. 2. Cylindrical Bessel's functions of 1-st, 2-nd and 3-th kind (solutions of Bessel's ODE in cylindrical coordinates) $J_\alpha(x)$, $Y_\alpha(x)$, $H_\alpha^{(1)}(x)$ and $H_\alpha^{(2)}(x)$.

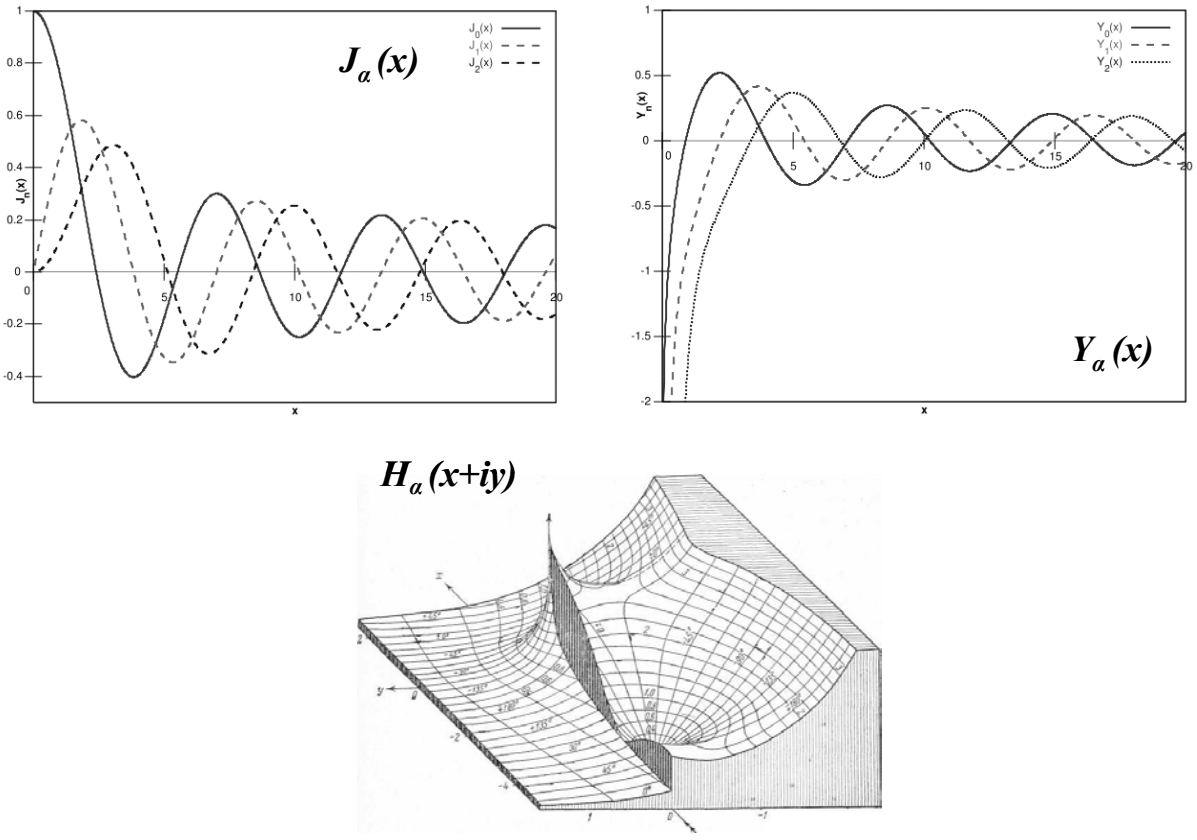

Fig. 3. Graphical representation of $J_\alpha(x)$, $Y_\alpha(x)$, and $H_\alpha(x+iy)$.

$$x^2\frac{d^2y}{dx^2}+x\frac{dy}{dx}-\left(x^2+\alpha^2\right)y=0$$

$$I_\alpha(x)=i^{-\alpha}J_\alpha(ix)$$

$$K_\alpha(x)=\frac{\pi}{2}\frac{I_{-\alpha}(x)-I_\alpha(x)}{\sin(\alpha\pi)}$$

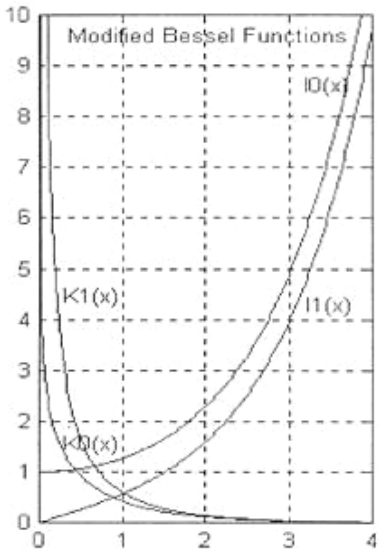

Fig. 4. Modified Bessel's functions I_α and K_α.

$$x^2\frac{d^2y}{dx^2}+2x\frac{dy}{dx}+\left[x^2-n(n+1)\right]y=0$$

$$j_n(x)=\sqrt{\frac{\pi}{2}}J_{n+1/2}(x)$$

$$y_n(x)=\sqrt{\frac{\pi}{2}}Y_{n+1/2}(x)$$

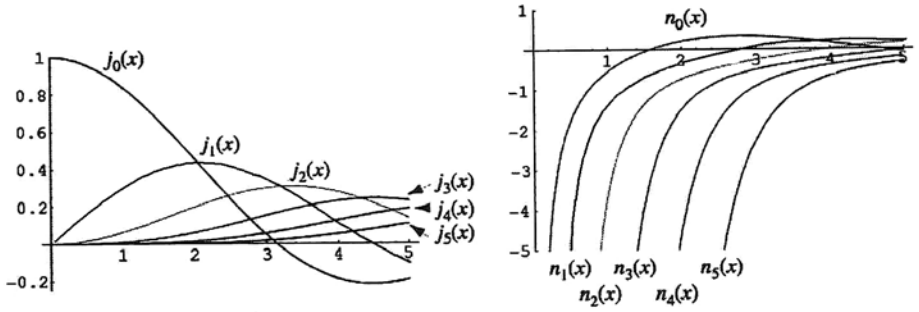

Fig. 5. Spherical Bessel's functions j_n and y_n.

Zeros of BF played crucial role in their implementation in practice. Relton [16] shows that the number of that zeros turns to infinity. In principle, their calculation is often very complex but if it was done once, they can be used repeatedly. At present the Bessel's ODE solutions and zero's calculation and their graphical representation are laid at the core of many modern software packages [17−19].

After this brief introduction to the mathematical apparatus connected to BF, some examples of chemical engineering processes in hydrodynamics, heat and mass transfer, bioprocesses and *etc*. will be described, in which modelling the BF appeared.

EXAMPLES OF BF APPLICATION TO MODELLING OF TRANSFER PROCESSES IN CHEMICAL ENGINEERING

Heat transfer

The classical example for illustration of MSV application in this area is the heat transfer in homogeneous infinite cylinder with surface area S and radius R_0. The mathematical process description is given by:

$$\frac{\partial U}{\partial t}=a^2\left(\frac{\partial^2U}{\partial r^2}+\frac{1}{r}\frac{\partial U}{\partial r}+\frac{1}{r^2}\frac{\partial^2U}{\partial\varphi^2}\right) \qquad (1)$$

$$U(r,0)=f(r), \quad U(R_0,t)\big|_S=0. \tag{2}$$

Assuming that at each point in the cylinder the temperature $U = U(r, \varphi, t)$ depends only on the radii r, the above equation will be simplified into next one:

$$\frac{\partial U}{\partial t}=a^2\left(\frac{\partial^2 U}{\partial r^2}+\frac{1}{r}\frac{\partial U}{\partial r}\right). \tag{3}$$

Let the MSV be applied, *i.e.*, we look for a non-trivial solution of the type $U(r, t) = R(r).T(t)$, which satisfies the boundary and initial conditions. After the substitution and rearrangement the next system of two ODEs follows:

$$\frac{T'(t)}{a^2T(t)}=\frac{r^2R''(r)+rR'(r)}{r^2R(r)}=-\lambda^2$$

or

$$\begin{cases} T'(t)+a^2\lambda^2T(t)=0 \\ r^2R''(r)+rR'(r)+\left(\lambda^2r^2-0\right)R(r)=0 \end{cases} \tag{4}$$

The constant λ is called "separation constant" and it is determined from the boundary (or similar to them) conditions. The second equation in (4) is Bessel's ODE towards coordinate r, λ_k are the eigenvalues with corresponding eigenfunctions $J_0(\lambda_k r)$. Finally, the exact solution of Eqn. (3) is given as:

$$U(r,t)=\sum_{k=1}^{\infty}A_kJ_0(\lambda_k r)\exp\left(-a^2\lambda_k^2t\right) \tag{5}$$

The obtained in this (or similar) way exact solution in terms of BF can be used to calculate several important parameters needed in design and construction of chemical engineering apparatuses and equipment like heat exchangers and their components. Typical example for the efficiency calculation of finned elliptical-tube heat exchangers, part of the drying system in Brazilian powdered milk plant, is considered in [20]. The efficiency η(θ) of a rectangular fin in an elliptical tube as a function of the polar coordinate θ is expressed by:

$$\eta(\theta)=\frac{2r_0(\theta)}{m\left[r_c^2-r_0^2(\theta)\right]}\cdot \frac{\left\{I_1(mr_c)K_1\left[mr_0(\theta)\right]-I_1\left[mr_0(\theta)\right]K_1(mr_c)\right\}}{\left\{I_0\left[mr_0(\theta)\right]K_1(mr_c)+I_1(mr_c)K_0\left[mr_0(\theta)\right]\right\}}, \tag{6}$$

$$m=\sqrt{\frac{2h_{sl}}{k_{fin}s}}$$

where I_0, I_1 and K_0, K_1 are modified BF of 1-st and 2-nd kind respectively, k_{fin} is the fin thermal conductivity, h_{sl} is the shell exchanger heat-transfer coefficient, s – the fin thickness, r_0, r_c– geometrical parameters of finned elliptical-tube.

An analogous situation exists in the calculation of cooling towers efficiency. The towers consist of the plate-finned tubes with external radius R [21]. These plate-finned tubes are approximately simulated through round tubes with an equivalent radius r_f, when a criterion for equal performance is adopted. The simplification based on the asymptotic properties of BF was considered likewise and finally the efficiency takes the form:

$$\eta=\tanh(mR\phi)/mR\phi$$

where

$$\phi=\left(\frac{r_f}{R}-1\right)\left[1+0{,}35\ln\frac{r_f}{R}\right] \tag{7}$$

In the case of more complex fin geometry – cylindrical fins with hyperbolic profile [22], two simple numerical procedures for solving general Bessel's ODE are proposed to estimate the temperature changes in such fins. The aim of these procedures is to evade the assessment of elegant, but sophisticated exact solution for temperature distribution and to correspond with fin's efficiencies expressed by modified BF of fractional order. In the later work [23] a new way to facilitate the calculations, manifesting modified BF with exponential functions, is suggested. The comparison made between the exact and approximated formulas in regard to efficiency shows that efficiency value can be calculated sufficiently precise with approximated formulae, which require using of electronic calculator only.

Another case when the BF arises is heat transfer modelling as considered in [24]. Here the problem of cross-flow streaming of heated object with large value of length to diameter ratio (like thermo-anemometer) is solved for small Pe numbers using the theory of analytic functions. After applying the right and reverse Fourier transform action and taking into account the integral form of modified BF [9] in the obtained solution, the following exact expression for the Nusselt number is worked out:

$$Nu = 2/K_0(Pe/4), \tag{8}$$

where Nu is the ratio of convective to conductive heat transfer across (normally to) the boundary, K_0 is a modified BF of 2-nd kind. The comparison done between Eqn. (8) and other theoretical relations is

very good, as well as a qualitative similarity to the experimental data was observed.

Mass transfer

Owing to the analogy between mathematical descriptions of heat and mass transfer processes, the BF arises again as solutions of various diffusion type of processes. In [25] a model is proposed describing changes in tracer (solid phosphorus) concentration profiles in the apparatus with circulation fluidized bed. Mixing of flow of dispersed particles in ascending line is characterized by the coefficients of axial and radial dispersion D_a and D_r. If the tracer injection like delta-function at the beginning is provided and the tracer concentration $c = c(t,x,r)$ profiles are evaluated by a dispersion model with ideal displacement, the diffusion and convection under conditions of steady flow is described by:

$$D_a \frac{\partial^2 c}{\partial x^2} + \frac{D_r}{r}\frac{\partial}{\partial r}\left(r\frac{\partial c}{\partial r}\right) - U_s \frac{\partial c}{\partial x} = \frac{\partial c}{\partial t} \qquad (9)$$

at the following boundary and initial conditions:

$$r = R, \quad \frac{\partial c}{\partial r} = 0; \quad r = 0, \quad \frac{\partial c}{\partial r} = 0, \quad x = -\infty, \quad c = 0;$$
$$c(t,x,r) = c_0.\delta(t,x,r) \qquad (10)$$

The analytical solution of the upper system has a dimensionless form:

$$\frac{c}{c_0} = \frac{\exp(\varphi\xi)}{2\pi\sqrt{\pi\theta}} \cdot \sum_{n=0}^{\infty} \frac{J_0(\beta_n \rho)}{J_0^2(\beta_n)} \left[-\frac{\xi^2}{4\theta} - (\varphi^2 + \beta_n^2)\theta \right] \qquad (11)$$

$$\rho = \frac{r}{R}, \quad \xi = \frac{z\sqrt{D_r}}{R\sqrt{D_a}}, \quad \varphi = \frac{U_s.R}{2\sqrt{D_a D_r}},$$
$$\theta = \frac{D_r.t}{R^2}, \quad Pe_a = \frac{U_s.L}{D_a}, \quad Pe_r = \frac{2U_s.R}{D_r}$$

Perhaps except only sections near the wall of air duct, the match between model and experiment is very good [25, Fig. 4−6]. The dimensionless equations, in which Peclet numbers are determined as a functions of Reynolds number and bed porosity, are derived too (mean error 10%).

In two consecutive works [26, 27] the problem of transfer modelling of one or more pollutants in anisotropic underground media into the horizontal and vertical direction has been studied. The respective system of advection-dispersion equation and initial and boundary conditions is solved analytically where values of axial and radial Pe numbers are unknown. They are determined later on by solving the inverse problem with Monte-Carlo method and experimental data for pollutants distribution.

$$\frac{\partial C}{\partial t} + u\frac{\partial C}{\partial x} = \frac{\eta}{Pe_R}\left(\frac{\partial^2 C}{\partial r^2} + \frac{1}{r}\frac{\partial C}{\partial r}\right) + \frac{1}{Pe_L}\frac{\partial^2 C}{\partial x^2} \qquad (12)$$
$$\left.\frac{\partial C(r,x,t)}{\partial r}\right|_{r=1} = 0, \quad \lim_{x\to+\infty} C(r,x,t) = 0,$$
$$\lim_{x\to+\infty} \frac{\partial C}{\partial x} = 0,$$
$$C(r,0,t) = C_0 H(t), \quad C(r,x,0) = 0;$$

Here L is the column length, R is the column radius, C_0 is the pollutant inlet concentration, $H(t)$ – Hevyside function, $\eta = L/R$. Because of its complicated mathematical expression the analytic solution is not presented in details here; it is a linear combination from BF of 1-st kind and two exponential functions whose arguments are Pe numbers. A very good coincidence is observed between the model and experimental values of pollutant concentrations [26 Fig. 2].

Another approach to modelling transfer process like osmotic transfer of water molecules in nanopores of the hexagonally packed carbon nanotube membranes is presented in ref. [28]. It was found through random walk model that the flow through any of the cylindrical membrane pores is stochastic. Then the final number of water molecules passing through each of the cylindrical pores for time t, is a function with the following distribution:

$$P[\Delta N(t) = \nu] = \exp(-k't)\left(\frac{p}{q}\right)^{\nu} I_{\nu}\left(2k'tp^{1/2}q^{1/2}\right), \qquad (13)$$

where $p,q = 1 - p$ are probabilities for water molecule to "hop" by one molecular diameter toward the salt-solution and pure-water compartments respectively, k' – "hopping" rate.

In the modelling of water diffusion in polymer particles (amorphous macromolecular systems and foods) with spherical or cylindrical shape, one is seeking a solution of the diffusion equation of the second law of Fick [29]. The solution obtained in [29, Eqn. (18)] for the normalized water uptake M_t is:

$$\frac{M_t}{M_\infty} = 1 - \sum_{n=1}^{\infty} \frac{4}{a^2\alpha_n^2} \exp\left[-D\alpha_n^2\, t\right], \qquad (14)$$

where $a\alpha_n$ are the roots of $J_0(a\alpha_n) = 0$, D is a diffusion coefficient. That solution is compared with the solutions of other simpler models. It is well seen [29, Fig. 2] that there is a qualitative difference in the behaviour of these solutions for M_t with respect to the time t, because without accounting for zeros

of the BF, the linearity of the other solutions is valid only for the first 15−20% of the entire process.

The consistent application of the fractal diffusion model, the MSV, and the construction of analytical continuation in eigenfunctions BF allow obtaining exact solution for the distribution of concentration in a limited volume of the vessel (reactor) in the case of CO_2 and N_2 diffusion in mesoporous materials (γ-alumina) [30]. This allows simulating and analyzing in detail the diffusion kinetics only through the use of BF of fractional order and their positive zeros.

In [31] it has been shown that the effectiveness factor for a catalyst pellet can be expressed for an irreversible first-order reaction by a single function, namely the modified Bessel function, independent of the shape of the pellet. Such a relation has been derived by transforming the Laplacian into a three-dimensional coordinate system, appearing in the differential mass balance equation of diffusion and reaction in a catalyst pellet, to the one-dimen-sional system. The order of the Bessel's function is strictly connected with the shape of the pellet, which is characterized by the geometrical shape parameter. The derived relationship thus enables the effectiveness factor to be calculated quickly for any simple shape of the catalyst pellet. It can therefore replace tedious and not always feasible rigorous calculations in the modelling and sizing of heterogeneous catalytic reactors.

Later, Argentinean scientists' team [32] developed models of Burghardt and found out that their one-dimensional model for the effectiveness factor of granules, already defined by the form factor, is applied with great precision in 3-D cases. Simplified procedures for calculating the efficiency of cylindrical pellets with arbitrary cross-section have been developed in [32], as an alternative for the same problem, if the form factor cannot be thus calculated, by a method of boundary elements. The study of the convergence of different equations for the degree of effectiveness of one cylindrical bead and disk expressed by modified BF has been worked out also by Asif [33]. It was found that the degree of effectiveness is increased if the factor of the form of granules differs from the spherical one.

Bioprocesses

Two-step reduction of benzene concentration in the bioreactor was studied: absorption in cylindrical polymer particles, and subsequent biodegradation of the rest in the liquid phase of benzene through the bioreactor after inoculation with *Alcaligenes xylosoxidans* [34]. The idea is to remediate partially the initial solution to a concentration of benzene, non-toxic to the environment. Benzene is first absorbed by the polymer to a concentration suitable for the microorganisms already present in the bioreactor, which are extracting it finally. Crank equations involving the BF are used [35] for calculation of the average effective diffusivity of benzene D_e within the solid cylindrical polymer particles, in [34, Eqn. (4)]:

$$\frac{\hat{M}_t}{\hat{M}_\infty} = 1 - \sum_{n=1}^{\infty} \frac{4\alpha(\alpha+1)\exp\left(\frac{-q_n^2 D_e t}{\bar{r}^2}\right)}{4 + 4\alpha + q_n^2\alpha^2}. \quad (15)$$

Here $\hat{M}_t$ is the mass of phenol absorbed from the medium by a single bead at time t, $\hat{M}_\infty$ is the total mass of phenol absorbed by a bead, $\bar{r}$ is the average radius of the beads, and q_n's are the roots of the following characteristic equation, including BF of 1-st kind:

$$\alpha q_n J_0(q_n) + 2J_1(q_n) = 0. \quad (16)$$

The coincidence between measured and calculated values in the above equation for the ratio $\hat{M}_t/\hat{M}_\infty$ is very good [34, Fig. 3].

Also in 2003, Japanese scientists' team studied the process of simultaneous nitrification and denitrification of wastewater in membrane bioreactor with aeration and biofilm fixed on the hollow fiber membrane surface [36]. The bacteria, oxidizing ammonium compounds, are concentrated mainly inside the biofilm and the bacteria, carrying out denitrification, are distributed outside. The constant speed of reaction of the 1-st order k_l for nitrification is determined by combining of experimentally measured concentration profiles of ammonia nitrogen/total nitrogen in biofilm, and the exact solution of the equation of mass balance within a biofilm:

$$D_A \frac{1}{r}\frac{d}{dr}\left(r\frac{dC_A}{dr}\right) = k_l C_A; \quad (17)$$

$$r = r_b,\ C_A = C_b;\ r = r_m,\ C_A = C_m$$

where C_A is the concentration of ammonia nitrogen, C_B – the concentration at the outside biofilm surface, C_m – the concentration at the outside membrane surface, D_A – the diffusion coefficient inside the biofilm. The exact solution of the above system includes modified BF I_0 and K_0 of 1-st and 2-nd kind:

$$C_A = A.I_0\left(\sqrt{\frac{k_l}{D_A}}r\right) + B.K_0\left(\sqrt{\frac{k_l}{D_A}}r\right), \quad (18)$$

where A and B are algebraic expressions, consisting

of the same functions and boundary value concentrations. Kinetic parameters are identified with its help – the rate of nitrification in three different axial positions in the reactor, diffusion coefficient, and experimental results show that nitrogen impurities are completely reduced at the exit of the apparatus.

Hydrodynamic

The influence of the superficially active substances (SAS) on the hydrodynamics was studied in [37]. The distribution of velocities in a thin laminar film, which was solved SAS, is determined. After a number of simplifying assumptions the non-homogeneous Bessel's differential equation about one velocity component is obtained, in which the influence of SAS appeared in its right side. Longitudinal velocity component is expressed by the BF of the first kind and argument, depending on the longitudinal coordinate, the initial thickness of the film, and the change of surface tension. It was found out that the surface concentration of SAS and the distribution on the surface of the film can be determined by the rate of adsorption.

Another problem connected with SAS is solved in [38]. In the presence of SAS considering the impact of the phases, limiting the film, the rate of thinning of emulsion films in the cylindrical coordinates and for semi-infinite area has been studied. The mechanism of SAS emerging is divided into 2 stages - the diffusion from volume of the film to the layer in immediate vicinity of the film surface, and adsorption of SAS from that layer to the film surface. Depending on the rate of these stages, slowed diffusion or delayed adsorption, respectively, were observed. Equations of the Navier-Stokes and boundary conditions are simplified and this leads to an analytical solution for determining the components of velocity in r and z in the surrounding film phase. This solution contains BF of 1-st kind.

The idea of modelling the process of spreading of a liquid flow in packed columns by the Gaussian normal distribution is started in [39], and subsequently is further developed in [40] and [41]. Based on this idea various mathematical models are developed subsequently, most of whose analytical solutions for the liquid density of irrigation in different cases of initial irrigation and other types of boundary conditions are derived [42−59]. The most common type of solution has been presented by converged infinite series and is a combination of exponents, BF and unknown coefficients, the latter being determined based on the boundary conditions. Table 1 shows some of the results obtained by different researchers on modelling the liquid density of irrigation in packed columns.

BF can be used in modelling of gas flow maldistribution in the packed columns too [60−62]. For the gas phase the analytical formula (from the dispersion model of [60]) for a gas flow maldistribution factor has been worked out. Later an additional term taking into account the effects of the discrete structure of the packing layer itself is added to this formula [61−62], since in the solution for the velocity given by dispersion model, the structure of layers is assumed to be homogeneous and isotropic medium:

$$\left(M_f^{\boldsymbol{real}}\right)^2 = \left(M_f^{\boldsymbol{model}}\right)^2 + \left(M_f^{\boldsymbol{noise}}\right)^2 \qquad (19)$$

In the modelling of the blood flow movement in arterial vessels different boundary conditions have been tested in cases of deformable or non-deformable arterial walls [63]. For determining appropriate choice of boundary condition of pulsative blood flow in the model, the solution of Womersley [64] has been chosen:

$$w(r,t) = \frac{2}{\pi R^2} B_0 \left[1 - \left(\frac{r}{R}\right)^2\right] + \qquad (20)$$

$$+ \sum_{n=1}^{N} \frac{B_n}{\pi R^2} \left[\frac{1 - \dfrac{J_0\left(\alpha_n \dfrac{r}{R} i^{3/2}\right)}{J_0\left(\alpha_n i^{3/2}\right)}}{1 - \dfrac{2J_1\left(\alpha_n i^{3/2}\right)}{\alpha_n i^{3/2} J_0\left(\alpha_n i^{3/2}\right)}}\right] \exp(in\omega t)$$

where R is the inlet radius of the considered arterial vessel, α_n are eigenvalues, i − imaginary unit. Pulsation of the flow is modelled by a Fourier series with coefficients B_0, B_n. Since they were unknown [63] they were determined by experimental data for blood velocity profile taken by ultrasonic Doppler method. The argument of the BF of the first kind contains the frequency ω of the cardiac cycle ~ 1s. The appropriate choice of Eqn. (20) upon comparing calculated and experimental data on the rate of blood flow can be seen in [63, Fig. 3].

The review of all selected examples of BF applications in all considered areas would be incomplete if the similarities between the diffusion boundary problem, dispersion model for spreading fluids and heat transfer problem are not mentioned [11]. The different cases of problems boundary conditions and the effects, which they are corresponding to, are discussed. In particular, the boundary condition, used in [47, 48] are considered. It is an assessment of the zeros of the BF of the first kind and 1-st order involved in that condition, using Newton-Rapson's method.

Table 1. Analytical solutions for liquid density of irrigation, expressed in BF for different boundary conditions.

Equation: $\frac{\partial^2 f(r,z)}{\partial r^2}+\frac{1}{r}\frac{\partial f(r,z)}{\partial r}=\frac{\partial f(r,z)}{\partial z}$

Boundary condition	Solution	Source
$f_{r=\infty}=Q$	$f=\frac{Q}{4\pi DH}\exp\left(-\frac{r^2}{4DH}\right)$	[41, 65–68]
$f(a,z)=Kw(z)$	$\frac{f(r,z)}{f_0}=\frac{K}{K+1}-4K\sum_{n=1}^{\infty}\frac{J_0(q_n r/a)\exp\left(-q_n^2 To\right)}{\left(4K+4K^2+q_n^2\right)J_0(q_n)}$	[69]
$-\frac{\partial f(r,z)}{\partial r}=B\{f(r,z)-CW\}$, for $r=1$	$f^u(r,z)=A_0+\sum_{n=1}^{\infty}A_n^u J_0(q_n r)\exp\left(-q_n{}^2 z\right)$; $A_0=\frac{C}{1+C}$; $A_n^u=\frac{2\left(q_n^2/B-2C\right)}{\left[\left(q_n^2/B-2C\right)^2+q_n^2+4C\right]J_0(q_n)}$	[44–46, 49, 50, 53–58]
$-2\pi aD\left(\frac{\partial f}{\partial r}\right)_{r=a}=kf(a,z)-k'w(z)$	$\frac{f}{f_0}=\frac{1}{1+\alpha}.(1+2(1+\alpha))\quad x$ $x\quad\sum_{n=1}^{\infty}\frac{q_n J_0(q_n r/a)\exp\left(-q_n^2 To\right)}{\left[\left(2\beta q_n^2-\frac{2}{\alpha}\right)^2+q_n^2+4\alpha\right]J_1(q_n)}$ $\alpha=\frac{k}{\pi a^2 k'}$, $\beta=\frac{\pi D}{k}$, $To=\frac{DH}{a^2}$	[47, 48]

REASONS FOR USING BF IN THE MODELING OF CHEMICAL ENGINEERING TRANSFER PROCESSES

- Heat transfer, diffusion and hydrodynamic processes of flow moving and flow state, can be modelled successfully by PDEs. There are methods for solving them by which they are restricted to the Bessel's type of ODE for some of the variables. The exact solution of the ordinary or modified Bessel's equation contains BF.

- The solution in BF is obtained when the system of linear PDE, with boundary and initial conditions is located in the area with simple boundaries – rectangle, circle, *etc*., and the presence of symmetry (cylindrical or spherical).

- In many cases it is possible to simplify the right exact solution, using the properties of BF (asymptotic at large or small value of the argument, orthogonality, recurrent relations between BF, integral representations). This saves time and resources in its calculation.

- Opportunity to compare the exact and other existing approximate solutions allows evaluating the details based on which it is determined as well as when to use which one, especially in the calculation of kinetic and other important indicators of the effectiveness of a transfer process.

NOMENCLATURE

A, B	constants, in the algebraic expressions, Eqn. (18);
a	thermal diffusivity, (m^2/s);
B_0, B_n	Fourier series coefficients;
C_A	concentration of ammonia nitrogen, (g/m^3);
C_b	concentration on the outside biofilm surface, (g/m^3);
C_m	concentration on the outside membrane surface, (g/m^3);
C_0	scale of pollutant concentration, (g/m^3);
c, c_0,	recent and initial relative concentrations of the phosphorus tracer, (−);
D	diffusion coefficient, (cm^2/s);

D_A diffusion coefficient inside the biofilm, (m^2/day);
D_a, D_r coefficients of axial and lateral solids dispersion, respectively, (m^2/s);
D_e average effective diffusivity of benzene inside the solid cylindrical polymer particles, (cm^2/s);
f function; liquid density of irrigation in Table 1, ($m^2/m^3 \cdot s$);
$H_a(x+iy)$ BF of 3-th kind, complex argument;
$H(t)$ Hevyside function;
h_{sl} shell exchanger heat-transfer coefficient, ($W/m^2 \cdot K$);
i imaginary unit;
I_α modified BF of 1-st kind, order $\alpha = 0,1,2 \ldots$;
J_α cylindrical BF of 1-st kind, order $\alpha = 0,1,2 \ldots$;
$j_n(x)$ spherical BF of 1-st kind;
K_α modified BF of 2-nd kind, order $\alpha = 0,1,2 \ldots$;
k_{fin} fin thermal conductivity, (W/m·K);
k, n summation indexes;
k' hopping rate, nm/s;
k_l constant rate of reaction of the 1st order for nitrification, (l/day);
L column length, (m);
M_f - gas maldistribution factor,(−);
M_t water uptake, in Eqn. (14), (mg);
$\hat{M}_t$ mass of phenol absorbed from the medium by a single bead at time t, in Eqn. (15), (mg);
M_∞ mass of water uptake as time approaches infinity, in Eqn. (14), (mg);
$\hat{M}_\infty$ the total mass of phenol absorbed by a bead, in Eqn. (15), (mg);
p probability of water molecule to "hop" by one molecular diameter toward the salt-solution;
$q = 1-p$ probability of water molecule to "hop" by one molecular diameter toward the pure-water compartments;
q_n roots of Eqn. (16);
R radius, (m);
R_0 cylinder radius, (m);
r radial coordinate, (m);
r_0, r_c geometrical parameters of finned elliptical-tube, (m);
r_f equivalent radius, (m);
$\bar{r}$ the average radius of a bead, (m);
S cylinder surface area, (m^2);
s fin thickness, (m);
t time, (s);
U_s superficial solids velocity, (m/s);
U temperature, (°C);
u dimensionless velocity in Eqn. (12);
x, y spatial coordinates, (m);
$Y_\alpha(x)$ BF of 2-nd kind;
$y_n(x)$ spherical BF of 2-nd kind;
$a\alpha_n$ roots of $J_0(a\alpha_n) = 0$;
α_n modified Womersley number, after [64];
β_n the n-th positive zero of J_1;
δ Dirac's function;
$\eta = \frac{L}{R}$ dimensionless parameter, (−);
$\eta(\theta)$ efficiency, (−);
θ polar coordinate, (m);
φ angular coordinate, (grad);
λ separation constant;
λ_k eigenvalues in Eqn. (5);
φ dimensionless parameter in Eqn. (7);
ω frequency of the cardiac cycle, (s).

ABBREVIATIONS

BF Bessel's functions;
MSV Method of separation of variables;
ODE ordinary differential equation;
PDE partial differential equation;
SAS surface active substances (surfactants).

REFERENCES

1. J. Mathews, R. L. Walker, Mathematical Methods of Physics, Atomizdat, Moskow, 1972 (in Russian).
2. G. Korn, T. Korn, Mathematical Handbook for Scientists and Engineers, 4-th edn., Nauka, Moskow, 1977. (in Russian).
3. V. I. Levin, Mathematical Methods of Physics, 2-nd edn., Uchpedgiz, Moskow, 1960 (in Russian).
4. P. N. Shankar, *Current Science*, **88**, 266 (2005).
5. http://en.wikipedia.org/wiki/Bessel_function.
6. http://ccrma.stanford.edu/~jos/mdft/Bessel_Functions.html.
7. http://www.inrne.bas.bg/wop/ARCHIVE/wop_1_2006/nauka_mater.pdf.
8. A. V. Efimov, Matematical Analysis (Special Sections) Part 1, Visshaya Shkola, Moscow, 1980 (in Russian).
9. M. Abramowitz, I. A. Stegun, (eds.), Modified Bessel Functions I and K, 9-th printing, Dover, New York, 1972.
10. B. G. Korenev, Bessel Functions and Their Applications, CRC Press, London, New York, 2002.
11. I. A. Furzer, *AIChE J.*, **32**, 325 (1986).
12. X. A. Lin, O. P. Agrawal, *J. Franklin Inst.*, **332**, 333 (1995).
13. E. A. Skelton, *J. Math. Anal. Appl.*, **267**, 338 (2002).

14. A. Grey, G. B. Mathews, A Treatise of Bessel Functions and Their Applications to Physics, Merchant Books, 2007.
15. D. Borwein, J. M. Borwein, O-Yeat Chan, *J. Math. Anal. Appl.,* **341**, 478 (2008).
16. http://www.du.edu/~jcalvert/math/bessels.htm - Comments on the book of F. E. Relton, Applied Bessel Functions, Blackie and Son, London, 1946.
17. K. Syverud, S. T. Moe, R. J. A. Minja, in: Proc. 10th Int. Symp. Wood and Pulping Chemistry, June 7–10, 1999, Yokohama, Japan, Part 2, p. 232.
18. L. F. de Moura, in: 1st Int. Conf. Foundations of Systems Biology in Engineering, August 7−10, 2005, Santa Barbara, California, USA.
19. http://www.higgins.ucdavis.edu/chemmath.php.
20. C. P. Ribeiro Jr., M. H. C. Andrade, *Braz. J. Chem. Eng.,* **21**, 345 (2004).
21. A. Hasan, K. Siren, *Appl. Therm. Eng*., **23**, 325 (2003).
22. A. Campo, B. Morrone, S. Chikh, *Int. J. Numer. Meth. Heat Fluid Flow*, **14**, 1002 (2004).
23. A. Campo, J. Cui, *J. Heat Transfer*, **130**, 054501-1 (2008).
24. V. Bertola, E. Cafaro, *Int. J. Heat Mass Transfer*, **49**, 2859 (2006).
25. F. Wei, Y. Jin, Zh. Yu, W. Chen, S. Mori, *J. Chem. Eng. Jpn*., **28**, 506 (1995).
26. F. Catania, M. Massabò, O. Paladino, Transactions of the 2nd Biennial Meeting of the iEMSs, University of Osnabruck, Germany, 14−17 June, 2004 (on CD).
27. F. Catania, M. Massabò, O. Paladino, *Environ. Metrics*, **17**, 199 (2006).
28. A. Kalra, Sh. Garde, G. Hummer, *Proc. Nat. Acad. Sci. U.S.A.*, **100**, 10175 (2003).
29. N. A. Peppas, L. Brannon-Peppas, *J. Food Eng*., **22**, 189 (1994).
30. Sh. Wang, Zh. Ma, H. Yao, *Chem. Eng. Sci*., **64**, 1318 (2009).
31. A. Burghardt; A. Kubaczka, *Chem. Eng. Process*., **35**, 65 (1996).
32. N. J. Mariani, S. D. Keegan, O. M. Marti'nez, G. F. Baretto, *Chem. Eng. Res. Des.*, **81**, 1033 (2003).
33. M. Asif, *Chem. Eng. Res. Des*., **82**, 605 (2004).
34. J. Daugulis, B. G. Amsden, J. Bochanysz, A. Kayssi, *Biotechnol. Lett.*, **25**, 1203 (2003).
35. J. Crank, The Mathematics of Diffusion, Clarendon Press, Oxford, viii, 1975.
36. K. Hibiya, A. Terada, S. Tsuneda, A. Hirata, *J. Biotechnol*., **100**, 23 (2003).
37. Hr. Boyadjiev, *Proc. Inst. Gen. Inorg. Chem. Bulg. Acad. Sci.*, **III**, 137 (1965). (in Bulgarian).
38. V. Beshkov, B. Radoev, I. Ivanov, God. Sofii. Univ. Khim. Fac., **63**, 197 (1968/1969) (in Bulgarian).
39. K. Thormann, Distillation und Rektifizieren, Spamer, Leipzig, 1928.
40. A. H. Scott, *Trans. Inst. Chem. Eng*. **13**, 211 (1935).
41. R. S. Tour, F. Lerman, *Trans. Am. Inst. Chem. Eng.,* **40**, 79 (1944).
42. Z. Cihla, O. Schmidt, *Collect. Czech. Chem. Commun*., **22**, 896 (1957).
43. Z. Cihla, O. Schmidt, *Collect. Czech. Chem. Commun*., **23**, 569 (1958).
44. V. Kolář, V. Staněk, *Collect. Czech. Chem. Commun*., **30**, 1054 (1965).
45. V. Kolář, V. Staněk, *Collect. Czech. Chem. Commun*., **32**, 4207 (1967).
46. V. Staněk, V. Kolàř, *Collect. Czech. Chem. Commun*., **33**, 1062 (1968).
47. E. Dutkai, E. Ruckenstein, *Chem. Engn. Sci.,* **23**, 1365 (1968).
48. E. Dutkai, E. Ruckenstein, *Chem. Engn. Sci*., **25**, 483 (1970).
49. V. Staněk, V. Kolàř, *Collect. Czech. Chem. Commun*., **38**, 1012 (1973).
50. V. Staněk, V. Kolàř, *Collect. Czech. Chem. Commun*., **38**, 2865 (1973).
51. E. Brignole, G. Zacharonek, J. Mangosio, *Chem. Engng. Sci*., **28**, 1225 (1973).
52. V. Staněk, V. Kolàř, *Collect. Czech. Chem. Commun*., **39**, 2007 (1974).
53. V. Staněk, Kr. Semkov, N. Kolev, G. Paskalev, *Collect. Czech. Chem. Commun*., **50**, 2685 (1985).
54. Kr. Semkov, N. Kolev, V. Stanek, P. Moravec, *Collect. Czech. Chem. Commun*., **52**, 1430 (1987).
55. Kr. Semkov, N. Kolev, V. Stanek, P. Moravec, *Collect. Czech. Chem. Commun*., **52**, 1440 (1987).
56. Kr. Semkov, N. Kolev, V. Stanek, *Collect. Czech. Chem. Commun*., **52**, 2438 (1987).
57. Kr. Semkov, T. Petrova, P. Moravec, *Bulg. Chem. Commun.*, **32**, 497 (2000).
58. T. Petrova, Kr. Semkov, P. Moravec, *Bulg. Chem. Commun*., **34**, 82 (2002).
59. K. Onda, H. Takeuchi, Y. Maeda, N. Takeuchi, *Chem. Eng. Sci*., **28**, 1677 (1973).
60. T. Petrova, Kr. Semkov, Ch. Dodev, *Chem. Eng. Process*., **42**, 931 (2003).
61. T. Petrova, Kr. Semkov, in: Proc. 11-th Workshop Transport Phenomena in Two-Phase Flow, September 1–5, 2006, Sunny Beach Resort, Bulgaria, J. Hristov (ed.), p. 93.
62. T. Petrova, PhD Thesis, Inst. Chem. Eng., Bulg. Acad. Sci., Sofia, 2008.
63. R. Torii, M. Oshima, T. Kobayashi, K. Takagi, T. E. Tezduyar, *Comput. Meth. Appl. Mech. Eng*., **195**, 1885 (2006).
64. J. R. Womersley, *J. Physiol.*, **127**, 553 (1955).
65. M. I. Kabakov, V. V. Dil'man, *Theor. Found. Chem. Eng*., **7**, 815 (1973).
66. N. N. Kolev, A. L. Boev, R. D. Darakchiev, *Theor. Found. Chem. Eng.*, **15**, 299 (1981).
67. D. Dzhonova-Atanasova, N. Kolev, S. Nakov, M. Gyupchanov, M. Hristov, *Compt. Rend. Acad. Bulg. Sci.*, **58**, 1281 (2005).
68. D. Dzhonova-Atanasova, N. Kolev, Sv. Nakov, *Chem. Eng. Technol*., **30**, 202 (2007).
69. K. E. Porter, M. C. Jones, *Trans. Inst. Chem. Eng*., **41**, 240 (1963).

ПРИЛОЖЕНИЕ НА БЕСЕЛЕВИТЕ ФУНКЦИИ В МОДЕЛИРАНЕТО НА ИНЖЕНЕРНО-ХИМИЧНИ ПРОЦЕСИ

Т. Ст. Петрова

Институт по инженерна химия, Българска академия на науките, ул. „Акад. Г. Бончев“, бл. 103, 1113 София

Постъпила на 18 март 2009 г.

(Резюме)

Показано е, че при определени условия диференциалните уравнения, описващи съответния преносен процес, допускат решение, изразяващо се чрез Беселевите функции (БФ). За целта е направено проучване върху широк кръг работи, обхващащ моделирането на преносни процеси както в химичното инженерство, така и в сродни и близки до него области. Разгледани са различни типове случаи от хидродинамиката, топлопроводността и дифузията, биопроцесите и др. В заключение са обособени основанията за използването на БФ при моделирането на преносни процеси в инженерната химия.

Bulgarian Chemical Communications, Volume 41, Number 4 (pp. 355–361) 2009

Biomethanation of black liquor in fluidized-bed bioreactor

Sk. M. Hossain[1,*], M. Das[2]

[1] *Centre for Advanced Studies and Research, Younus College of Engineering & Technology, Vadakkevila, 691010 Kollam, India*

[2] *Department of Chemical Engineering, University of Calcutta, 92 A P C Road, 700009 Kolkata, India*

Received November 14, 2007; Revised April 17, 2009

Attempts were made to optimize bioprocess parameters for maximum production of methane and removal of chemical oxygen demand (COD) and biological oxygen demand (BOD) from black liquor in the process of biomethanation in three-phase fluidized bioreactor. The optimum hydraulic retention time (HRT) is 8 h and optimum initial pH of the feed was observed to be 7.5. The optimum feed temperature is 40°C and optimum feed flow rate is 16 L/min at organic loading rate (OLR) of 45.158 kg COD·m^{-3}·h^{-1} respectively. The maximum methane constitutes 64.82% (v/v) of the total biogas generation. The maximum biogas yield rate is 0.723 m^3/kg COD·m^{-3}·h^{-1} with methane yield rate of 0.530 m^3/kg COD·m^{-3}·h^{-1} respectively at optimum biomethanation parameters. The maximum COD and BOD remediation of the black liquor are 79.65% (w/w) and 81.54% (w/w) with maximum OLR of 11.686 kg COD·m^{-3}·h^{-1} respectively.

Key words: anaerobic**,** biogas, biomethanation, black liquor, fluidized-bed, optimum.

INTRODUCTION

The energy crisis of the early 1970s brought into sharp focus the vital importance of the biomass energy in the face of destabilized global trade in fossil energy. Much of the present-day technology is fuelled by biomass of carboniferous era. To a varying extent, this fossil biomass energy resource is supplemented all over the world by energy obtainable from extant biomass. The unique ability to capture photons from solar radiation and to store the energy in the form of sugars, starch, cellulose materials, *etc*. implies renewable energy supply given appropriate conversion technologies.

A reassessment of conventional biomass energy production and conversion technologies is pertinent at this stage. The bulk of biomass energy is currently derived from agricultural crop wastes [1−7]. Biogas production is of major importance for the sustainable use of agrarian biomass as renewable energy source. In a few instances, municipal wastes and peat form additional sources of biomass energy [8−14]. Attempts are being made to exploit other forms of biomass such as seaweeds, and algae. While these other sources could add substantially to the world biomass energy supply, their exploitation could lead to ecological disasters. A more possible alternative is to use industrial cellulose wastewaters and effluents to satisfy the ecological balances and pollution abatement [15−32].

The conversion of complex organic matter to methane and carbon dioxide is accomplished in general by four groups of bacteria [1−7] namely hydrolytic, acetogenic, acetoclasic and hydrogen-utilizing, respectively. The various groups of bacteria essential to the biomethanation are interdependent. They all perform under anaerobic conditions, *i.e.* in the absence of molecular oxygen at highly negative redox potential, but the activity of each group depends on the activities of the others. The actual ratio of methane to carbon dioxide (CO_2) varies with the substrate, temperature (mesophilic or thermophilic) and bioprocess conditions [1−7, 26−32].

Perez *et al.* [18] examined the effect of organic loading rate (OLR) on the removal efficiency of chemical oxygen demand (COD) and total organic carbon (TOC) using anaerobic thermophilic fluidized-bed reactor (AFBR) in the treatment of cutting-oil wastewaters at different hydraulic retention time (HRT) conditions. Acharya *et al.* [19] studied the anaerobic digestion of wastewater from a distillery industry having very high COD and biological oxygen demand (BOD), which was fed in a continuous upflow fixed film column reactor using different support materials such as charcoal, coconut coir and nylon fibres under varying hydraulic retention time (HRT) and organic loading rates (OLR) respectively. This study indicated that fixed film biomethanation of distillery spent wash using coconut coir as the support material appeared to be a

* To whom all correspondence should be sent:
E-mail: skmhossain@yahoo.co.in

cost effective and promising technology for mitigating the problems caused by distillery effluent. Jantsch *et al*. [20] investigated anaerobic biodegradation of fermented spent sulphite liquor. Batch experiments with diluted liquor and pretreated liquor indicated a potential of 12−22 l of methane per litre liquor, which corresponds to 0.13−0.22 l of methane $(gVS)^{-1}$ and COD removal of up to 37%. COD removal in a mesophilic upflow anaerobic sludge blanket (UASB) reactor ranged from 10% to 31% at an organic loading rate (OLR) of 10−51 $g\cdot(L\cdot d)^{-1}$ and hydraulic retention time from 3.7 to 1.5 days. The biogas productivity was 3 $l\cdot(L_{reactor}\cdot d)^{-1}$, with an yield of 0.05 l gas $(gVS)^{-1}$.

Encouraged by the above work, continuous investigations are being undertaken to develop an effective anaerobic biomethanation of black liquor (wastewaters from craft pulping) using actively digested sludge from a sewage plant for biogas generation in three-phase fluidized-bed bioreactor. Attempts are also made to optimize hydraulic retention time (HRT), initial feed pH, feed temperature and feed flow rate to obtain maximum methane gas generation and bioremoval of chemical oxygen demand (COD) and biological oxygen demand (BOD) from black liquor wastewaters.

EXPERIMENTAL

Collection of seed and suspension culture preparation. Activated sewage sludge collected from a local sewage plant constitutes the ideal "seed" material. It is transferred to suspension culture media, prepared earlier and incubated in an incubator at 30°C for 7 days for sufficient bacterial growth. The resulting mixed bacterial cell suspensions are filtered through several layers of sterile adsorbent cotton. The mixed bacterial population is counted [33] as 7.1×10^8 number of cells per ml of the suspension culture (Luckey Drop Method). The suspension culture media contained the following constituents per liter: KH_2PO_4 – 20 g, $MgSO_4.7H_2O$ − 5.0 g, $CaCl_2$ − 1.0 g, $MnSO_4.7H_2O$ − 0.05 g, $FeSO_4.7H_2O$ − 0.10 g, $CaCl_2.6H_2O$ − 0.10 g, $AlK(SO_4)_2.12H_2O$ − 0.01 g, $Na_2MoO_4.2H_2O$ − 0.01 g.

Collection and analysis of black liquor

The black liquor wastewater sample was collected from indigenous sources and stored at 4°C. The sample was analyzed [34]. The chemical oxygen demand (COD) is 28.565 mg/l and biological oxygen demand (BOD) is 17.750 mg/l respectively.

Experimental setup

The experimental setup of three-phase fluidized-bed bioreactor (Appex Innovations Ltd.) is shown in Fig. 1. The wastewaters enter at the bottom and pass through the fluidized-bed bioreactor and leave at the top. The flow has a velocity sufficient to expand the bed without necessarily causing vigorous agitation, which results in complete mixing of the wastewaters and mixed activated sludge bacteria. The increase in effective surface area of the medium, achieved by fluidizing and expanding in the bioreactor bed, provides an opportunity for higher organic loading rates, greater yield of cell mass and greater resistance to intimidators. Wastewaters flow in expanded bed only. Recycle of the feed is done (Fig. 1). The biogas is collected in a gas holder. The gas holder is normally an airproof steel container, which floats like a ball on the fermentation mix and cuts off air to the reactor and collects the gas generated. It is fitted with a Flame-Ionization Detector (FID). After each operation, the effluents (digested feed) are discharged through a valve.

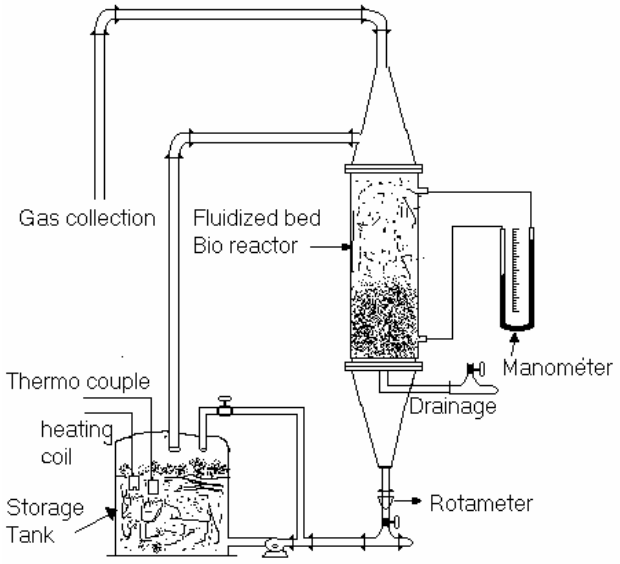

Fig. 1. Experimental setup of fluidized-bed reactor.

General method

The anaerobic biomethanation of black liquor is studied in a three-phase fluidized-bed bioreactor of 18.6 l capacity. Experiments are carried out in 50 l plastic tank containing 20 l of raw wastewaters as feed to be digested for biogas generation. 20 l of suspension mixed activated bacterial culture as inoculums are added to the feed tank. The inoculum is taken from a seven-days-old suspension culture. 2.0 L of suspension culture media is added to the feed tank contents. The initial pH of feed in tank is maintained at 6.0 by using 0.1 N H_2SO_4 acid and/or 1 M $CaCO_3$ slurry. The temperature of the feed is maintained at 30°C by means of heating coil fitted with off/on temperature controller. The temperature of the feed is measured by a thermocouple. The feed

is pumped to three-phase fluidized-bed bioreactor from the feed tank. The initial feed flow rate is maintained at 10 l/min (OLR is 28.224 kg COD·m^{-3}·h^{-1}) through a rotameter (Fig. 1). Outlet digested feed is recycled to the feed tank. The biogas is collected in the gas holder.

Effect of hydraulic retention time. The concentrations of methane gas in the generated biogas are measured at regular interval of time. 50 ml of digested feed is taken out after 2, 4, 6, 8, and 10 h of HRT, filtered, followed by analysis of COD and BOD respectively.

Effect of initial feed pH. The general method is repeated at various initial pH values of the feed in the tank such as 6.5, 7.0, 7.5 and 8.0 respectively to optimize initial pH. The concentrations of methane gas are measured at optimal HRT of 8 h at each pH value. 50 ml of digested feed is taken out at optimal HRT, filtered, followed by analysis of COD and BOD at each pH value respectively.

Effect of feed temperature. The general method is repeated at different temperatures of the feed in the tank such as 35, 40 and 45°C respectively. The initial pH of the feed in the tank is maintained at optimum of 7.5. The methane gas concentrations are measured at optimal HRT of 8 h at each temperature. 50 ml of digested feed is taken out at optimal HRT, filtered, followed by analysis of COD and BOD respectively at each temperature.

Effect of feed flow rate. The general method is repeated at different feed flow rates (organic loading rate) in the three-phase fluidized-bed bioreactor such as 12, 14, 16 and 18 l/min respectively. The corresponding organic loading rates (OLR) are 33.867 kg COD·m^{-3}·h^{-1}, 39.513 kg COD·m^{-3}·h^{-1}, 45.158 kg COD·m^{-3}·h^{-1} and 50.803 kg COD·m^{-3}·h^{-1} for 12, 14, 16 and 18 l/min respectively. The initial pH value of the feed in the tank is maintained at optimum of 7.5. The temperature of the feed in the tank maintained at optimum 40°C. The methane (CH_4) gas concentrations are measured at optimal HRT of 8 h for each feed flow rate. 50 ml of digested feed is taken out after optimal HRT, filtered, followed by analysis of COD and BOD respectively at each flow rate.

Analysis of methane in biogas

The analysis of biogas [35] containing methane gas is carried out by the Flame-Ionization Detector (FID). The eluate coming from the column is mixed with hydrogen (the fuel) and then burned in a stream of air (the oxidant) to form a combustible mixture in FID (Ametek Process Instruments, Inc.). The ignited mixture yields a flame, which provides the energy to ionize sample component in the eluate. The temperature (1800−1900°C) of the air-hydrogen flame is used to ionize only carbon compounds. The positive ions thus formed during ionization in the flame are attracted to a negative "Collector" electrode and repelled by a positive "Repeller" electrode. The repeller electrode is either the metal burner or an electrode placed near the base of the flame. Upon striking the collector electrode, the positively charged ions cause a current to flow in the external circuit, connecting the positive and negative electrodes. The current is amplified and recorded. Because the hydrogen-air flame itself generates relatively few ions, it has a non-zero base line. The current flowing through the circuit is proportional to the number of ions striking the collector, which in its turn is proportional to the amount (concentrations) of methane gas entering the flame. Since the number of the positive ions formed in the flame is proportional to the number of carbon atoms in the sample component, the detector's response is also proportional to the number of carbons in the sample component molecule [35]. The FID responds only to such substances, which can be ionized in the air-hydrogen flame. For that reason, the FID does not respond to most inorganic components present in biogas including carbon dioxide, hydrogen sulphide, *etc*.

RESULTS AND DISCUSSION

Effect of hydraulic retention time

The effect of hydraulic retention time (HRT) on methane (CH_4) gas generation from black liquor and bioremediation of pollution load in fluidized-bed bioreactor with mixed activated sludge is shown in Figures 2 and 3 respectively.

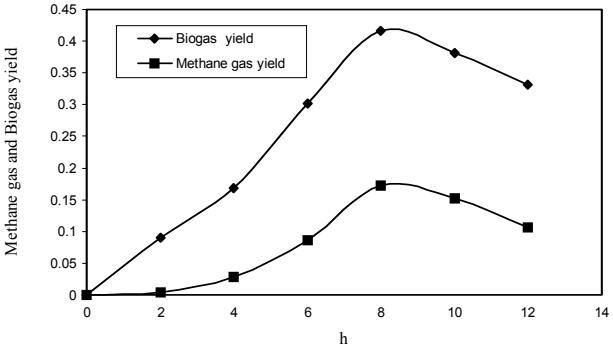

Fig. 2. Effect of hydraulic retention time.

The concentration and yield of methane gas increase with increase of HRT up to 8 h and then both decline (Fig. 2). The concentrations and yields of methane gas from black liquor are proportional to optimal HRT of 8 h. It is observed that maximal biogas yield from black liquor is 0.416 m^3/kg COD·m^{-3}·h^{-1} at optimal 8 h HRT (Fig. 2). The

maximal methane gas concentration is 41.53% (v/v) at optimal 8 h HRT in the biogas (Fig. 3). The recycling time is also included in the HRT measurements. Maximal methane gas yield is 0.172 m^3/kg COD·m^{-3}·h^{-1} at an optimum of 8 h HRT (Fig. 2). It is also noticed that the maximal removal of COD and BOD from black liquor are 49.53% (w/w) and 56.72% (w/w) respectively at an optimum of 8 h HRT (Fig. 3). After 8 h of HRT, the removal of COD and BOD from wastewaters decreases (Fig. 3) and yields of biogas and methane gas also decline (Figs. 2 and 3). Therefore, HRT of 8 h is taken as an optimum for further studies in the fluidized-bed bioreactor to optimize other biomethanation process parameters.

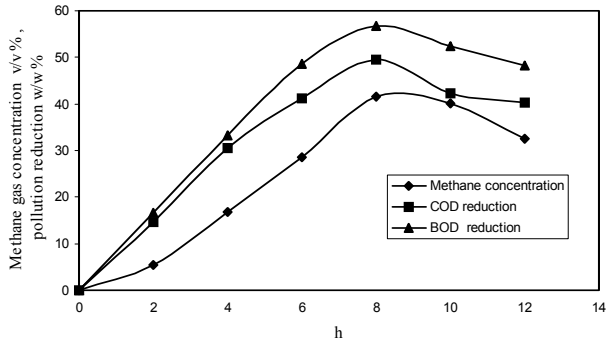

Fig. 3. Effect of hydraulic retention time.

It is evident from the Figures 2 and 3 that as the HRT increases, the yields and concentrations of methane gas by the mixed bacteria increase up to optimal value, then both decrease. This is because of bacterial populations in the reactor that can affect biomethanation of black liquor. At the early stage of biomethanation, which coincided with lag-phase of bacterial growth, the removal of COD and BOD and yield of methane gas are very low (Figs. 2 and 3). The extent of lag-phase is dependent on feed compositions, which initially contain high values of COD and BOD, respectively. Lag-phase time is required for adaptation to black liquor media for proper growth of the mixed bacteria [36−37]. The transition of bacterial growth from the lag-phase to exponential phase (maximum growth) led to a notable increase in methane gas, which proceeded in the same way until it reaches maximum at optimal HRT of 8 h as well (Figs. 2 and 3).

Effect of initial feed pH

The effect of initial feed pH on the anaerobic biomethanation of black liquor in three-phase fluidized-bed bioreactor is shown in Figures 4 and 5 respectively. Initial pH of feed is taken both in acidic and basic medium range. The optimal HRT of 8 h is maintained for the optimization of feed pH. The increase in yields and concentrations of methane gas are observed with increase in initial feed pH up to 7.5 and then both declined. It is observed that maximal biogas yield from sugar industry wastewaters in fluidized-bed bioreactor is 0.618 m^3/kg COD·m^{-3}·h^{-1} at optimal feed pH of 7.5 (Fig. 4).

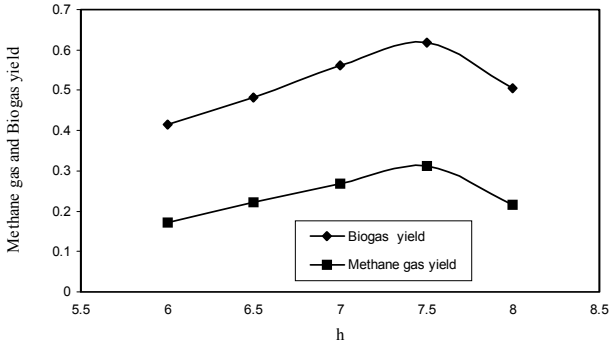

Fig. 4. Effect of feed pH.

The maximum methane gas concentration is 50.76% (v/v) at optimum feed *p*H of 7.5 with mixed activated sludge bacteria (Fig. 5). The maximal methane gas yield is 0.313 m^3/kg COD·m^{-3}·h^{-1} at optimal feed pH of 7.5 (Fig. 4). With increase in feed pH value beyond 7.5, the concentrations as well as the yields of methane gas decrease sharply (Figs. 4 and 5). It is also observed that maximal COD removal from black liquor in the biomethanation process is 58.75% (w/w) at optimal feed pH of 7.5 (Fig. 5).

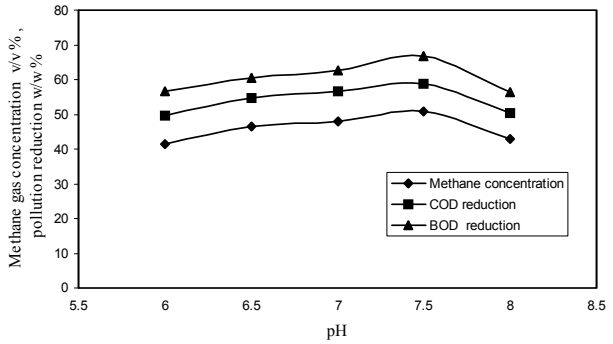

Fig. 5. Effect of feed pH.

Maximal BOD removal from wastewaters in the biomethanation process is 66.85 % (w/w) at optimal feed pH of 7.5 (Fig. 5). The removals of COD and BOD decrease after optimal feed pH (Fig. 5). Therefore, the initial feed pH of 7.5 is the optimum for maximum yield of methane gas and the removal of COD and BOD from black liquor in a three-phase fluidized-bed bioreactor and it is taken for further optimization of biomethanation parameter studies.

Variations in the pH of the feed result in changes in the activity of the mixed bacteria and hence the

bacterial growth as well as in the methane gas generation. Methagenic bacteria are very active over a certain pH range. When pH differs from the optimal value, the maintenance energy requirements increase [36−37] that leads to decrease in bacterial population and biogas yields.

Effect of feed temperature

The effect of feed temperature on the anaerobic biomethanation of black liquor in three-phase fluidized-bed bioreactor is shown in Figures.6 and 7 respectively. The feed temperature is in the mesophilic range. With increase in feed temperature, the yields and concentrations of methane gas increase up to temperature of 40ºC and then both decrease. It is noticed that maximal biogas yield from black liquor in fluidized-bed bioreactor is 0.686 m^3/kg COD·m^{-3}·h^{-1} at optimal feed temperature of 40ºC (Fig. 6). The maximum concentration of methane gas is 56.37% (v/v) at optimal feed temperature of 40ºC (Fig. 7). The maximal methane gas yield in fluidized-bed bioreactor is 0.386 m^3/kg COD m^{-3}·h^{-1} at optimal temperature of 40ºC (Fig. 6). It is also observed that maximal COD removal from the wastewaters is 67.82% (w/w) at optimal feed temperature of 40ºC (Fig. 7). Maximal BOD removal from the waste waters is 70.91% (w/w) at optimal feed temperature of 40ºC at optimal biomethanation process parameters (Fig. 7). With increase in feed temperature beyond 40ºC, the biogas and methane gas yields and the removal of COD and BOD from wastewaters decline as well (Figs.6 and 7). Therefore, feed temperature of 40ºC is the optimum for maximum yield of methane gas and removal of COD and BOD from black liquor in a three-phase fluidized-bed bioreactor and it is taken for further optimization of biomethanation process parameter studies.

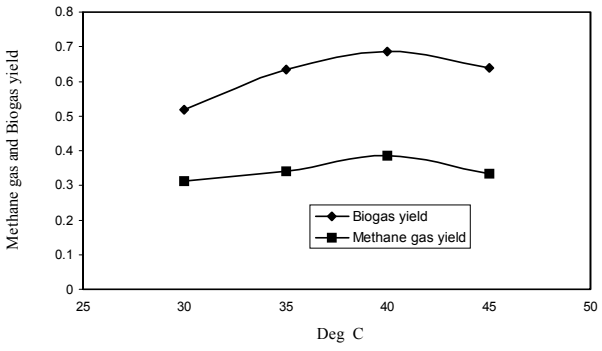

Fig. 6. Effect of feed temperature.

Every type of bacteria has an optimal, minimal and maximal growth temperature. Temperatures below the optimum for growth depress the rate of metabolism of bacterial cells. Above the optimal temperature, the growth rate decreases and thermal death may occur. At high temperature, death rate exceeds the growth rate [36−37], which causes a net decrease in the populations of viable bacterial cells with lowering of methane gas generation as well as COD and BOD removal.

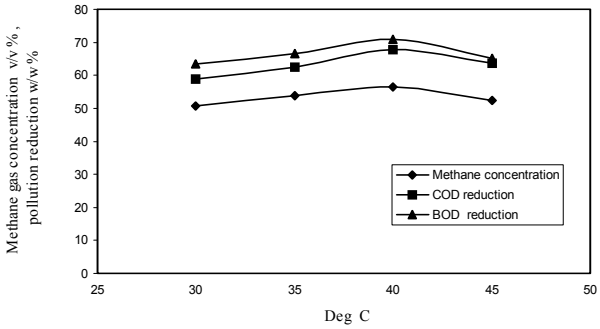

Fig. 7. Effect of feed temperature.

Effect of feed flow rate

The effect of feed flow rate (organic loading rate) on the anaerobic biomethanation of black liquor in three-phase fluidized-bed bioreactor is shown in Figures 8 and 9, respectively. The organic loading rates (OLR) are calculated on the basis of COD inlet in the bioreactor with different feed flow rates. With increase in feed flow rate, the yields and concentrations of methane gas increase up to 16 l/min and then both decrease. It is noticed that maximal biogas yield from wastewaters in anaerobic fluidized-bed bioreactor is 0.748 m^3/kg COD·m^{-3}·h^{-1} at optimal feed flow rate of 16 l/min (Fig. 8).

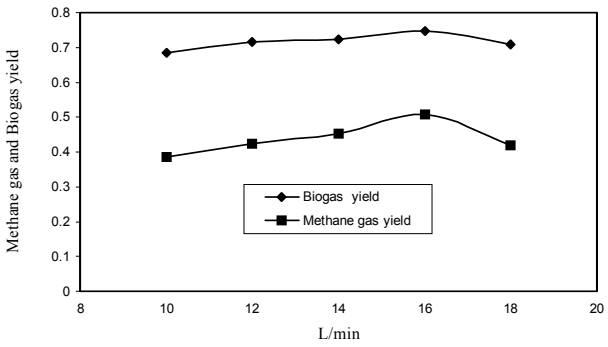

Fig. 8. Effect of feed flow rate.

The maximal concentration of methane gas is 64.82% (v/v) at optimal flow rate of 16 l/min respectively (Fig. 9). The maximal methane gas yield in anaerobic fluidized-bed bioreactor is 0.508 m^3/kg COD·m^{-3}·h^{-1} at optimal feed flow rate of 16 l/min (Fig. 8). With increase in feed flow rate as well as OLR beyond 16 l/min (the corresponding OLR is 45.158 g COD·m^{-3}·h^{-1}), the yield and concentration of methane gas decline (Fig. 9). It is also observed that the maximal COD removal from the

wastewaters is 79.65% (w/w) at optimal feed flow rate of 16 l/min (Fig. 9). It is noticed that maximal BOD removal from the wastewaters is 81.54% (w/w) at optimal feed flow rate of 16 l/min (Fig. 9). With increase in feed flow rate beyond 16 l/min, the methane gas yield and concentration and the removal of COD and BOD from wastewaters decrease as well (Figs. 8 and 9). Feed flow rate of 16 l/min is the optimum for maximal yield of methane gas and maximal bioremoval of COD and BOD from black liquor in the process of biomethanation in a three-phase fluidized-bed bioreactor.

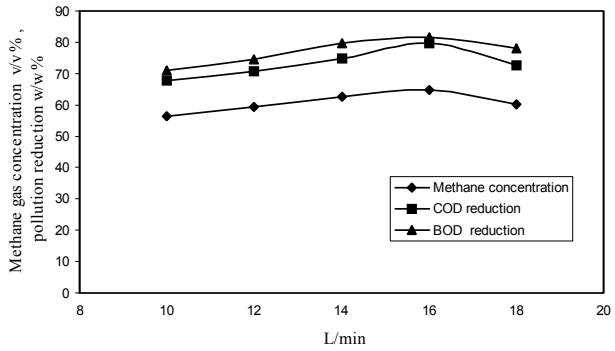

Fig. 9. Effect of feed flow rate.

In the three-phase fluidized-bed bioreactor, there exists a pressure drop between inlet and outlet of the feed. Increase in mechanical forces (increase in flow rates) can disturb the elaborate shape of enzyme molecule of the bacteria to such a degree that denaturation of the protein occurs and it deactivates the bacterial growth [36−37]. Therefore, the maximal yields of methane gas and removal of pollution load decrease with increase in feed flow rate beyond 16 l/min as well. The characteristic mechanical fragility of bacteria may impose limit on the fluid forces, which can be tolerated in fluidized-bed reactor. Since the surface tension of the interface between methane gas and water is high, it causes denaturation of proteins adsorbed at the methane-water interface [36−37]. In addition extensional flow, cavities, metal contamination and surface denaturation at cavities may influence bacterial growth [36−37] causing a decrease in population of viable bacterial cells as well as in methane yield and pollution load, respectively.

CONCLUSION

Generation of methane (CH_4) gas from black liquor in fluidized-bed bioreactor using activated sewage sludge mixed bacteria is an effective biomethanation process. The optimal HRT is 8 h and optimal initial pH of feed is found to be 7.5 respectively. The optimal flow rate of feed in fluidized-bed bioreactor is 16 l/min with organic loading rate (OLR) of 45.158 kg $COD \cdot m^{-3} \cdot h^{-1}$ respectively. Optimal temperature of feed is 40ºC. The maximal biogas yield rate is 0.748 $m^3/kg\ COD \cdot m^{-3} \cdot h^{-1}$ with CH_4 yield rate of 0.530 $m^3/kg\ COD \cdot m^{-3} \cdot h^{-1}$ respectively at optimal biomethanation parameters. The maximal concentration of methane (CH_4) gas is found as 64.82% (v/v) at optimal biomethanation parameters in the fluidized-bed bioreactor. The maximal COD and BOD removals from black liquor are 79.65% (w/w) and 81.54% (w/w) at optimal anaerobic bio-methanation parameters respectively.

REFERENCES

1. M. J. McInerney, M. P. Bryant, in: Fuel Gas Production from Biomass, vol. 1, D. L. Wise (ed.), C. R. C. Press, Boca Raton, FL, USA, 1981, p. 19.
2. M. J. McInerney, M. P. Bryant, in: Anaerobes and Anaerobic Infections, P. N. Gottschalk, S. Werner (eds.), Gustaro Fischer Verlag, Stuttgart West, Germany, 1980, p. 117.
3. J. Lamptey, M. Moo-Young, H. F. Sullivan, in: Bioenergy, A. V. Desai (ed.), Wiley Eastern Ltd., International Development Research Centre, Ottawa, United Nations University, Tokyo, Japan, 1990, p. 6.
4. N. L. Brown, P. B. S. Tata, in: Bioenergy, A. V. Desai (ed.), Wiley Eastern Ltd., International Development Research Centre, Ottawa, United Nations University, Tokyo, Japan, 1990, p. 67.
5. B. L. Vandan, K. J. Kennedy, in: Energy from Biomass and Waste VI, The Institute of Gas Technology, Chicago, IL, USA, 1982, p. 401.
6. D. I. Klass, in: Energy from Biomass and Waste VII, The Institute of Gas Technology, Chicago, IL, USA, 1983, p. 1.
7. J. Higgin, J. H. Krieger, *Chem. Eng. News*, **71**, 28 (1993).
8. M. Henze, P. Harremoes, *Water Sci. Technol.,* **28**, 1 (1996).
9. L. Lastella, C. Testa, G. Cornacchlia, M. Notornicola, F. Voltasio, V. K. Sharma, *Energy Conserv. Manag*., **43**, 63 (2002).
10. J. Biswas, R. Chowdhury, P. Bhattacharya, *Enzyme Microbial. Technol*., **38**, 493 (2006).
11. W. Chun-Sheng, H. Ju-Sheng, C. Hsin-Hsien, *Water Res*., **40**, 126 (2006).
12. L. H. Pol, G. Lettinga, *Water Sci. Technol*., **18**, 41 (1986).
13. L. Vandan Berg, K. J. Kennedy, *Water Sci. Technol.,* **15**, 359 (1982).
14. L. Neves, E. Goncalo, R. Oliveira, M. M. Alves, *Waste Manag*., **26**, 965 (2008).
15. A. Gangagni, A. N. Bapat, *Bioresource Technol.,* **97**, 2311 (2006).
16. A. Isci, L. Demirer, *Renewable Energy*, **32**, 750 (2007).
17. H. N. Chanakya, B. V. V. Reddy, J. Modak, *Renewable Energy*, **34**, 416 (2009).

18. M. Perez, R. Rodriguez-Cano, L. I. Romero, D. Sales, *Bioresource Technol.,* **98**, 3456 (2007).
19. B. K. Acharya, S. Mohana, M. Datta, *Biomass Bioenergy*, **31**, 247 (2007).
20. T. G. Jantsch, I. Angelidaki, J. E. Schmidt, B. E. Braña de Hvidsten, B. K. Ahring, *Chem. Eng. J*., **106**, 53 (2005).
21. G. Lettinga, A. F. M. Van Velsen, W. de Zeeuw, S. W. Hobma, *Biotechnol. Bioeng*., **22**, 699 (1980).
22. I. Zawiejn, L. Wolny, P. Wolski, *Desalination*, **222**, 186 (2008).
23. D. L. Manjunath, I. Mehrotra, R. P. Mathur, *IAWPC Tech. Annual*, **15**, 23 (1988).
24. H. Patel, D. Madamwar, *Process Biochem.,* **36**, 613 (2001).
25. M. Olthof, J. Oleszkiewicz, *Chem. Eng. J*., **89**, 121 (2005).
26. A. Gohil, G. Nakhia, *Bioresource Technol*., **97**, 2141 (2006).
27. A. P. Buzzini, E. C. Pires, *Bioresource Technol*., **98**, 1838 (2007).
28. J. Bjorklund, U. Geber, T. Rydberg, *Resource Conserv*., **99**, 293 (2008).
29. V. K. Verma, Y. P. Singh, J. P. N. Rai, *Bioresource Technol.,* **31**, 7941 (2001).
30. K. Nand, S. S. Devi, P. Viswanath, S. Deepak, R. Sarada, *Process Biochem.,* **26**, 1 (1991).
31. K. B. Cantrell, T. Ducey, K. S. Ro, P. G. Hunt, *Bioresource Technol*., **98**, 1664 (2007).
32. I. Ferrer, S. Poush, F. Vazquez, X. Font, *Biochem. Eng.,* **42**, 186 (2008).
33. R. K. Trivedy, P. K. Goel, Chemical and Biological Methods for Water Pollution Studies, Environmental Publications, Karad, India, 1986, p.125.
34. C. N. Sawyer, P. L. McCarty, G. F. Parkin, Chemistry for Environmental Engineering, 4th edn., McGraw-Hill, Inc., New York, U S A, 1994.
35. R. D. Braun, Introduction to Chemical Analysis, McGraw-Hill, Inc., Aucland, 1982, p. 410.
36. M. L. Shulter, F. Kargi, Bioprocess Engineering Basic Concept, Parentice-Hall of India Pvt Ltd., New Delhi, India, 2000.
37. M. J. Pclczar, E. C. S. Chan, N. R. Kring, Microbiology, 5th edn., Tata McGraw-Hill Publ. Co. Ltd., New Delhi, India, 2004.

БИОМЕТАНИЗАЦИЯ НА ЧЕРНА ЛУГА В БИОРЕАКТОР С ФЛУИДИЗИРАН СЛОЙ

Ск. М. Хосаин[1,]*, М. Дас[2]

[1] *Център за съвременни изследвания, Юнус Инженерен и технологичен колеж, Вадакевила, 691010 Колам, Индия*

[2] *Департамент по инженерна химия, Университет на Калкута, 92 А. П. С. шосе, 700009 Колката, Индия*

Постъпила на 14 ноември 2007 г.; Преработена на 17 април 2009 г.

(Резюме)

Извършени са опити по оптимизирането на параметрите за максимално продуциране на метан и намаляване на химическия потребен кислород (ХПК) и на биологически потребния кислород ($БПК_5$) на черна луга при биометанизацията в трифазен биореактор с флуидизиран слой. Оптималното времепребиваване (HRT) е 8 часа, а оптималната стойност на pH – 7.5. Оптималната температура на захранващия поток е 40°C, а оптималния му дебит – 16 L/min при натоварване с органична материя (OLR) съответно от 45.158 kg ХПК$\cdot m^{-3}\cdot h^{-1}$. Максималното съдържание на метан в биогаза е 64.82 об.% . Максималният дебит на добивания биогаз е 0.723 m^3/kg ХПК$\cdot m^{-3}\cdot h^{-1}$ с добив на метан от 0.530 m^3/kg COD$\cdot m^{-3}\cdot h^{-1}$ при оптималните определени параметри. Максималното понижение на ХПК и $БПК_5$ на използваната черна луга са съответно 79.65% (тегл.) и 81.54% (тегл.) при максимално натоварване с органична материя от 11.686 kg COD$\cdot m^{-3}\cdot h^{-1}$.

Bulgarian Chemical Communications, Volume 41, Number 4 (pp. 362–367) 2009

Novel routes to triazino[5,6-b]indole and indolo[2,3-b]quinoxaline derivatives

N. I. Abdel-Sayed

Chemistry Department, Faculty of Women for Arts, Sciences and Education, Ain Shams University, Heliopolis, P. O. Box 11757, Cairo, A.. R. Egypt

Received November 14, 2008; Revised April 14, 2009

The reaction of isatin with *o*-phenylenediamine afforded 6*H*-indolo[2,3-b]quinoxaline**.** While the reaction of isatin with semicarbazide hydrochloride afforded 2-(2-oxoindolin-3-ylidene)hydrazine carboxamide, which cyclizes to 2*H*-[1,2,4]triazino[5,6-b]indol-3(5*H*)-one. The 1,2,4-triazino[5,6-b]indolo derivatives were synthesized starting from the latter compound**.** 6*H*-Indolo[2,3-b]quinoxaline reacted with chloroacetone to afford 1-(6*H*-indolo[2,3-b]quinoxalin-6-yl)propan-2-one, which coupled readily with benzenediazonium chloride to yield the aryl hydrazone derivative from which, the indolo[2,3-b]quinoxalinyl thieno[3,4-d]pyridazine and the indolo[2,3-b]quinoxalinyl pyridazine derivatives could be prepared. The indolo[2,3-b]quinoxalinyl pyridine derivative was prepared from the enaminone 4-(N,N-dimethylamino)-3-(6*H*-indolo[2,3-b]quinoxalin-6-yl)-2-butanone. Chemical and spectroscopic evidences for the new compounds are described.

Key words: enaminone, isatin, indolo[2,3-b]quinoxaline, *o*-phenylenediamine, triazino[5,6-b]indole.

INTRODUCTION

Polynuclear condensed heterocyclic compounds or polynuclear compounds having another noncondensed heterocycle in their molecules are noted for the significant biological activity. Their cancerostatic and virostatic effects are based especially on intercalation into the double helix of DNA or inhibition of topoisomerase [1, 2]. Therefore, indole and quinoxaline derivatives display diverse pharmacological activities [3−5]. Quinoxaline derivatives have been synthesized by many research groups [4, 6−8]. In continuation of our work [9−11] the present study focuses on the synthesis of new indoloquinoxaline (**1**) and indolotriazine (**3**) derivatives. The results of the investigation on the reactivity of **1** and **3** towards nitrogen and carbon electrophiles are reported.

RESULTS AND DISCUSSION

The reaction of isatin with *o*-phenylenediamine in a solution of sodium bicarbonate afforded in good yield the indoloquinoxaline **1** (Scheme 1). The structure of the isolated product was confirmed on the basis of elemental analysis and spectral data.

However treatment of isatin with semicarbazide hydrochloride yielded the hydrazonocarboxamide derivative **2**, which cyclized to the triazino[5,6-b]indole **3** by boiling in acetic acid (Scheme 1).

The condensation of compound **3** with malononitrile in dimethylformamide (DMF) solution containing triethylamine yielded the triazinoindolyl malononitrile derivative **4**. The latter reacted with urea and/or thiourea in sodium ethoxide to afford the triazinoindolyl pyrimidine derivatives **5a**, **b** (Scheme 1).

Compound **6** could be easily prepared via reacting **1** with chloroacetone in refluxing toluene and in the presence of equivalent amount of triethylamine. The ^{1}H NMR spectrum of compound **6** displayed two singlets, one at δ = 2.15 ppm for the CH_3 protons of the acetyl group, and the second at δ = 4.70 ppm assigned for the methylene protons.

Coupling **6** with benzenediazonium chloride in ethanolic sodium acetate solution produces the corresponding aryl hydrazone **7** in good yield. Condensation of **7** with phenylhydrazine afforded diphenylhydrazone derivative **8** that has already been obtained by an alternative method, via coupling the phenylhydrazone derivative **10** with benzenediazonium chloride. Compound **10** could be prepared *via* condensing **6** with phenylhydrazine in refluxing acetic acid. Reaction of compound **6** with benzylidenemalononitrile yielded the addition product **9** (Scheme 1). Compound **7** condensed readily with malononitrile to yield the indolo[2,3-b]quinoxalinyl pyridazine derivative **13** (Scheme 2). Compound **13** reacted with sulphur in refluxing DMF in the presence of piperidine to yield the indolo[2,3-b]quinoxalinyl thieno pyridazine derivative **14.** Compound **7** also condensed with dimethylformamide dimethylacetal (DMFDMA) in refluxing toluene to afford the indolo[2,3-b]quinoxalinyl pyridazine

* E-mail: nadia_iskandar@yahoo.com

derivative **16** (Scheme 2).

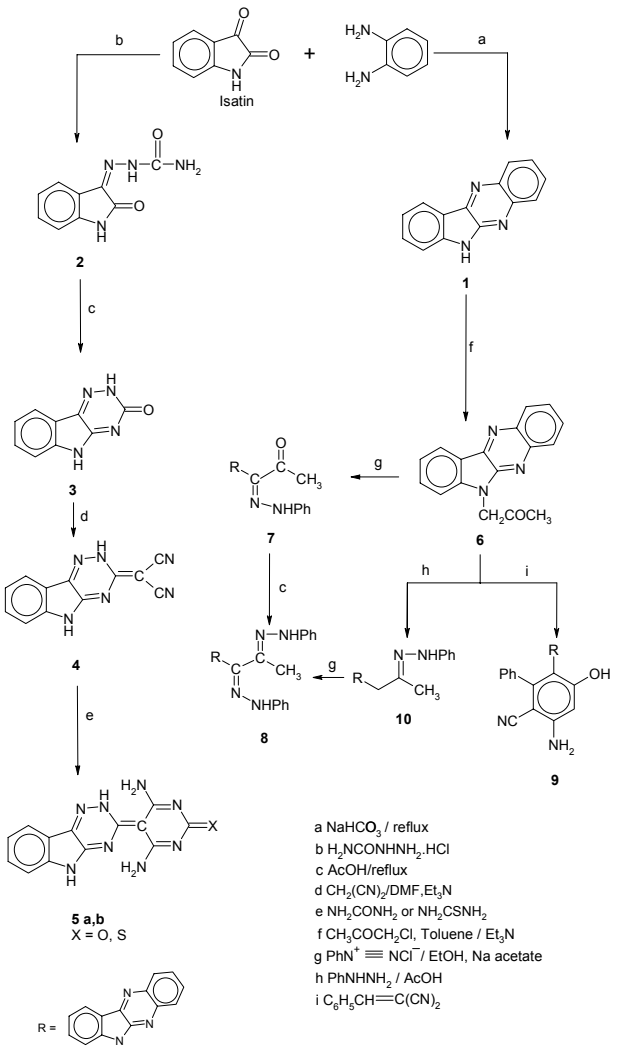

Scheme 1.

Treatment of **16** with malononitrile afforded the ylidenomalononitrile derivative **17**. Further on, the pyrimidine derivatives **18a**, **b** were obtained by refluxing **17** in sodium ethoxide with urea or thiourea respectively (Scheme 2).

Treatment of **6** with DMFDMA in dry xylene at reflux temperature afforded the enaminone **19** in a good yield (Scheme 3). The structure of the isolated product revealed a singlet at δ = 2.30 ppm indicating the presence of six protons of $N(CH_3)_2$.

The reaction of **19** with malononitrile in refluxing ethanol and in the presence of piperidine yielded a product that could be formulated as **23**. The formation of the latter is assumed to proceed via initial addition of the active methylene reagent across the double bond in **19** producing the intermediate Michael's adduct **20** that then cyclizes into **21,** which undergoes Dimroth's type of rearrangement and aromatizes *via* loss of a water molecule and dimethylamine to yield the final isolated product **23** (Scheme 3). The ^{1}H NMR spectrum of compound **23** showed a resonance at δ_H = 1.99 ppm corresponding to methyl protons and a signal at δ_H = 8.433 ppm assigned to pyridinyl 4-*H*. Alternatively, initial condensation of **19** with malononitrile could yield the initial condensation product **24** that is further hydrolysed into **25** and subsequently cyclizes to **26.** The product failed to react with sulphur to yield a condensed thiophene, as it is characteristic of azines with vicinal methyl and carbonitrile substituents [12], so structure **26** was ruled out and the product was assigned to be **23**. Compound **23** reacts with hydrazine hydrate in refluxing ethanolic solution to give the pyrazolo pyridyl indolo quinoxaline derivative **27** (Scheme 3).

EXPERIMENTAL

All melting points are uncorrected. The IR spectra (KBr) were recorded on a Pye Unicam SP-100 spectrophotometer. ^{1}H NMR spectra (DMSO-d_6, as a solvent) were obtained on a Varian Gemini 200 MHz spectrometer, using TMS as internal standard. Chemical shifts in δ (ppm) values; Mass spectra: AEI MS 30 mass spectrometer operating at 70 eV; microanalytical data were obtained from Microanalytical Data Unit at Cairo University.

6H-Indolo[2,3-b]quinoxaline (**1**). Isatin (1.71 g, 11.6 mmol) was dissolved in refluxing aqueous sodium bicarbonate solution (2.38 g, 28.3 mmol in 160 ml water). *o*-Phenylenediamine (1.44 g, 13.29 mmol) was added and the mixture was refluxed for 20 min. After cooling down to the room temperature the solution was acidified with acetic acid and left to stay overnight. The precipitate was filtered, washed with water and dried in air.

Yield 90%; yellow crystals from ethanol; m.p. 283°C; IR (KBr) ν (cm^{-1}): 1615 (C=N), 3448 (NH), 3065 (CH aromatic); ^{1}H NMR (DMSO-d_6) δ: 11.98 (s, 1H, NH), 7.31−8.33 (m, 8H, $2C_6H_4$); MS: m/z = 219 [M^+]; Anal. Calcd. for $C_{14}H_9N_3$: C, 76.69; H, 4.14; N, 19.16%. Found: C, 76.81; H, 4.03; N, 19.28%.

2-(2-Oxoindolin-3-ylidene)hydrazinecarboxamide (**2**). Isatin (0.74 g, 5 mmol) was dissolved in a refluxing solution of sodium bicarbonate (1.03 g, 12.3 mmol) in water (150 ml). Semicarbazide hydrochloride (0.70 g, 6.3 mmol) was added to this solution and the mixture was left to stay at room temperature for two days. The mixture was filtered and the filtrate was acidified with acetic acid. After two days, the precipitated solid was filtered, washed with water and dried.

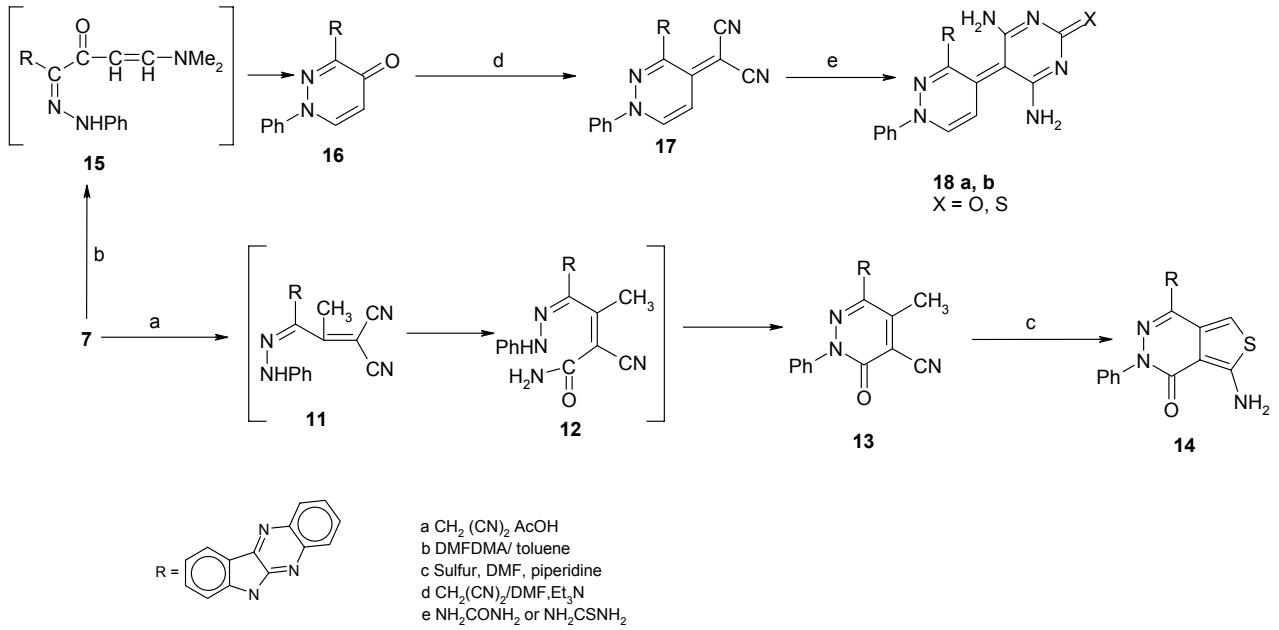

Scheme 2.

Yield 95%; yellow crystals from water; m.p. 262°C; IRS (KBr) ν (cm^{-1}): 1700, 1690 (C=O), 1612 (C=N), 3310, 3330, 3468 (NH, NH_2); ^{1}H NMR (DMSO-d_6) δ: 9.5 (br, 2H, NH_2), 10.58, 12.0 (2br s, 2H, 2NH), 6.91−7.59 (m, 4H, C_6H_4); MS: m/z = 204 [M^+]; Anal. Calcd. for $C_9H_8N_4O_2$: C, 52.94; H, 3.95; N, 27.44%. Found: C, 52.89, H, 3.99; N, 27.51%.

2H-[1,2,4]Triazino[5,6-b]indol-3(5H)-one (**3**). Compound **2** (1.22 g, 6 mmol) was refluxed in acetic acid (100 ml) for 2 h. After cooling, the solid was filtered, washed with water and dried.

Yield 93%; yellow crystals from acetic acid; m.p. 280°C; IRS (KBr) ν (cm^{-1}): 3336 (NH), 1698 (C=O), 1634 (C=N); ^{1}H NMR (DMSO-d_6) δ: 7.37−8.01 (m, 4H, C_6H_4), 11.79, 13.47 (2br s, 2H, 2NH); MS: m/z = 186 [M^+]; Anal. Calcd. for $C_9H_6N_4O$: C, 58.06; H, 3.25; N, 30.09%. Found: C, 58.11; H, 3.28; N, 30.28%.

General procedure for the synthesis of compounds (**4**) *and* (**17**)

To each solution of **3** (1.9 g, 10 mmol) or **16** (3.9 g, 10 mmol) in DMF (40 ml), containing triethylamine (1 ml), malononitrile (0.66 g, 1 mmol) was added. The reaction mixture was heated under reflux for 3 h. The solid product formed upon dilution with water, containing a few drops of HCl, was collected by filtration.

2-(2H-[1,2,4]Triazino[5,6-b]indol-3(5H)-ylidene) malononitrile (**4**). Yield 90%; yellow crystals from dioxane; m.p. 292°C; IRS (KBr) ν (cm^{-1}): 3330 (NH), 2220, 2225 (2CN), 1630 (C=C), 1650 (C=N), ^{1}H NMR (DMSO-d_6) δ: 7.21−7.55 (m, 4H, C_6H_4), 12.3, 13.0 (2br s, 2H, 2NH); MS: m/z = 234 [M^+]; Anal. Calcd. for $C_{12}H_6N_6$: C, 61.54; H, 2.58; N, 35.88%. Found: C, 61.46; H, 2.49; N, 35.98%.

1-Phenyl-3-(6H-indolo[2,3-b]quinoxalin-6-yl)-4-(ylidene-2-malononitrile)pyridazine (**17**). Yield 78% pale yellow crystals from dioxane; m.p. 320°C; IRS (KBr) ν (cm^{-1}): 2220, 2225 (2CN), 1620 (C=N), 1600 (C=C); ^{1}H NMR (DMSO-d_6) δ: 7.91, 6.80 (2d, 2H, pyridazinyl 6-H, 5-H), 7.30−7.88 (m, 13H, $2C_6H_4$, C_6H_5); MS: m/z = 437 [M^+]; Anal. Calcd. for $C_{27}H_{15}N_7$: C, 74.13; H, 3.46; N, 22.41%. Found: C, 73.18; H, 3.44; N, 22.58%.

General procedure for the synthesis of compounds (**5a**, **b**) *and* (**18a**, **b**)

Urea (0.6 g, 10 mmol) or thiourea (0.8 g, 10 mmol) was added to each solution of **4** (2.3 g, 10 mmol) or **17** (4.4 g, 10 mmol) in sodium ethoxide (10 mmol) [prepared by adding sodium metal (0.23 g, 10 mmol) to absolute ethanol (40 ml)] and the mixture was heated under reflux on a steam bath for 4−6 h. The solid product formed upon pouring onto ice water containing a few drops of HCl (until pH 6) was collected by filtration.

5-(2H-[1,2,4]Triazino[5,6-b]indolo-3(5H)-ylidene)-4,6-diaminopyrimidine-2-one (**5a**). Yield 85%; orange crystals from dioxane; m.p. > 360°C; IRS (KBr) ν (cm^{-1}): 3430, 3330, 3310 (NH, NH_2), 1650 (C=N), 1630 (C=C), 1690 (CO); ^{1}H NMR (DMSO-d_6) δ: 7.24−7.50 (m, 4H, C_6H_4), 12.3, 13.0 (2br s, 2H, 2NH), 2.5, 3.4 (2s, 4H, $2NH_2$), MS: m/z = 294 [M^+]; Anal. Calcd. for $C_{13}H_{10}N_8O$: C, 53.06; H, 3.42; N, 38.0%. Found: C, 53.10; H, 3.40; N, 38.25%.

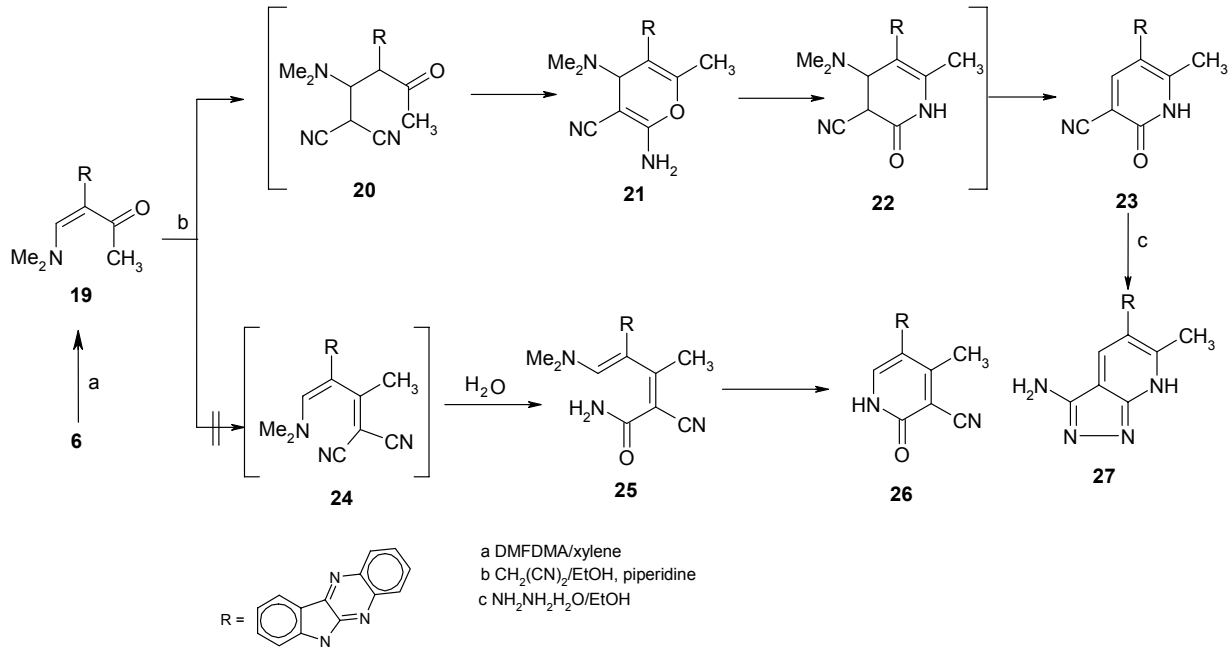

Scheme 3.

5-(2H-[1,2,4]Triazino[5,6-b]indolo-3(5H)-ylidene)-4,6-diaminopyrimidine-2-thione (**5b**). Yield 85%; yellow solid from DMF; m.p. > 360°C; IRS (KBr) ν (cm^{-1}): 1200 (C=S), 3440, 3330, 3310 (NH, NH_2), 1650 (C=N), 1630 (C=C); ^{1}H NMR (DMSO-d_6) δ: 7.23−7.45 (m, 4H, C_6H_4), 12.3, 13.0 (2br s, 2H, 2NH), 2.45, 3.38 (2s, 4H, $2NH_2$); MS: m/z = 310 [M^+]; Anal. Calcd. for $C_{13}H_{10}N_8S$: C, 50.31; H, 3.25; N, 36.11; S, 10.33%. Found: C, 50.33; H, 3.30; N, 36.28; S, 10.38%.

5-[3-(6H-Indolo[2,3-b]quinoxalin-6-yl)-4-ylidene-1-phenylpyridazine]-4,6-diaminopyrimidine-2-one (**18a**). Yield 68%; yellow crystals from ethanol/dioxane; m.p. > 360°C; IRS (KBr) ν (cm^{-1}): 1690 (CO), 3430, 3310 (NH_2), 1650 (C=N), 1635 (C=C); ^{1}H NMR (DMSO-d_6) δ: 7.91, 6.8 (2d, 2H, pyridazinyl 6-H, 5-H), 2.45, 3.38 (2s, 4H, $2NH_2$), 7.31–7.89 (m, 13H, C_6H_5, $2C_6H_4$); MS: m/z = 497 [M^+]; Anal. Calcd. for $C_{28}H_{19}N_9O$: C, 67.59; H, 3.85; N, 25.34%. Found: C, 67.68; H, 3.84; N, 25.38%.

5-[3-(6H-Indolo[2,3-b]quinoxalin-6-yl)-4-ylidene-1-phenylpyridazine]-4,6-diaminopyrimidine-2-thione (**18b**). Yield 65%; pale yellow solid from ethanol/dioxane; m.p. > 360°C; IRS (KBr) ν (cm^{-1}): 1200 (C=S), 3430, 3310 (NH_2), 1650 (C=N), 1635 (C=C); ^{1}H NMR (DMSO-d_6) δ: 7.92, 6.8 (2d, 2H, pyridazinyl 6-H, 5-H), 2.40, 3.39 (2s, 4H, $2NH_2$), 7.32−7.86 (m, 13H, C_6H_5, $2C_6H_4$); MS: m/z = 513 [M^+]; Anal. Calcd. for $C_{28}H_{19}N_9S$: C, 65.48; H, 3.73; N, 24.55; S, 6.24%. Found: C, 65.51; H, 3.75; N, 24.61; S, 6.28%.

1-(6H-Indolo[2,3-b}quinoxalin-6-yl]propan-2-one (**6**). A solution of **1** (2.2 g, 10 mmol) in dry toluene (30 ml) was treated with chloroacetone (0.93 g, 10 mmol) in the presence of triethylamine (1 ml). The reaction mixture was refluxed for 7 h. The solvent was evaporated under vacuum and the solid product, so formed, was collected by filtration.

Yield 85%; pale yellow crystals from benzene; m.p. 295°C; IRS (KBr) ν (cm^{-1}): 2960, 2840 (CH_3, CH_2), 1680 (CO); ^{1}H NMR (DMSO-d_6) δ: 2.15 (s, 3H, CH_3), 4.70 (s, 2H, CH_2), 7.4−8.35 (m, 8H, $2C_6H_4$); MS: m/z = 275 [M^+]; Anal. Calcd. for $C_{17}H_{13}N_3O$: C, 74.17; H, 4.76; N, 15.26%. Found: C, 74.20; H, 4.77; N, 15.47%.

1-(6H-Indolo[2,3-b]quinoxalin-6-yl)-1-(2-phenylhydrazono)propan-2-one (**7**). A cold solution of benzenediazonium chloride (10 mmol) [prepared by the addition of sodium nitrite (0.7 g in 5 ml water) to a cold solution (0.5°C) of aniline (0.93 g, 10 mmol) containing the appropriate amount of hydrochloric acid], was added to a solution of **6** (2.75 g, 10 mmol) in ethanol (50 ml) containing sodium acetate (3 g). The reaction mixture was stirred at room temperature for 2 h, and left to stay overnight in the refrigerator. The solid product, so formed, was collected by filtration.

Yield 83%; orange crystals from ethanol; m.p. 330°C; IRS (KBr) ν (cm^{-1}): 3215 (NH), 1680 (CO); ^{1}H NMR (DMSO-d_6) δ: 2.19 (s, 3H, $COCH_3$), 7.3−7.80 (m, 13 H, C_6H_5, 2 C_6H_4), 9.80 (s 1H, NH); MS: m/z = 379 [M^+]; Anal. Calcd. for $C_{23}H_{17}N_5O$: C, 72.81; H, 4.52; N, 18.46%. Found: C, 72.80; H, 4.55; N, 18.77%.

6-[1,2-Bis(2-phenylhydazono)propyl]-6H-indolo-[2,3-b]quinoxaline (**8**). *Method (A).* A mixture of compound **7** (0.38 g, 1 mmol) and phenylhydrazine

(0.11 g, 1 mmol) and acetic acid (1 ml) was heated at 120°C for 10 min. The reaction mixture was triturated with ethanol, the solid product, so formed, was collected by filtration.

Method (B). The same experimental procedure as it is described for the synthesis of compound **7** was adopted using **10** instead of compound **6**.

Yield 78%; dark red crystals from ethanol; m.p. 320°C; IRS (KBr) ν (cm^{-1}): 3430 (NH), 2980, 2850 (CH_3); ^1H NMR (DMSO-d_6) δ: 2.65 (s, 3H, CH_3), 7.2−8.25 (m, 18H, $2C_6H_5$, $2C_6H_4$), 8.12, 8.15 (2br s, 2H, 2NH); MS: m/z = 469 [M^+]; Anal. Calcd. for $C_{29}H_{23}N_7$: C, 74.18; H, 4.94; N, 20.88%. Found: C, 74.30; H, 4.92; N, 21.22%.

3-Amino-5-hydroxy-6-(6H-indolo[2,3-b]quinoxalin-6-yl)biphenyl-2-carbonitrile (**9**). Benzylidene malononitrile (1.5 g, 10 mmol) was added to a solution of **6** (2.8 g, 10 mmol) in dioxane (30 ml) in the presence of few drops of piperidine. The reaction mixture was heated under reflux for 6 h. The amount of solvent was reduced under vacuum, the mixture was diluted with water and acidified with dilute hydrochloric acid. The solid product obtained was collected by filtration.

Yield 70%; brown solid from ethanol; m.p. 325°C; IRS (KBr) ν (cm^{-1}): 3400 (OH), 3420, 3330 (NH_2), 2210 (CN); ^1H NMR (DMSO-d_6) δ: 8.72 (br s, 2H, NH_2), 9.68 (s, 1H, OH), 7.3−8.10 (m, 14H, $2C_6H_4$, C_6H_5, C_6H); MS: m/z = 427 [M^+]; Anal. Calcd. for $C_{27}H_{17}N_5O$: C, 75.86; H, 4.01; N, 16.38%. Found: C, 75.84; H, 4.10; N, 16.59%.

1-(6H-Indolo[2,3-b]quinoxalin-6-yl)-2-phenylhydrazonopropane (**10**). The same experimental procedure as it was described for the synthesis of **8** (Method A) was adopted using compound **6** instead of **7**.

Yield 92%; orange crystals from ethyl alcohol; m.p. 315°C; IRS (KBr) ν (cm^{-1}): 3240 (NH); ^1H NMR (DMSO-d_6) δ: 2.62 (s, 3H, CH_3), 4.45 (s, 2H, CH_2), 7.33−8.10 (m, 13H, C_6H_5, $2C_6H_4$), 8.20 (br s, 1H, NH); MS: m/z = 365 [M^+]; Anal. Calcd. for $C_{23}H_{19}N_5$: C, 75.59; H, 5.24; N, 19.16%. Found: C, 75.56; H, 5.25; N, 19.68%.

5-Cyano-3-(6H-indolo[2,3-b]quinoxalin-6-yl)-4-methyl-6-oxo-1-phenylpyridazine (**13**). Malononitrile (0.66 g, 10 mmol) was added to compound **7** (3.79 g, 10 mmol) in the presence of acetic acid (1 ml) and anhydrous ammonium acetate (1 g). The reaction mixture was heated at 120°C for 15 min, then triturated with ethanol. The solid product, so formed, was collected by filtration.

Yield 85%; dark yellow solid from ethanol; m.p. 345°C; IRS (KBr) ν (cm^{-1}): 2230 (CN), 1680 (CO); ^1H NMR (DMSO-d_6) δ: 2.5 (s, 3H, CH_3), 7.5−8.4 (m, 13 H, C_6H_5, $2C_6H_4$); MS: m/z = 428 [M^+]; Anal. Calcd. for $C_{26}H_{16}N_6O$: C, 72.89; H, 3.76; N, 19.61%. Found: C, 72.92; H, 3.80; N, 19.95%.

4-Amino-7-(6H-indolo[2,3-b]quinoxalin-6-yl)-3-oxo-2-phenylthieno[3,4-d]pyridazine (**14**). Elemental sulphur (0.32 g, 10 mmol) was added to a solution of compound 13 (4.28 g, 10 mmol) in DMF (30 ml) in the presence of piperidine (0.5 ml). The reaction mixture was heated for 6 h. The solvent was reduced to half of its volume, poured onto water and neutralized with HCl, the solid product, so formed, was collected by filtration.

Yield 73%; yellow crystals from ethanol; m.p. > 360°C; IRS (KBr) ν (cm^{-1}): 3420, 3310 (NH_2), 1685 (CO); ^1H NMR (DMSO-d_6) δ: 5.75 (s, 1H, thienyl 5-H), 7.03−8.20 (m, 15 H, $2C_6H_4$, C_6H_5, NH_2); MS: m/z = 460 [M^+]; Anal. Calcd. for $C_{26}H_{16}N_6SO$: C, 67.81; H, 3.50; N, 18.25; S, 6.96%. Found: C, 67.67; H, 3.55; N, 18.58; S, 7.15%.

3-(6H-Indolo[2,3-b]quinoxalin-6-yl)-4-oxo-1-phenylpyridazine (**16**). A mixture of compound **7** (4.5 g, 12 mmol) and DMFDMA (1.19 g, 10 mmol) in toluene (30 ml) was heated for 18 h. The solvent was evaporated under vacuum and the solid product, so formed, was collected by filtration.

Yield 80%; pale yellow crystals from ethanol; m.p. 340°C; IRS (KBr) ν (cm^{-1}): 1700 (CO); ^1H NMR (DMSO-d_6) δ: 7.10−8.30 (m, 13H, $2C_6H_4$, C_6H_5), 6.98, 9.09 (2d, 2H, pyridazine 5-H, 6-H); MS: m/z = 389 [M^+]; Anal. Calcd. for $C_{24}H_{15}N_5O$: C, 74.02; H, 3.88; N, 17.98%. Found: C, 74.13; H, 3.86; N, 18.30%.

4-(N,N-Dimethylamino)-3-(6H-indolo[2,3-b]quinoxalin-6-yl)-2-butanone (**19**). A mixture of **6** (2.8 g, 10 mmol) and DMFDMA (1.4 g, 12 mmol) in xylene (30 ml) was refluxed for 14 h. The reaction mixture was evaporated in vacuum to afford the enaminone **19**.

Yield 92%; yellow crystals from dioxane; m.p. 300°C; IRS (KBr) ν (cm^{-1}): 1690 (CO), 1600 (C=C, olefinic); ^1H NMR (DMSO – d_6) δ: 6.0 (s, 1H, CH), 2.30 (s, 6H, NMe_2), 2.15 (s, 3H, CH_3), 7.31−8.0 (m, 8H, $2C_6H_4$); MS: m/z = 330 [M^+]; Anal. Calcd. for $C_{20}H_{18}N_4O$: C, 72.71; H, 5.49; N, 16.96%. Found: C, 72.75; H, 5.52; N, 17.41%.

3-Cyano-5-(6H-indolo[2,3-b]quinoxalin-6-yl)-6-methyl-2-oxo-1H-pyridine (**23**). A mixture of compound 19 (3.3 g, 10 mmol) and malononitrile (0.66 g, 10 mmol) in absolute ethanol (50 ml) and a few drops of piperidine was stirred for 1 h. The solvent was evaporated under reduced pressure. The solid product, so formed, was collected by filtration.

Yield 90%; dark yellow solid from dimethyl formamide/ethanol; m.p. 317°C; IRS (KBr) ν (cm^{-1}): 3400 (NH), 2220 (CN), 1660 (CO); ^1H NMR (DMSO-d_6) δ: 1.99 (s, 3H, CH_3), 8.43 (s, 1H,

pyridinyl 4-H), 7.3−8.0 (m, 8H, $2C_6H_4$), 13.20 (br, 1H, NH), MS: m/z = 351 [M^+]; Anal. Calcd. for $C_{21}H_{13}N_5O$: C, 71.78; H, 3.73; N, 19.93%. Found: C, 71.75; H, 3.74; N, 20.01%.

7-Amino-3H-5-(6H-indolo[2,3-b]quinoxalin-6-yl)-4-methylpyrazolo[3,4-b]pyridine (**27**). Hydrazine hydrate (0.5 g, 10 mmol) was added to a solution of **23** (3.5 g, 10 mmol) in ethanol (40 ml). The reaction mixture was heated under reflux for 8 h, then evaporated in vacuum. The remaining product was triturated with diethyl ether then collected by filtration.

Yield 80%; yellow crystals from dioxane; m.p. > 360°C; IRS (KBr) ν (cm^{-1}): 1620 (C=N), 3440, 3310 (NH, NH_2), 1600 (C=C); ^{1}H NMR (DMSO-d_6) δ: 7.31−8.35 (m, 10H, $2C_6H_4$, NH_2), 2.56 (s, 3H, CH_3), 11.23 (br s, 1H, NH), 6.88 (s, 1H, pyridyl 4-H); MS: m/z = 365 [M^+]; Anal. Calcd. for $C_{21}H_{15}N_7$: C, 69.04; H, 4.14; N,26.83%. Found: C, 69.06; H, 4.17; N, 27.13%.

REFERENCES

1. B. C. Baguley, *Anti-Cancer Drug Des.*, **6**, 1 (1991).
2. M. Binaschi, F. Zunino, G. Capranico, *Stem Cells,* **13**, 369 (1995).
3. G. Olayiwola, C. A. Obafemi, F. O. Taiwo, *African J. Biotechn.,* **6**, 777 (2007).
4. H. M. Refaat, A. A. Moneer, O. M. Khalil, *Arch. Pharmacol. Res.,* **27,** 1093 (2004).
5. U. J. Ries, H. W. Priekpe, N. H. Havel, S. Handschuh, G. Mihm, J. M. Stassen, W. Nienen, H. Nar, *Bioorg. Med. Chem. Lett.,* **13,** 2297 (2003).
6. J. Ohmori, S. Sakamoto, H. Kupota, M. Shimizu-Sasamata, M. Okada, S. Kawasaki, K. Hidaka, J. Togami, T. Furuya, K. Murase, *J. Med. Chem.,* **37,** 467 (1994).
7. J. Saloň, V. Milata, N. Prónáyová, J. Leško, *Collect. Czech. Chem. Commun.,* **66,** 1691 (2001).
8. J. Saloň, V. Milata, M. Chudik, N. Prónayová, J. Leško, M. Seman, A. Belicová, *Monatsh. Chem.,* **135,** 283 (2004).
9. R. M. Mohareb, N. I. Abdel-Sayed, S. M. Sherif, *Phosphorus, Sulfur Silicon,* **63,** 119 (1991).
10. R. M. Mohareb, Y. M. Elkholy, N. I. Abdel-Sayed, *Phosphorus, Sulfur Silicon,* **106,** 193 (1995).
11. S. M. Sherif, N. I. Abdel-Sayed, S. M. El-Kousy, R. M. Mohareb, *Monatsh. Chem.,* **126,** 601 (1995).
12. F. Al-Omran, M. M. Abdel-Khalik, H. Al-Awadi, M. H. Elnagdi, *Tetrahedron*, **52,** 11915 (1996).

НОВИ ПРОЦЕДУРИ ЗА СИНТЕЗ НА ТРИАЗИНО[5,6-b]ИНДОЛ И ИНДОЛО[2,3-b]ХИНОКСАЛИНОВИ ПРОИЗВОДНИ

Н. И. Абдел-Сайед

Химически департамент, Девически факултет по изкуства, науки и образование, Университет Аин Шамс, Хелиополис, ПК 11757, Кайро, А. Р. Египет

Постъпила на 14 ноември 2008 г.; Преработена на 14 април 2009 г.

(Резюме)

При реакцията на изатин с *о*-фенилендиамин е получен 6*H*-индоло[2,3-b]хиноксалин. При реакцията на изатин със семикарбазид хидрохлорид е получен 2-(2-оксоиндолин-3-илиден)хидразин карбоксамид, който циклизира до 2*H*-[1,2,4]триазино[5,6-b]индол-3(5*H*)-он. От последното съединение са синтезирани 1,2,4-триазино[5,6-b]индоло производни. 6*H*-Индоло[2,3-b]хиноксалин при реакция с хлороацетон дава 1-(6*H*-индоло[2,3-b]хиноксалин-6-ил)пропан-2-он, който лесно се сдвоява с бензендиазониев хлорид до арилхидразоново производно, от което се получават индоло[2,3-b]хиноксалинилтиено[3,4-d]пиридазин и индоло[2,3-b]хиноксалинилпиридазинови производни. Производни на индоло[2,3-b]хиноксалинилпиридин са синтезирани от 4-(N,N-диметиламино)-3-(6*H*-индоло[2,3-b]хиноксалин-6-ил)-2-бутанон. Представени са химични и спектрални доказателства за новите съединения.

Bulgarian Chemical Communications, Volume 41, Number 4 (pp. 368–373) 2009

Toxicity of some solvents and extractants towards *Lactobacillus casei* cells

N. A. Marinova, D. S. Yankov*

Institute of Chemical Engineering, Bulgarian Academy of Sciences,
Acad. G. Bonchev St., Block 103, 1113 Sofia, Bulgaria

Received October 30, 2008; Revised April 23, 2009

Various organic compounds used as diluents, modifiers and extractants in lactic acid extraction have been tested to determine their toxicity towards *Lactobacillus casei* cells. The toxicity on molecular and phase level has been investigated. In general, the tested hydrocarbons were non-toxic on molecular level and showed variable toxicity on phase level. Among the tested alcohols octanol and oleyl alcohol were non-toxic, whereas decanol and dodecanol were toxic on the molecular level. All the alcohols showed high phase toxicity. The tested extractants were very toxic both on molecular (except for tridodecylamine) and on phase level. Two extraction systems composed of trioctylamine/oleyl alcohol and tridodecylamine/oleyl alcohol have also been studied. Both systems were non-toxic on molecular level and showed medium toxicity on phase level. They can be used successfully for *in situ* extractive fermentation of lactic acid.

Key words: solvent toxicity, *in-situ* extraction, lactic acid, *Lactobacillus casei.*

INTRODUCTION

The product separation or *in situ* product removal is the limiting stage in the manufacturing of various organic compounds, produced via microbial transformations, because of low concentration and water solubility of the product. The product recovery step is very expensive and energy consuming. The fermentative lactic acid production is a typical example of an end-product inhibited process. Besides, the rate decreasing due to inhibition, accumulation of the acid leads to decrease in pH value of the system, often out of the optimum range for fermentation. In case of such fermentations processes where the continuous removal of the product is obligatory, successful organization of the process is very complicated. Different approaches, such as solvent extraction [1, 2], electro-dialysis [3, 4], membrane separation [5, 6], ion-exchange [7, 8] or aqueous two-phase systems [9] have been used for overcoming the arising problems. Each one of above mentioned methods possesses its own advantages and draw-backs.

Solvent extraction, especially extraction with long-chain tertiary aliphatic amines, has been recognized as a promising alternative to conventional calcium-salt precipitation method for separation and purification of the lactic acid. The major problem in this case is the toxicity of the commonly used organic solvents. The mechanism of toxicity caused by the organic solvents is still not clear, but it is generally accepted that the interaction of the solvents with membrane lipids leads to disturbance of essential membrane functions, inactivation or denaturation of membrane-bound enzymes, breakdown of transport mechanisms and at high concentrations to solvolysis of the cells [10–12]. The solvents interact with the cells by two routes: direct contact of the cells with the water immiscible organic phase and by solvent molecules dissolved in fermentation broth. The former mechanism is named "phase" toxicity and the latter – "molecular" toxicity.

Chen and Lee [5] have investigated the toxicity of three diluents, three modifiers and 5 solvent mixtures towards *Lactobacillus delbrueckii* strain. They have concluded that kerosene and oleyl alcohol are nontoxic and have chosen the system composed of 20% Alamine 336, 40% kerosene and 40% oleyl alcohol for *in situ* extraction of lactic acid.

Seevaratnam *et al*. [13] have reported that Aliquat 336, Amberlite LA-2, Adogen 464 and trioctyl amine (TOA) are highly toxic towards *Lactobacillus delbrueckii* cells even at 0.1% concentration. What is more, Aliquat 336 and Adogen 464 formed third phase during extraction, when dissolved in paraffin oil in order to improve their physical properties.

Tong *et al*. [14] have studied 10 extractants and solvents in regard to their toxicity to *Lactobacillus rhamnosus* cells and have used a mixture of TOMAC (trioctylmethylammoniumchloride, 0.2 kmol/m^3) in oleyl alcohol, in spite of the high toxicity of TOMAC.

* To whom all correspondence should be sent:
E-mail: yanpe@bas.bg

Demirci *et al*. [15] have made a screening of 12 solvents and 8 carrier compounds in different combinations, with respect to their toxicity on *Lactobacillus casei* strain. Hexadecane:tributyl phosphate, *n*-dodecane:tri-*n*-octylamine, and kerosene:tri-*n*-octylphosphine oxide demonstrated the least microbial toxicity among the tested blends with excess solvent media. Whereas hexanes:Alamine 304 and xylenes: Alamine 304 were non-toxic in solvent saturated media.

Choudhury *at al*. [16] have also investigated the toxicity of TOA in three different solvents (methyl-isobutyl ketone (MIBK), octanol, paraffin) on *Lactobacillus delbrueckii* strain. While TOA was found to be highly toxic on the molecular and on the phase level, the paraffin liquid was totally non-toxic.

The data presented in the literature varied and they are often contradictory. It seems that the toxicity of organic solvents and extractants is closely related to the type of used microorganism.

The aim of the present study was to investigate the solvent toxicity towards *Lactobacillus casei* strain of various organic solvents and extractants, frequently used for extraction of lactic acid from fermentation broth.

EXPERIMENTAL

Materials and Methods

Extractants. Tributylphosphate (TBP) − Merck; Tridodecylamine (TdDA) – Fluka; Dioctylamine (DOA) − Fluka; Tri-*n*-octylamine (TOA) – Acros Organics; Alamine 336 (a mixture of tri-*n*-octylamine and tri-*n*-decylamine) – Henkel and Aliquat 336 (tri(C_8C_{10})methylammonium chloride) − Acros Organics.

Modifiers. 1-Octanol − Fluka; 1-decanol − Merck; 1-dodecanol − Merck; oleyl alcohol − Acros Organics.

Diluents. n-Octane – Fluka; *n*-Decane – Merck; Dodecane – Prolabo; kerosene – technical grade, distillation fraction from 175−190°C with $\rho^{20} \sim 0.778$ kg/dm^3.

All chemicals, except for kerosene, were p.a. purity grade. Kerosene was distillated from a technical grade, taking the 198−212°C fraction. Before further use, the organic chemicals were washed threefold with distilled water under vigorous mixing for 10 min in order to eliminate any water-soluble impurities. At the same time, the organic chemicals were saturated with water.

Microorganism. *Lactobacillus casei* strain (NBMCC-1013) was used in the present study.

Media. The strain was maintained on a semi-synthetic medium containing (g/l): yeast extract 10; peptone 10; sodium acetate 5; $MgSO_4.7H_2O$ 0.1; $MnSO_4.4H_2O$ 0.05; agar 20; distilled water to 1l.

The culture was inoculated into semi-synthetic medium containing (g/l): yeast extract 5.5; peptone 12.5; KH_2PO_4 0.25; K_2HPO_4 0.25; sodium acetate 10.0; $MgSO_4.7H_2O$ 0.1; $MnSO_4.4H_2O$ 0.05; $FeSO_4.7H_2O$ 0.05; distilled water to 1l. The pH value was adjusted to 6.8. The culture media were sterilized at 121°C for 20 min. The bacterial cells were transferred from agar slants into the medium and were incubated for 24 h at 38°C in a rotatory shaker New Brunswick Scientific Co., Ink., Edison, NY, USA, (100−120 rpm). In a conventional fermentation process, 10 ml of the inoculum were added to 100 ml of the culture medium. The fermentation was carried out in flasks without any pH correction for 48 h.

Molecular level toxicity experiments. Ten millilitres of washed chemicals were mixed with 100 ml of distilled water and were shaken for 15 min in a shacking machine. After phase separation, the solvent saturated water was used for culture medium preparation. After fermentation without any pH control, samples were taken at 24 h and 48 h intervals and were analyzed for produced lactic acid and bacterial growth. The results were compared with those of control sample, where the medium was prepared with distilled water.

Phase level toxicity experiments. For these experiments water saturated organic solvents were sterilized and 25 ml of each one of them were added to 100 ml of culture media. The fermentation process was carried out as it was described above and the results were compared to the control sample.

Analysis

Counting of microbial cells. After appropriate dilution of the sample the number of the cells in one ml was counted with the help of a Bürker camera.

Lactic acid analyses. An HPLC system composed of Perkin-Elmer Series 10 Pump, LC-25RI detector, Shimadzu C-R6A Chromatopac integrator and Aminex HPX-87H column was used. The mobile phase was 0.01 N H_2SO_4 at 0.6 ml/min flow rate. Pure (98%) crystalline L-(+)-lactic acid (Sigma) was used as the standard.

RESULTS AND DISCUSSION

In order to divide the used organic compounds into groups according to their toxicity, the classification proposed by Martak *et al*. [17] was used:

- *Non-toxic solvents* when practically no toxic effect was observed and the production rate was at most 25% lower than in the control cultivation sample.

- *Solvents with medium toxicity* when the production rate was higher than 25% of that in control cultivation sample.

- *Toxic solvents*, when no biological activity was observed in their presence or the production rate was less than 25% of that in control cultivation sample.

Molecular level toxicity

Diluents. All the investigated hydrocarbons are non-toxic on molecular level. Both culture growth and lactic acid production are at least 80% of the control sample at 24 h and 48 h of fermentation. The results are represented in Figure 1.

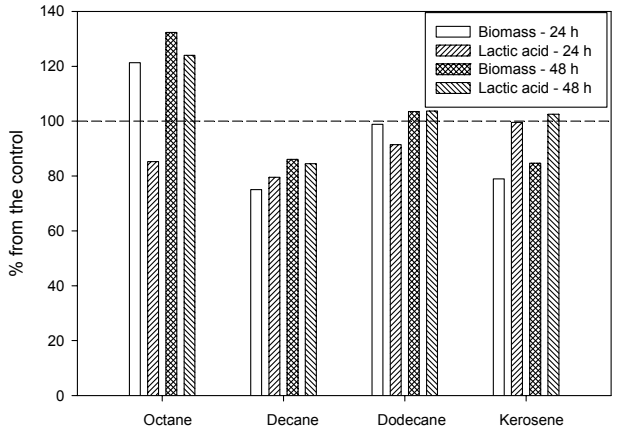

Fig. 1. Influence of some diluents on the cell growth and lactic acid production of *Lactobacillus casei* - molecular level.

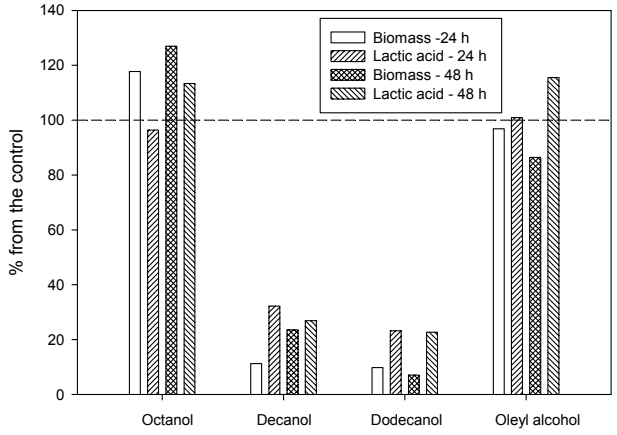

Fig. 2. Influence of some modifiers on the cell growth and lactic acid production of *Lactobacillus casei* - molecular level.

Dodecane and kerosene had the same behavior at two points of comparison, whereas the production of lactic acid in case of octane increased at 48 h and decreased in the presence of decane.

Modifiers. The toxicity of the investigated alcohols differs considerably. The octanol and oleyl alcohol are non-toxic and their results are close to the control sample ones. The bacterial growth (11% and 10% at 24 h; 24% and 23% at 48 h) and the lactic acid production (32% and 23% at 24 h and 23% and 7% at 48 h) for decanol and dodecanol were very low. The results obtained are shown in Figure 2.

Extractants. Among all extractants used, only tridodecylamine is not-toxic on molecular level (Fig. 3).

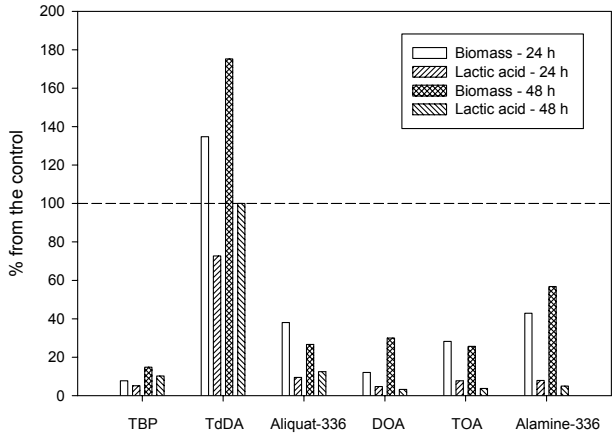

Fig. 3. Influence of some extractants on the cell growth and lactic acid production of *Lactobacillus casei* - molecular level.

What is more the number of the cells is greater than in the control sample (135% at 24 h and 175% at 48 h). It is necessary to mention that the bacterial cells look differently. They look not like small sticks, but like circles. If a sample of these cells is inoculated in normal fermentation medium they restore their initial shape, as well as the growth rate and productivity. This phenomenon has to be additionally investigated. For all other extractants the number of the cells does not exceed 60% and the lactic acid produced − 15%.

Phase level toxicity

Diluents. The results obtained (Fig. 4) demonstrate considerable phase toxicity of the investigated hydrocarbons, regardless of the high number of the cells. In case of octane and decane the number of the cells is 2 to 4 time higher than in the control sample. Again the cells look like small circles and do not have their usual shape. The increased number of the cells does not result in increase of the lactic acid production. The lactic acid production in the presence of octane and decane (compared to the control sample) is 11% and 21% at 24 h and 42%

and 33% at 48 h respectively. The dodecane is non-toxic on the phase level, whereas the kerosene fraction is very toxic – (25% and 33% biomass, 14% and 13% lactic acid).

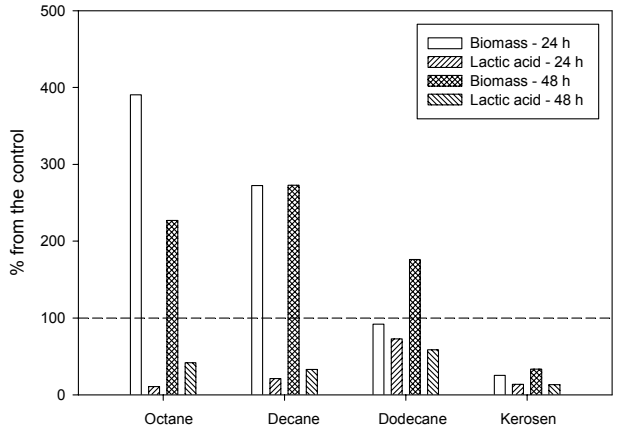

Fig. 4. Phase level toxicity of some diluents on *Lactobacillus casei* cells.

Modifiers. Similarly to the hydrocarbons, the corresponding alcohols (octanol and decanol) showed high phase toxicity. In the case of octanol, on the 24 h, the biomass is only 2% of the control sample, increasing slightly to 8% at 48 h – (Fig. 5).

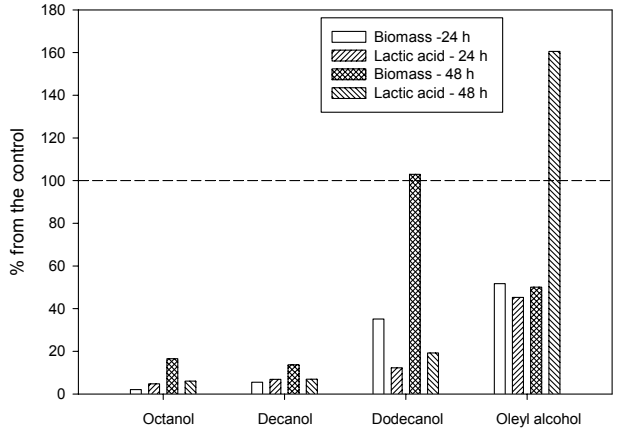

Fig. 5. Phase level toxicity of some modifiers on *Lactobacillus casei* cells.

The results for lactic acid production are analogous – 5% at 24 h and 7% at 48 h. For decanol we obtained - 6% and 7% biomass at the 24 h and 48 h and 7% lactic acid for both points of analysis. The results for the dodecanol are very different comparing the biomass growth and lactic acid production. Whereas at the 24 h the biomass is only about 35% of the control sample, at the 48 h the biomass is equal to that of the control sample. At the same time the production of the lactic acid is low – 12% and 19%. Probably in this case the acid production has started at the late stage of fermentation, because the cells were viable and with normal shape. In the case of oleyl alcohol the phase toxicity is low. In spite of the fact that the biomass is only about 50% at the 24 h and 48 h, at the end of the fermentation, the produced lactic acid is 160% compared to the control sample.

Extractants. All the studied extractants showed high phase level toxicity. The number of the cells did not exceed 45% of the control sample and produced lactic acid – 11% (Fig. 6).

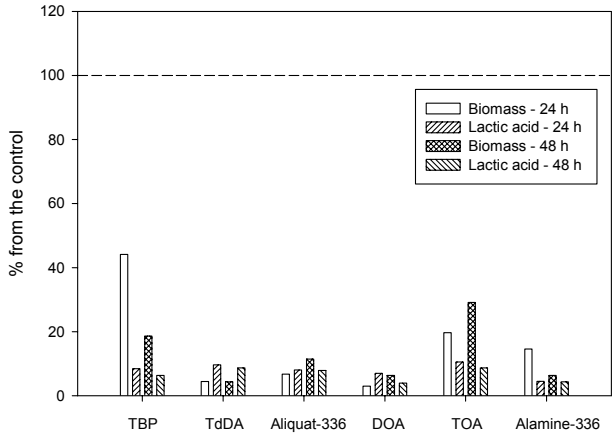

Fig. 6. Phase level toxicity of some extractants on *Lactobacillus casei* cells.

The lactic acid was analyzed only in water phase and we had no information for the quantity of the extracted acid. This will be done on the next stage of the investigations. In any case, if there is some extracted acid the results will be better. At the same time the cells have normal shape and it is possible that the presence of organic phase prolonged the lag phase. The results obtained at two points of comparison do not give enough information about the cell growth in the presence of organic reagents. Additional investigations are necessary and the fermentation process should be monitored at shorter time intervals during entire process.

Systems extractant/modifier. On the basis of the results obtained it has been decided to check two systems, composed of TOA/oleyl alcohol and TdDA/oleyl alcohol at volume ratio 30/70.

On the molecular level both systems showed no toxicity. The results at 24 h are very close to those of the control sample and decreased to about 70% for the biomass and 60% for lactic acid at 48 h (Fig. 7a). The results with TdDA/oleyl alcohol system are similar to those with pure TdDA, whereas the system TOA/oleyl alcohol is less toxic than the pure TOA.

On the phase level of toxicity the chosen systems are better, compared to the pure extractants. The cell growth in the system TOA/oleyl alcohol is about 70% of the control sample and in the system TdDA/oleyl alcohol it is even higher than that in the

control sample (Fig. 7b). The produced lactic acid is about 25% for both systems, ignoring the quantity of acid extracted by the amine.

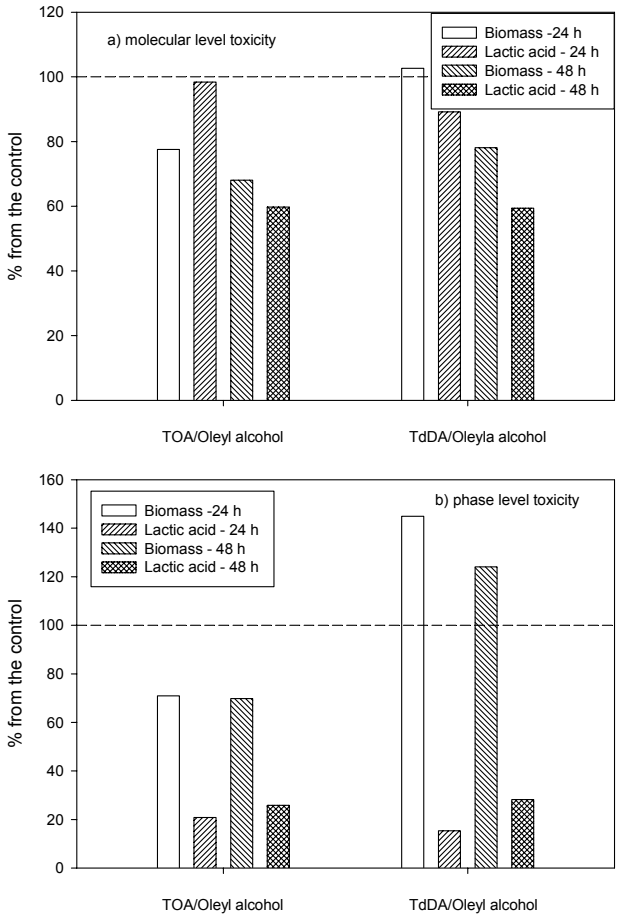

Fig. 7. Molecular (a) and phase level (b) toxicity of the systems TOA/oleyl alcohol and TdDA/oleyl alcohol on the *Lactobacillus casei* cells.

CONCLUSIONS

Among all the tested diluents and modifiers only decanol and dodecanol were toxic on molecular level, as well as all the extractants, except for tridodecylamine. All other chemicals were non-toxic on molecular level.

Regarding phase level toxicity, only dodecane, dodecanol and oleyl alcohol showed low toxicity, while all the extractants were highly toxic.

The results obtained with systems extractant/ diluent demonstrated that the use of non-toxic diluents decreases the toxicity of the system in comparison to pure extractants.

Further investigations are necessary to determine whether lower lactic acid production is due to the prolonged lag-phase in bacterial growth, as well as on the influence of ratio extractant to diluent on the lactic acid production.

REFERENCES

1. K. Ye, Sh. Jin, K. Shimizu, *J. Ferment. Bioeng*., **81**, 240 (1996).
2. N. Tik, E. Bayraktar, Ü. Mehmetoglu, *J. Chem. Techn. Biotechnol.*, **76**, 764 (2001).
3. L. Xuemei, L. Jianping, L. Mo'e, C. Peilin, *Bioprocess Eng*., **20**, 231 (1999).
4. K.B. Lee, *Bioresource Technol*., **96**, 1505 (2005)
5. 5. R. Chen, Y. Y. Lee, *Appl. Biochem. Biotechn*., **63-65**, 435 (1997).
6. Y. Tong, M. Hirata, H. Takanashi, T. Hano, F. Kubota, M. Goto, F. Nakashio, M. Matsumoto, *J. Membrane Sci.,***143**, 81, (1998).
7. A. V. Sosa, J. Ochoa, N. I. Perotti, *Bioseparation*, **9**, 283 (2001).
8. W.-Y. Tong, X.-Y. Fu, S.-M. Lee, J. Yu, J.-W. Liu, D.-Zh. Wei, Y.-Mo Koo, *Biochem. Eng. J.,* **18**, 89 (2004).
9. J. Planas, A. Kozlowski, J. M. Harris., F. Tjerneld, B. Hanh-Hagerdal, *Biotechnol. Bioeng*., **66**, 211 (1999).
10. P. Nikolova, O. P. Ward, *J. Ind. Microb.,* **12**, 76 (1993).
11. R. Leon, P. Fernandes, H. M. Pinheiro, J. M. S. Cabral, *Enz. Microb. Techn*., **23**, 483, (1998).
12. Y. Sardessai, S. Bhosle, *Res. Microbiol*., **153**, 263 (2002).
13. S. Seevaratnam, S. Holst, O. Hjörleifsdottir, B. Mattiasson, *Bioprocess Eng.,* **6**, 35 (1991).
14. Y. Tong, M. Hirata, H. Takanishi, T. Hano, M. Matsumoto, Sh. Miura, *Sep. Purif. Techn*., **33**, 1439 (1998).
15. A. Demirci, A. L. Pometto III, K. R. Harkins, *Bioseparation,* **7**, 297 (1999).
16. B. Choudhury, A. Basha, T. Swaminathan, *J. Chem. Techn. Biotechn*., **73**, 111 (1998).
17. J. Marták, E. Sabolová, Š. Schlosser, M. Rosenberg, L. Krištofiková, *Biotechnol. Techn.,* **11**, 71 (1997).

ТОКСИЧНОСТ НА НЯКОИ РАЗТВОРИТЕЛИ И ЕКСТРАГЕНТИ КЪМ КЛЕТКИ НА *LACTOBACILLUS CASEI*

Н. А. Маринова, Д. С. Янков*

Институт по инженерна химия, Българска академия на науките, ул. „Акад. Г. Бончев", бл. 103, 1113 София

Постъпила на 30 октомври 2008 г., Преработена на 23 април 2009 г.

(Резюме)

Различни органични съединения, използвани като разтворители, модификатори и екстрагенти при екстракцията на млечна киселина са изследвани, за да се определи токсичността им спрямо клетки на *Lactobacillus casei*. Изследвана бе токсичността на молекулно и фазово ниво. Изследваните въглеводороди са нетоксични на молекулно ниво и показват различна токсичност на фазово ниво. Измежду изследваните алкохоли октанолът и олеиловият алкохол са нетоксични, а деканолът и додеканолът са токсични на молекулно ниво. Всички алкохоли показват висока токсичност на фазово ниво. Изследваните екстрагенти са силно токсични както на молекулно (с изключение на тридодециламина), така и на фазово ниво. Две екстракционни системи, съставени от триоктиламин/олеилов алкохол и тридодециламин/олеилов алкохол също бяха изследвани. И двете системи са нетоксични на молекулно ниво и са средно токсични на фазово ниво. Те успешно могат да се използват за *in situ* екстрактивна ферментация на млечна киселина.

Bulgarian Chemical Communications, Volume 41, Number 4 (pp. 374–379) 2009

Fluorescein as corrosion inhibitor for carbon steel in well water

J. Sathiyabama[1], S. Rajendran[1,2]*, J. A. Selvi[3], J. Jeyasundari[4]

[1] *Department of Chemistry, GTN Arts College, Dindigul - 624005, Tamilnadu, India*
[2] *Corrosion Research Centre, Department of Physical Sciences, Servite College of Education for Women, Thogaimalai - 621 313, Tamilnadu, India*
[3] *Department of Chemistry, Vinayaga Mission University, Aarupadai Veedu Institute of Technology, OMR, Paiyanur - 603104, India*
[4] *Department of Chemistry, SVN College, Madurai, India*

Received January 10, 2009; Revised April 23, 2009

The inhibition efficiency of fluorescein in controlling corrosion of carbon steel, immersed in well water, has been evaluated by mass loss method both in the absence and presence of zinc ion. The formulation consisting of 60 ppm of Fluorescein (FN) and 50 ppm of Zn^{2+} offers 98% inhibition efficiency to carbon steel immersed in well water. A synergistic effect exists between FN and Zn^{2+}. The inhibition efficiency (IE) of the FN-Zn^{2+} system decreases with increases in immersion period. Addition of N-cetyl-N,N,N-trimethyl ammonium bromide (CTAB) sodium dodecyl sulphate (SDS), sodium sulphite (Na_2SO_3) does not change the excellent inhibition efficiency of the FN-Zn^{2+} system. Polarization study suggests that the FN-Zn^{2+} functions as an anodic inhibitor system. AC impedance spectra reveal the presence of a protective film on the metal surface. FTIR spectra indicate that the protective film consists of Fe^{2+}-FN complex and $Zn(OH)_2$.

Key words: carbon steel, corrosion inhibition, fluorescein, dyes and synergistic effect.

INTRODUCTION

Several compounds such as nitrate [1, 2] phosphates [3, 4] silicates [5] sodium salicylate [6] sodium cinnamate [7] molybdate [8, 9] phosphoric acids [10, 12] polyacrylamide [13] and caffeine [14, 15] have been used as corrosion inhibitors. Talati and Gandhi [16, 18] have studied the effect of some dyes as corrosion inhibitors for B26S aluminium in hydrochloric acid. The inhibition efficiency (IE) of triphenylmethane dyes such as Victoria Blue, Fast Green, Light Green, Malachite Green, Fuchsine base, Fuchsine acid, Crystal Violet and Methyl Violet 6B in controlling corrosion of aluminium in phosphonic acid has been studied by Talati and Daraji using mass loss and polarization studies [19]. Though several dyes have been used as corrosion inhibitors, the mechanistic aspects of corrosion inhibition have not been studied in detail. This prompted us to investigate (i) the inhibition efficiency of fluorescein in controlling the corrosion of carbon steel immersed in well water in the absence and presence of zinc ion (ii) the influence of pH and immersion period (iii) to analyze the protective film formed on the metal surface by FTIR spectroscopy (iv) to propose a suitable mechanism of corrosion inhibition based on the results of electrochemical studies such as polarization and AC impedance and FTIR spectra.

EXPERIMENTAL

Preparation of the specimens

Carbon steel specimens (0.0267% S, 0.06% P, 0.4% Mn, 0.1% C and the rest iron) of the dimensions 10×4.0×0.2 cm were polished to mirror finish and degreased with trichloroethylene and used for mass loss method and surface examination studies.

Mass loss method. Relevant data on the well water, used in this study, are given in Table 1.

Table 1. Parameters of well water.

Parameter	Value
pH	8.38
Conductivity	3110×10^{-4} S·m^{-1}
TDS	2013 ppm
Chloride	665 ppm
Sulphate	14 ppm
Total hardness	1100 ppm

Carbon steel specimens, in triplicate were immersed in 100 ml of well water and various concentrations of fluorescein in the presence and absence of Zn^{2+} (as $ZnSO_4.7H_2O$) for a period of one day. The corrosion products were cleaned with Clarke's solution [20]. The weight of the specimens before and after immersion was determined using Shimadzu

* To whom all correspondence should be sent:
E-mail: susairajendran@gmail.com

balance AY62. The corrosion inhibition efficiency was calculated based on Eqn (1):

$$IE = 100\,[1-W_2/W_1], \quad \% \qquad (1)$$

Where W_1 is the corrosion rate in the absence of the inhibitor and W_2 is the corrosion rate in the presence of inhibitor.

Surface examination study

FTIR spectra. The carbon steel specimens were immersed in various test solutions for one day. The specimens were taken out of the test solutions and dried. The film formed on the metal surface was carefully removed and thoroughly mixed with KBr so as to make it uniform throughout. The FTIR spectra were recorded on a Perkin-Elmer 1600 spectrophotometer.

Potentiodynamic polarization study. Polarization study was carried out by H and CH Electrochemical Impedance Analyzer Model CHI 660A using a three electrode cell assembly. Carbon steel was used as working electrode with platinum as counter electrode and saturated calomel electrode (SCE) as reference electrode. The corrosion parameters such as corrosion potential (E_{corr}) corrosion current (I_{corr}) and Tafel's slopes (anodic slope b_a and cathodic slope b_c) were calculated.

AC Impedance spectra. AC impedance spectra were recorded by the same instrument used for polarization study using the same type of three electrode cell assembly. The real part (Z') and imaginary part (Z'') of the cell impedance were measured in ohms at various frequencies. The charge transfer resistance (R_t) and double layer capacitance (C_{dl}) values were calculated.

Decolourization process. The optical density of FN solution before and after decolourization was measured by the instrument Photoelectric Calorimeter-112. The carbon steel was immersed in 100 ml of the formulation consisting of 60 ppm of FN and 50 ppm of Zn^{2+} for one day. After one day immersion, the carbon steels were removed and the solution was subjected to electrochemical decolourization process. The platinized titanium electrode was used as the anode and the graphite was used as the cathode. The electrolysis was carried out in an undivided cell with a stirring bar.

RESULTS AND DISCUSSION

Analysis of results from mass loss study

The calculated inhibition efficiencies (*IE*) of fluorescein in controlling the corrosion of carbon steel immersed in well water both in the absence and presence of zinc ion have been tabulated in Table 2. The calculated values indicate the ability of fluorescein to be a good corrosion inhibitor. The inhibition efficiency is found to be enhanced in the presence of zinc ion.

Table 2. Corrosion rates (*CR*) of carbon steel in well water in the absence and presence of inhibitors and the inhibition efficiencies obtained by mass loss method. Inhibitor system: Fluorescein (FN)+Zn^{2+}. Immersion period: one day.

Zn^{2+}/FN, ppm	0	10	25	50
0	-	3	7	15
20	13	35	70	96
60	16	38	75	98
100	22	45	82	98
140	25	50	83	98
180	30	65	90	98
	CR(mdd)			
0	59.09	59.09	59.09	59.09
20	51.40	38.41	17.23	2.36
60	50.32	36.64	14.77	1.18
100	46.09	36.64	14.77	1.179
140	44.32	29.54	10.04	1.178
180	41.36	20.68	5.91	1.175

Influence of immersion period on inhibition efficiency. The *IE* of FN (60 ppm)-Zn^{2+} (50 ppm) (Table 3) system is found to decrease as the immersion period increases. This indicates that the protective film, formed on the metal surface, is unable to withstand the continuous attack of corrosive ions such as Cl^- ion (665 ppm) present in well water for long time. There is a competition between the formations of $FeCl_2$ (and also $FeCl_3$) and Fe-FN complex on the anodic sites of the metal surface. The formation of $FeCl_2$ is favoured, compared to the formation of Fe-FN complex [21, 22].

Table 3. Influence of immersion period on the inhibition efficiency of FN (60 ppm)+Zn^{2+} (50 ppm) system.

Immersion period, day	1	3	5	7
System: well water CR, mdd	59.09	21.52	14.9	17
System: well water + FN (60 ppm) + Zn^{2+} (50 ppm) CR, mdd	1.18	1.29	1.49	3.06
IE%	98	94	90	82

Influence of N-cetyl N,N,N-trimethyl ammonium bromide (CTAB) on the inhibition efficiency of FN (60 ppm) + Zn^{2+} (50 ppm) system. The influence of CTAB on the inhibition efficiency of FN (60 ppm) + Zn^{2+} (50 ppm) system is given in Table 4. It is interesting to find that the *IE* of the FN-Zn^{2+} system is not changed upon the addition of CTAB. CTAB is a biocide. It can control the corrosion caused by bacteria. The present study reveals that the formulation consisting of FN, Zn^{2+} and CTAB has

excellent corrosion inhibition efficiency. It is expected that this formulation will have also excellent biocidal efficiency. Hence, this formulation may be used in cooling water system.

Influence of sodium dodecyl sulphate (SDS) on the inhibition efficiency of FN (60 ppm) - Zn^{2+} (50 ppm) system. The influence of SDS on the inhibition efficiency of FN (60 ppm) - Zn^{2+} (50 ppm) system is given in Table 4. The IE of FN-Zn^{2+} system is not changed by the addition of SDS. It can control the corrosion caused by bacteria. The present study reveals that the formulation consisting of FN, Zn^{2+} and SDS has excellent corrosion inhibition efficiency. It is expected that this formulation will also have excellent biocidal efficiency.

Influence of sodium sulphite (Na_2SO_3) on the inhibition efficiency of FN (60 ppm)-Zn^{2+} (50 ppm) system. The influence of Na_2SO_3 on the inhibition efficiency of FN-Zn^{2+} system is given in Table 4. Addition of Na_2SO_3 has no influence on the inhibition efficiency of FN (60 ppm) + Zn^{2+} (50 ppm) system.

Table 4. Influence of N-Cetyl-N,N,N-trimethyl ammonium bromide (CTAB) on the inhibition efficiency of FN (60 ppm) + Zn^{2+} (50 ppm) system. Inhibitor system: FN (60 ppm) + Zn^{2+} (50 ppm) + CTAB; FN (60 ppm) + Zn^{2+} (50 ppm) + SDS; FN (60 ppm) + Zn^{2+} (50 ppm) + Na_2SO_3. Immersion period: one day.

FN, ppm	Zn^2, ppm	CTAB/SDS/Na_2SO_3, ppm	CR, mdd	IE, %
0	0	0	59.09	--
60	50	50	1.18	98
60	50	100	1.179	98
60	50	150	1.178	98
60	50	200	1.176	98
60	50	250	1.175	98

Table 5. Influence of various pH on the inhibition efficiency of FN + Zn^{2+} system. Inhibitor system: FN (60 ppm) + Zn^{2+} (50 ppm) + Na_2SO_3. Immersion period: one day.

pH	6	8	11
System: well water; CR, mdd	17.27	59.09	3.64
System: well water + FN (60 ppm) + Zn^{2+} (50 ppm); CR, mdd	16.55	1.18	0.546
IE%	72	98	85

Influence of pH on inhibition efficiency. The *IE* of the FN-Zn^{2+} system has been studied at different pH of the solutions and it is calculated. *IE* values have been tabulated in Table 5. At pH 6 the *IE* is found to be 72%. This decrease in *IE* is due to the fact that the protective film formed on the metal surface is broken by the attack of H^+ ions. At pH 8 the *IE* is 98%. Further increase in pH of the solution lowers *IE* substantially. The experimental results suggest that the amount of Zn^{2+} available to transport FN towards the metal surface decreases at high pH. This may be due to the fact that zinc ions in the bulk of the solution might have been precipitated as zinc hydroxide.

Analysis of polarization curves

The potentiodynamic polarization curves of carbon steel immersed in well water in the absence and presence of inhibitors are shown in Fig. 1a, b and c. The corrosion parameters are given in Table 6.

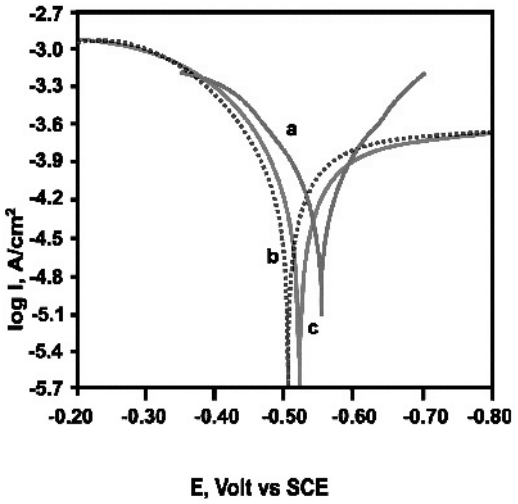

Fig. 1. Polarization curves of carbon steel immersed in test solution. a. well water; b. well water + FN (60 ppm); c. well water + FN (60 ppm) + Zn^{2+} (50 ppm).

When carbon steel is immersed in well water the corrosion potential is −550 mV vs SCE (Saturated Calomel Electrode). The corrosion current is 5.2480×10^{-4} A/cm^2. When FN (60 ppm) and Zn^{2+} (50 ppm) are added to the above system the corrosion potential shifts to the anodic side (−522 mV vs SCE). This suggests that this formulation controls the anodic reaction predominantly. In the presence of this inhibitor system, the corrosion current decreases from 5.2480×10^{-4} A/cm^2 down to 4.365×10^{-5} A/cm^2. This suggests the inhibitive nature of this inhibitor system.

Table 6. Corrosion parameters of carbon steel immersed in well water in the absence and presence of inhibitors. Inhibitor: FN (60 ppm) + Zn^{2+} (50 ppm).

FN, ppm	Zn^{2+}, ppm	E_{cor}, mV vs SCE	b_a, mV	b_c, mV	I_{corr}, A/cm^2
0	0	−550	115	125	5.2480×10^{-4}
60	0	−509	100	186	5.1095×10^{-5}
60	50	−522	71	114	4.365×10^{-5}

Analysis of AC impedance spectra

The AC impedance spectra of carbon steel of our study are shown in Fig. 2a, b and c.

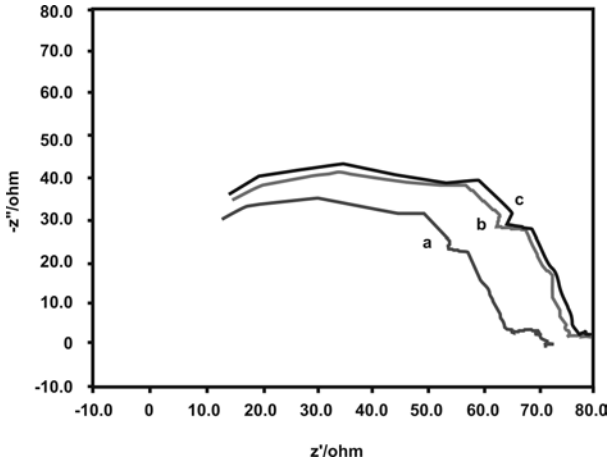

Fig. 2. AC Impedance spectra of carbon steel immersed in test solution: a - well water; b - well water + FN (60 ppm); c - well water + FN (60 ppm) + Zn^{2+} (50 ppm).

The impedance parameters have been tabulated in Table 7. When carbon steel is immersed in well water the charge transfer resistance R_t is 59.6 ohm·cm^2. The double layer capacitance C_{dl} is 4.8854×10^{-8} μF/cm^2. When the formulation consisting of FN and Zn^{2+} is added the R_t value increases to 66.66 ohm·cm^2 and the C_{dl} value decreases to 4.367×10^{-9} μF/cm^2. This increase in charge transfer resistance value (R_t) and the decrease in the double layer capacitance value (C_{dl}) confirm the formation of a protective film on the surface of the metal. This accounts for the better inhibition efficiency of the FN-Zn^{2+} system.

Table 7. AC Impedance parameters of carbon steel immersed in well water in the absence and presence of inhibitors. Inhibitors: FN (60 ppm) + Zn^{2+} (50 ppm).

FN ppm	Zn^{2+}, ppm	R_t, ohm·cm^2	C_{dl}, μF/cm^2
0	0	59.6	4.8854×10^{-8}
60	0	60.63	4.8236×10^{-8}
60	50	66.66	4.367×10^{-9}

Analysis of FTIR spectra

The FTIR spectrum (KBr) of pure fluorescein is shown in Fig. 3a. The FTIR spectrum (KBr) of the film formed on the surface of the carbon steel after immersion in solution containing 60 ppm of FN and 50 ppm of Zn^{2+} is shown in Fig. 3b. The OH stretching frequency shifts from 3428 cm^{-1} to 3463. The C=O stretching frequency shifts from 1592 cm^{-1} to 1625. The C–O–C asymmetric bending vibration frequency shifts from 1091 to 1078 cm^{-1}. It was inferred that fluorescein has co-ordinated with Fe^{2+} through oxygen atom of OH group carboxyl oxygen and aromatic II electron resulting in the formation of Fe^{2+}-FN complex on the anodic sites of the metal surface. The band at 1338 cm^{-1} is due to $Zn(OH)_2$ formed on the cathodic sites of the metal surface [22−24]. Thus FTIR spectral study leads to the conclusion that the protective film consists of Fe^{2+}-FN complex and $Zn(OH)_2$.

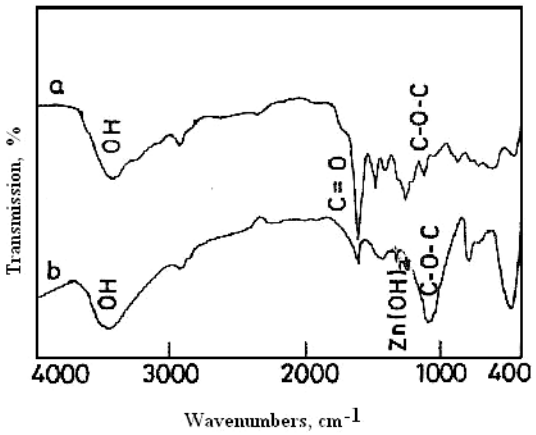

Fig. 3. FTIR spectra (KBr) of pure FN (a) and of film formed on the surface of the metal immersed in test solution FN (60 ppm) + Zn2+ (50 ppm) (b).

Decolourization process

Platinized titanium anode and graphite cathode were immersed in the solution to be decolourized. Current was passed for 10 min without addition of NaCl. The potential was 6 volts and current density was 0.25 A/cm^2. There was no decolourization, when 2 g of NaCl was added (2% solution) partial decolurization took place after passing a current for 10 min. However, very interestingly when 5 g of NaCl was added (5% solution) the solution was decolourized completely, within a few seconds. Hence this formulation, namely 5% solution of NaCl, platinized titanium anode, graphite cathode, passing a current density of 0.25 A/cm^2 and a potential of 6 volts, for a few seconds may be used to decolourize the test solution of FN.

The supporting electrolyte plays an important role in the oxidation process [23]. When NaCl solution is electrolysed, the active species produced is Cl^+ [24, 25]. The latter oxidized the coloured material into colourless product.

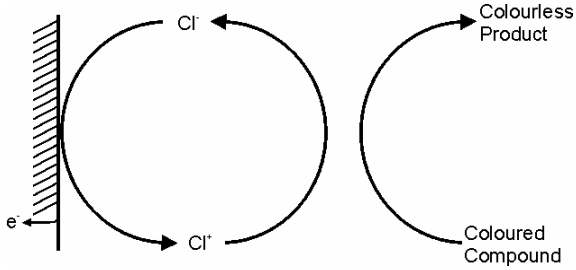

Scheme 1. Electrochemically regenerated Cl^+.

The optical density value for the coloured solution before decolourization was 0.50 and after

decolourization was 0.03. Hence, the efficiency of decolourization is 94%.

The main objection in case of using dyes as corrosion inhibitors in cooling water system is the colour of the dye. The present study has revealed a method of decolourizing the coloured inhibitor solutions.

Mechanism of corrosion inhibition

Following these discussions, a mechanism can be proposed for the corrosion inhibition of carbon steel immersed in well water by FN (60 ppm)-Zn^{2+} (50 ppm) system.

- When the formulation consists of 60 ppm of FN and 50 ppm of Zn^{2+} in well water there is formation of FN-Zn^{2+} complex in solution.

- When carbon steel is immersed in this solution FN-Zn^{2+} complex diffuses from the bulk of the solution towards the metal surface.

- FN-Zn^{2+} complex is converted into FN-Fe^{2+} complex on the anodic sites of the metal surface with the release of zinc ion:

$$Zn^{2+}\text{–FN} + Fe^{2+} \rightarrow Fe^{2+}\text{–FN} + Zn^{2+}$$

- The released Zn^{2+} combines with OH^- to form $Zn(OH)_2$ on the cathodic sites of the metal surface:

$$Zn^{2+} + 2OH^- \rightarrow Zn(OH)_2 \downarrow$$

- Thus the protective film consists of FN-Fe^{2+} complex and $Zn(OH)_2$.

- In nearly neutral aqueous solution the anodic reaction is the formation of Fe^{2+}. This anodic reaction is controlled by the formation of FN-Fe^{2+} complex on the anodic site of the metal surface. The cathodic reaction is the generation of OH^-, which is controlled by the formation of $Zn(OH)_2$ on the cathodic sites of the metal surface.

$$Fe \rightarrow Fe^{2+} + 2e^- \qquad \text{(Anodic reaction)}$$

$$2H_2O + O_2 + 4e^- \rightarrow 4OH^- \text{ (Cathodic reaction)}$$

- This accounts for the synergistic effect of the FN-Zn^{2+} system.

CONCLUSIONS

To summarize, fluorescein acts as a corrosion inhibitor for carbon steel in well water. Its efficiency is increased due to the transporting ability of zinc ion through the formation of the FN-Zn^{2+} complex. A suitable mechanism has been proposed for the corrosion inhibition based on the results of electrochemical studies such as polarization and AC impedance and FTIR spectra. Perusal of the spectral analysis suggests that the protective film consists of Fe^{2+}-FN complex on the anodic sites and $Zn(OH)_2$ on the cathodic sites on the metal surface, which confirms that FN-Zn^{2+} system functions as a anodic inhibitor system.

***Acknowledgement**: The authors are thankful to their management and University Grants Commission, India for help and encouragement.*

REFERENCES

1. M. Cohen, *Corrosion*, **32**, 461 (1976).
2. S. Sanyal, *Bull. Electrochem*., **6**, 392 (1990).
3. J. L. Mansa, Szybalski, *Corrosion*, **8**, 381 (1952).
4. K. S. Rajagopalan, K. Venu, *Indian J. Techn*., **6**, 239 (1968).
5. J. W. Wood, J. S. Beecher, P. S. Lawrence, *Corrosion*, **13**, 41 (1957).
6. E. V. Bogatyreva, S. A. Balezin, *Zh. Prikl. Khim*., **35**, 1071 (1962).
7. E. V. Bogatyreva, V. V. Nagaev, *Zh. Prikl. Khim*., **35**, 550 (1962).
8. S. Rajendran, B. V. Apparao, N. Palaniswamy, *J. Electrochem. Soc., India*, **47**, 43 (1998).
9. S. Rajendran, B. V. Apparao, A. Mani, N. Palaniswamy, *Anti-Corros. Methods Mater.*, **45**, 25 (1998).
10. Y. I. Kuzentzov, T. I. Bardasheva, *Zashch. Met*., **24**, 234 (1988).
11. K. Airey, R. D. Armstrong, T. Handside, *Corros. Sci*., **28**, 449 (1998).
12. S. Rajendran, B. V. Apparao, N. Palaniswamy, *Anti-Corros. Methods Mater.*, **47**, 294 (2000).
13. S. Rajendran, B. V. Apparao, N. Palaniswamy, *Anti-Corros. Methods Mater.*, **44**, 308 (1997).
14. S. Rajendran, S. Vaibhavi, N. Anthony, D. C. Trivedi, *Corrosion*, **59**, 529 (2003).
15. S. Rajendran, A. J. Amalraj, M. J. Joice, N. Anthony, D. C. Trivedi, M. Sunderavadivelu, *Corros. Rev*., **22**, 233 (2004).
16. J. D. Talati, D. K. Gandhi, *Werkst. Korros*., **33**, 155 (1982).
17. J. D. Talati, D. K. Gandhi, *Indian J. Technol*., **20**, 312 (1982).
18. J. D. Talati, D. K. Gandhi, *Corrosion*, **40**, 88 (1984).
19. J. D. Talati, J. M. Daraji, *J. Electrochem. Soc., India*, **35**, 175 (1986).
20. G. Wranglan, Introduction to Corrosion and Protection of Metals, Chapman and Hall, London, UK, 1985, p. 236.
21. S. K. Selvaraj, A. J. Kennedy, A. J. Amalraj, S. Rajendran, N. Palaniswamy, *Corros. Rev*., **22**, 219 (2004).
22. S. Rajendran, S. M. Reenkala, N. Anthony, R. Ramaraj, *Corros. Sci*., **44**, 449 (2002).
23. S. Durai, S. Chellammal, N. Balasubramanian, C. A. Basha, *J. Trans. SAEST*, **39**, 113 (2004).
24. S. Rajendran, D. C. Trivedi, *Synthesis*, Feb. 1995, p. 153
25. R. L. Dotson, R. W. Lynch, *J. Electrochem. Soc*., **128**, 798 (1981).

ФЛУОРЕСЦЕИН КАТО ИНХИБИТОР НА КОРОЗИЯ НА ВЪГЛЕРОДНА СТОМАНА ВЪВ ВОДНИ КЛАДЕНЦИ

Дж. Сатиябама[1], С. Раджендран[1,2]*, Дж. А. Селви[3], Дж. Джеясундари[4]

[1] Департамент по химия, ГТН колеж по изкуства, Диндигул 624005, Тамилнаду, Индия
[2] Център за изследване на корозията, Департамент по физически науки, Сервит Колеж за образование на жените, Тогаймалай 621313, Тамилнаду, Индия
[3] Департамент по химия, Университет Винаяга, Аарупадай Вееду Технологичен институт, ОМР, Пайянур 603104, Индия
[4] Департамент по химия, С. В. Н. Колеж, Мадурай, Индия

Постъпила на 10 януари 2009 г.; Преработена на 23 април 2009 г.

(Резюме)

Определено е инхибиторното действие на флуоресцеин за контролиране на корозията на въглеродна стомана потопена в воден кладенец чрез загубата на маса в отсъствие и присъствие на цинкови йони. Рецептурата включваща 60 ppm флуоресцеин (FN) и 50 ppm Zn^{2+} дава 98% ефикасност за въглеродна стомана потопена във воден кладенец. Намерен е синергичен ефект между FN и Zn^{2+}. Инхибиторното действие на системата FN-Zn^{2+} намалява с увеличаване на периода на потапяне. Добавянето на N-цетил-N,N,N-триметиламониев бромид (CTAB), натриев додецилсулфат (SDS), натриев сулфит (Na_2SO_3) не променят отличното инхибиторно действие на системата FN-Zn^{2+}. Резултатът от поляризационно изследване предполага, че системата FN-Zn^{2+} действа като анодна инхибираща система. Импедансни спектри показват присъствие на защитен филм върху повърхността на метала. ИЧ спектри показват, че защитния филм сесъстои от комплекс Fe^{2+}-FN и $Zn(OH)_2$.

Bulgarian Chemical Communications, Volume 41, Number 4 (pp. 380–384) 2009

Synthesis and spectrophotometric studies of some benzothiazolylazo dyes – determination of copper, zinc, cadmium, cobalt and nickel

K. Shanthalakshmi*, S. L. Belagali

Department of Studies in Environmental Science, University of Mysore, Mysore-570006, Karnataka, India

Received January 5, 2009; Revised May 6, 2009

4-(2-Benzothiazolylazo)-2-amino-3-hydroxypyridine and its derivatives 4-(4-methyl-2-benzothiazolylazo), 4-(6-chloro-2-benzothiazolylazo) and 4-(6-bromo-2-benzothiazolyl-azo)-2-amino-3-hydroxypyridines have been synthesized. All these dyes are very sensitive chromogenic reagents for the determination of copper, cadmium, zinc, cobalt and nickel. The reagents react with the metal ions to form purple-coloured complexes (λ_{max} 540−570 nm) in aqueous acetone solution within the pH range 2.8 to 4.6. Copper can be selectively determined at pH 2.8 and most of the metal ions do not interfere except for nickel and cobalt. Cadmium, zinc, cobalt and nickel can be determined at pH 4−5. Their mutual interference can be eliminated using suitable masking reagents. A further advantage of this method is that an extraction procedure is not required and therefore the analytical procedure is very simple.

Key words: 2-aminobenzothiazole, azodyes, 2-amino-3-hydroxypyridine, spectrophotometry, analytical reagents, metal ions.

INTRODUCTION

In search of new sensitive and selective organic reagents, a thorough study of some heterocyclic azo dyes has been made. Among the heterocyclic reagents pyridylazo, thiazolylazo and benzothiazolylazo dyes are extensively used for the spectrophotometric determination of metal ions [1−22]. In this work 4-(2-benzothiazolylazo)-2-amino-3-hydroxypyridine (BTAAHP), 4-(4-methyl-2-benzothiazolylazo)-2-amino-3-hydroxy-pyridine (MBTAAHP), 4-(6-chloro-2-benzothiazolylazo)-2-amino-3-hydroxypyridine (CBTAAHP) and 4-(6-bromo-2-benzothiazolylazo)-2-amino-3-hydroxypyridine, (BBTAAHP) were prepared and a spectrophotometric method was developed for the determination of copper, zinc, cadmium, cobalt and nickel. The authors have already reported the synthesis of 4-(2-benzothiazolylazo)-2-amino-3-hydroxypyridine (BTAAHP) and the spectrophotometric determination of copper by this reagent [1].

All the reagents react instantaneously with Cu (II), Zn (II), Cd (II) and Co (II) to form reddish purple complexes. However, the formation of Ni (II) complexes requires 30 minutes time. These complexes are stable for an hour. Metal ions like Fe^{2+}, Hg^{2+}, Pb^{2+} do not interfere.

MATERIALS AND METHODS

Apparatus

Shimadzu UV double-beam spectrophotometer was used for the spectrophotometric measurements. pH adjustments were carried out with Digisun electronic pH meter model 7007. 2000 Perkin Elmer FTIR was used for IRS measurements and Thermo DFS double focusing magnetic sector mass spectrometer was applied for mass spectral measurements. Graphite furnace atomic absorption spectrometer was used for the determination of the analytes in water samples

Chemicals

2-Aminobenzothiazole and 2-amino-4-methyl-benzothiazoles were prepared by cyclization of the corresponding α-phenyl thioureas [23] with thionyl chloride as described previously [24]. 2-amino-6-chloro- and 2-amino-6-bromobenzo-thiazoles were prepared from the corresponding α-phenyl thioureas, using sulphuric acid and hydrobromic acid as cyclization agents [25]. 2-amino-3-hydroxypyridine was purchased from Acros Organics (New Jersey, USA). 0.2 M sodium acetate and 0.2 M acetic acid were used for pH adjustments. BTAAHP, MBTAAHP, CBTAAHP and BBTAAHP solutions of concentration 10^{-4} M were prepared by dissolving a suitable quantity of the substance in AR acetone and these solutions were stable for several months, if stored in amber coloured bottles. All other solutions, including standard solutions of

* To whom all correspondence should be sent:
E-mail: shanthi1806@yahoo.co.in

metal ions, were prepared from purified reagents in redistilled water.

EXPERIMENTAL

Synthesis of BTAAHP. Synthesis and analysis of BTAAHP were already reported by the authors [1].

Synthesis of MBTAAHP. 1.64 g of 2-amino-4-methylbenzothiazole was dissolved in concentrated sulphuric acid (14 mL) and diluted with 24 mL of water. The amine was diazotized using nitrosyl sulphuric acid (prepared by adding 0.72 g of sodium nitrite to 5 mL of concentrated sulphuric acid at 70−90°C) at 0−5°C [7]. The diazotized mixture was kept for 2 hours at 0−5°C and then added to a solution containing 1.1 g of 2-amino-3-hydroxypyridine in 400 mL of 7% NaOH. The pH of the mixture was adjusted to 5 with ammonia and acetic acid, it was kept overnight and filtered. Brownish-red solid of MBTAAHP was dried and recrystallized from chloroform. The reagent was further purified by column chromatography using silica gel and 10% acetone in chloroform as eluent.

4-(6-chloro-2-benzothiazolylazo)-2-amino-3-hydroxypyridine (CBTAAHP) (and 4-(6-bromo-2-benzothiazolylazo)-2-amino-3-hydroxypyridine (BBTAAHP) were prepared as it was described above starting with 2-amino-6-chlorobenzothiazole (1.84 g) and 2-amino-6-bromobenzothiazole (2.29 g). The structure of the obtained substances is shown in Fig. 1.

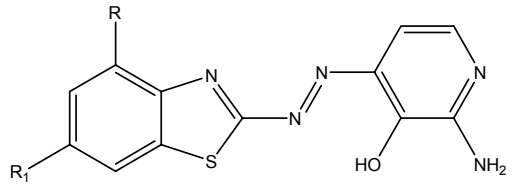

BTAAHP [R = H, R_1 = H],
MBTAAHP [R = CH_3, R_1 = H]
CBTAAHP [R = H, R_1 = Cl],
BBTAAHP [R = H, R_1 = Br].

Fig. 1. Structure of the dye.

Analysis of MBTAAHP. $C_{13}H_{11}N_5OS$ requires 54.74% C, 3.86% H and 24.56% N; found 54.8% C, 3.78% H and 24.5% N; reddish-brown powder (m.p. 242°C decomposes). Mass spectrum: M^+ ion peak at 285. IR spectrum (KBr pellets): 3472, 3431 cm^{-1} (str) (N–H), 3301 cm^{-1} (str) (O–H), 1473 cm^{-1} (str) (N=N).

Analysis of CBTAAHP. $C_{12}H_8N_5OSCl$ calculated 47.13% C, 2.62% H and 22.91% N; found 47.1% C, 2.6% H and 22.89% N; reddish-brown powder (m.p. 248°C decomposes). Mass spectrum: M^+ ion peak is at 305.5. IR spectrum (KBr pellets): 3461 cm^{-1}, 3432 cm^{-1} (str) (N–H), 3332 cm^{-1} (str) (O–H), 1471 cm^{-1} (str) (N=N).

Analysis of BBTAAHP: $C_{12}H_8N_5OSBr$ calculated 41.14% C, 2.28% H and 20.0% N; found 41.2% C, 2.26% H and 20.0% N; reddish-brown powder (m.p. 252°C decomposes). Mass spectrum: M^+ ion peak is at 350 m/z. IR spectrum (Nujol): 3478 cm^{-1}, 3448 cm^{-1} (str) (N–H), 3348 cm^{-1} (str) (O–H), 1490 cm^{-1} (str) (N=N). Spectral data for these dyes are represented in Table.1.

Table 1. Spectral data for the azo dyes.

Parameters	BTAAHP	MBTAAHP	CBTAAHP	BBTAAHP
Color in acetone	Reddish-orange	Reddish-orange	Reddish-orange	Reddish-orange
λ_{max}	470 nm	470 nm	470 nm	470 nm
ε_{max}, $L\cdot mol^{-1}\cdot cm^{-1}$ (in acetone)	5.52×10^4	3.85×10^4	4.26×10^4	2.42×10^4
ε_{max}, $L\cdot mol^{-1}\cdot cm^{-1}$ (pH 2.8)	4.4×10^4	3.55×10^4	3.88×10^4	2.39×10^4
ε_{max}, $L\cdot mol^{-1}\cdot cm^{-1}$ (at pH 4.45)	3.16×10^4	3.68×10^4	2.97×10^4	2.0×10^4
ε_{max}, $L\cdot mol^{-1}\cdot cm^{-1}$ (pH 4.63)	3.78×10^4	3.63×10^4	2.0×10^4	2.5×10^4

Preparation of metal standard solutions. Stock solutions (10^{-5} M) of copper, zinc, cadmium, cobalt were prepared from their corresponding analytical grade acetate salts; that of nickel was prepared from its sulphate salt.

General procedure for determination of metal ions. 5 mL of the standard dye solutions of concentration 5×10^{-4} M were diluted to 100 mL with acetone. From these solutions, 5 mL were used for the determination of metal ions. Absorption measurements were made at 540−580 nm, depending upon the kind of metal ions at a pH value, where the absorption was maximal. The reagent blank was prepared by pipetting 5 mL of the dilute dye solution (0.02 $mg\cdot L^{-1}$) to 5 mL of buffer solution and 10 mL of acetone, making up to 25 mL with water.

RESULTS AND DISCUSSION

Effect of pH

The absorbance of various metal chelates of BTAAHP, MBTAAHP, CBTAAHP and BBTAAHP at different pH values was measured. The pH of maximal absorption was selected for the pH range for the determination of the metal ions, as listed in Table 2.

The copper complexes of all the dyes were determined at pH 2.8 at λ_{max} = 540 nm, the selectivity of the reagents is excellent and metal ions like

zinc, cadmium, iron, lead, mercury, do not interfere except for nickel and cobalt.

Metal ions like Cu^{2+}, Zn^{2+}, Cd^{2+},$Co^{2+}$and Ni^{2+} show strong interference with one another within the pH range 4 to 5. Therefore, determination of any one of these metal ions requires either complete separation or masking of the other four metal ions.

Characteristics of the complexes

BTAAHP, MBTAAHP, CBTAAHP, and BBTAAHP form 1:1 (1igand to metal) complexes with copper, zinc, cadmium, cobalt and nickel. Calibration graphs were drawn by the general procedure. Beer's law was obeyed in the concentration range 0.03−0.3 $mg{\cdot}L^{-1}$.

The reagents react instantaneously with copper, zinc, cadmium and cobalt at the pH values listed in Table 2 to form reddish-purple coloured complexes. The reagents require 30 minutes to form a stable nickel complex. All these complexes were stable in aqueous acetone solution for an hour. The empirical formulae of the complexes were determined by Job's and mole ratio methods. The optical characteristics such as optimum range for the determination of metals, molar absorptivity, Sandell's sensitivity (S) are shown in Table 2.

The empirical formulae of the complexes were determined by Job's and mole ratio methods. The optical characteristics such as optimal range for the determination of metals, molar absorptivity and Sandell's sensitivity (S) are shown in Table 2.

To test the validity of the method, the experimental data were interpreted statistically by the linear regression method. The high correlation coefficient (r) (about 0.98) is evidence for the linear dependence of the absorbance on metal ion concentration. Correlation coefficients (r), slopes and intercepts for the various metal ion complexes are listed in Table 2.

Effect of diverse ions

The selectivity of BTAAHP, MBTAAHP, CBTAAHP, and BBTAAHP for copper, zinc, cadmium, cobalt and nickel is excellent. The effect of foreign ions with respect to MBTAAHP is represented in Table 3.

Copper determination in industrial effluents

Effluent samples were collected from battery producing industries and electroplating industries. These effluents contain mainly copper, cadmium, zinc and lead in trace amounts. Suitable amounts of the effluent solutions were completely evaporated and 10 mL of concentrated nitric acid were added to these solutions. The mixtures were heated until decomposition of all nitrates. The obtained residues were extracted with diluted acetic acid made up to 25 mL with redistilled water. The determination of copper ions was carried out as it is described in the general procedure using BTAAHP as analytical reagent. The results obtained by the proposed method agreed with those of the AAS method (Table 4).

Table 2. Spectral data for the metal complexes at various pH conditions.

Metal complex	pH	λ_{max}, nm	$\varepsilon_{max} \times 10^4$ $L{\cdot}mol^{-1}{\cdot}cm^{-1}$	Beer-Lambert's range, $mg{\cdot}L^{-1}$	Sensitivity ($\mu g{\cdot}cm^{-2}$)	Linear regression equation		
						Correlation coefficient r	Intercept	Slope
Cu-BTAAHP	2.8	540	4.4	0.316−1.0	1.71×10^{-3}	0.9794	−0.068	0.1278
Zn-BTAAHP	4.63	545	2.9750	1.8−0.53	2.2×10^{-3}	0.9952	0.005	0.1956
Cd-BTAAHP	4.63	545	2.2750	0.074−1.0	4.94×10^{-3}	0.9991	0.0003	0.3523
Co-BTAAHP	4.45	555	3.0	0.25−0.57	2×10^{-3}	0.9964	−0.006	0.2255
Ni-BTAAHP	4.63	550	3.78	1.27−0.26	1.6×10^{-3}	0.9780	0.018	0.1699
Cu-MBTAAHP	2.8	540	2.9513	0.23−0.47	2.14×10^{-3}	0.9824	−0.002	0.1588
Zn-MBTAAHP	4.63	550	3.0945	0.24−0.48	2.1×10^{-3}	0.9998	−0.001	0.2327
Cd-MBTAAHP	4.63	550	2.5605	0.25−0.6	4.4×10^{-3}	0.9999	−0.001	0.4829
Co-MBTAAHP	4.45	570	3.6891	0.12−0.28	1.6×10^{-3}	0.9788	0.025	0.1962
Ni-MBTAAHP	4.63	560	4.6756	0.13−0.35	1.62×10^{-3}	0.9998	−0.001	0.1275
Cu-CBTAAHP	2.8	540	4.259	0.06−0.27	1.72×10^{-3}	0.9954	0.002	0.5515
Zn-CBTAAHP	4.63	540	1.98	0.01−0.29	3.3×10^{-3}	0.9947	0.002	0.2811
Cd-CBTAAHP	4.63	550	1.52	0.165−0.58	7.39×10^{-3}	0.9922	−0.001	0.5069
Co-CBTAAHP	4.45	560	3.51	0.081−0.201	1.7×10^{-3}	0.9599	0.0155	0.1996
Ni-CBTAAHP	4.63	550	3.810	0.109−0.22	1.54×10^{-3}	0.9800	−0.001	0.1266
Cu-BBTAAHP	2.8	540	2.3275	0.038−0.195	2.7×10^{-3}	0.9982	−0.002	0.0883
Zn-BBTAAHP	4.63	540	2.3275	0.08−0.363	2.8×10^{-3}	0.9946	−0.003	0.5548
Cd-BBTAAHP	4.63	540	1.7456	0.82−1.16	6.44×10^{-3}	0.9738	−0.003	1.561
Co-BBTAAHP	4.45	560	2.4568	0.019−0.071	2.4×10^{-3}	0.9426	0.014	0.5572
Ni-BBTAAHP	4.63	550	3.3624	0.02−0.085	1.76×10^{-3}	0.9746	0.005	0.1611

Table 3. Effect of interferents on the spectrophotometric determination of metal ions with MBTAAHP.

Substance	Amount added, $mg·L^{-1}$	Copper added (3.12 $mg·L^{-1}$)		Nickel added (2.27 $mg·L^{-1}$)		Cobalt added (1.7 $mg·L^{-1}$)		Zinc added (1.36 $mg·L^{-1}$)		Cadmium added (1.97 $mg·L^{-1}$)	
		Cu found, $mg·L^{-1}$	Error, $mg·L^{-1}$	Ni found $mg·L^{-1}$	Error, $mg·L^{-1}$	Co found, $mg·L^{-1}$	Error, $mg·L^{-1}$	Zn found, $mg·L^{-1}$	Error, $mg·L^{-1}$	Cd found, $mg·L^{-1}$	Error, $mg·L^{-1}$
KCl	296	3.12	0.0	2.27	0.0	1.73	0.03	1.36	0.0	1.97	0.0
K_2SO_4	696	2.84	−0.28	1.98	−0.29	1.48	−0.22	1.25	−0.11	1.73	−0.24
KNO_3	399	3.12	0.0	2.27	0.0	1.70	0.0	1.36	0.0	1.97	0.0
Thiourea	320	2.76	−0.36	2.0	−0.27	1.48	−0.22	1.29	−0.07	1.81	−0.16
NaF	168	3.4	0.28	1.74	−0.53	1.76	0.06	1.26	−0.1	1.88	−0.09
Na-K Tartrate	250	2.5	−0.62	1.45	−0.82	0.7	−1.00	0.68	−0.68	1.22	−0.75
Dimethyl-glyoxime	2387	3.0	0.12	0.1	−2.17	1.0	−0.7	1.23	−0.13	1.61	−0.36
H_2O_2 (6%)	0.1 mL	3.02	0.1	1.9	−0.37	0.0	−1.7	1.10	−0.26	1.83	−0.14
EDTA (0.1 M)	0.05 mL	0	−3.12	0	−2.27	0	−1.7	0	−1.36	0	−1.97
NaH_2PO_4	400	3.3	0.19	2.01	−0.26	1.64	−0.06	0.65	−0.71	1.9	−0.07
Hg^{2+}	0.54	3.06	−0.06	2.0	−0.27	1.68	−0.02	1.20	−0.16	1.79	−0.18
Pb^{2+}	0.41	2.98	−0.14	2.18	−0.09	1.6	−0.1	1.3	−0.06	1.92	−0.05
Fe^{2+}	2.84	3.01	−0.11	2.01	−0.26	1.54	−0.16	1.12	−0.24	1.89	−0.08
Cd^{2+}	0.97	3.12	0.0	3.24	0.97	2.6	0.9	2.34	0.98	-	-
Zn^{2+}	1.47	3.12	0.0	3.74	−1.47	3.17	1.47	-	-	3.44	1.47
Co^{2+}	1.94	5.28	2.16	4.21	1.94	-	-	3.3	1.94	3.91	1.94
Ni^{2+}	1.82	6.39	3.27	-	-	3.5	1.8	3.18	1.82	3.79	1.82
Cu^{2+}	1.56	-	-	3.83	1.56	3.26	1.56	2.92	1.56	3.53	1.56

Table 4. Determination of Cu(II) and Zn(II) in industrial effluents with BTAAHP.

Sample	Copper determination by proposed method, mg L^{-1}	Copper determination by AAS, $mg·L^{-1}$	Error, $mg·L^{-1}$	Zinc determination by proposed method, $mg·L^{-1}$	Zinc determination by AAS, $mg·L^{-1}$	Error, $mg·L^{-1}$
1	0.0204	0.02	−0.004	0.062	0.07	0.008
2	0.0224	0.02	−0.0024	0.0098	0.01	0.0002
3	0.0315	0.03	−0.015	0.008	0.01	0.002
4	0.367	0.35	−0.017	6.6	6.8	0.2

Zinc determination in industrial effluents

Copper, zinc and cadmium form complexes with BTAAHP. As the effluent solutions contain all the three ions, the determination of each one of them requires masking of the other two. The determination of zinc was carried out in a suitable aliquot of the effluent solution as it is described in the general procedure using BTAAHP as analytical reagent and masking copper and cadmium with 1 mL of 2% $Na_2S_2O_3$. The results are represented in Table 4.

CONCLUSION

BTAAHP, MBTAAHP, CBTAAHP and BBTAAHP are sensitive spectrophotometric reagents for the determination of metal ions - copper, zinc, cadmium, cobalt and nickel due to their high absorptivity and the reasonable stability of their complexes. Determination of copper by these reagents at pH 2.8 is relatively free from interference; hence copper can be determined in the presence of metal ions like zinc and cadmium. Determination of zinc, cadmium, cobalt and nickel can be done above pH 4−5. Zinc can be determined in the presence of copper and cadmium by masking them with 1 ml of 2% $Na_2S_2O_3$ solution. The method was successfully applied tor the determination of copper and zinc in industrial effluents.

***Acknowledgements**: The authors gratefully acknowledge helpful discussions with Prof. V. Keshavan, retired Professor of Chemistry, RIE, Mysore. Mr. J. Kodiyan, Chief technician, SAF, Kuwait University, Kuwait is thanked for the analysis. Dr. G. R. Prakash, Reader in Chemistry and Principal Prof. G. T. Bhandage RIE, Mysore are thanked for their continuous encouragement.*

REFERENCES

1. K. Shanthalakshmi, S. L. Belagali, *Res. J. Chem. Environ*., 12, 59 (2008).
2. M. Furukawa, *Anal. Chim. Acta,* **140**, 281 (1982).
3. K. Veda, D. Yamamoto, *Microchim. Acta*, 103, (1984),
4. T. Katami, T. Hayakawa, M. Furukawa, S. Shibata. *Analyst*, **109**, 1511 (1984).
5. K. Ohshita, H. Wada, G. Nakagawa, *Anal. Chim. Acta*, **176**, 41 (1985).
6. T. Katami, T. Hayakawa, M. Furukawa, S. Shibata. *Analyst*, **110**, 399 (1985).
7. K. Grudpan, C. G. Taylor, *Talanta*, **36**, 1005 (1989).

8. M. S. Abu-Bakr, A. S. EI-Shahawy, A. M. Seddique, *J. Solution Chem*., **22**, 663 (1993).
9. M. Fenggin, L. Junyu, X. Zhongmei, D. Hongguang, Q. Dayong, *Huaxue Shiji*, **17**, 371 (1995); *CA* **123**, 305474.
10. M. Carvalho, I. C. S. Fraga, K. C. M. Neto, E. Q. S. Filho, *Talanta*, **43**, 1675 (1996).
11. Z.-L. Ma, Y.-P. Wang, C.-X. Wang, F.-Z. Miao, W.-X. Ma, *Talanta,* **44**, 743 (1997).
12. Z. Jiaoqiang, F. Xuezhong, L. Hengchuan, L. Jianyan, *Huaxue Fence*, **35**, 195 (1999); *CA,* **131**, 153163.
13. T. Yan, S. Youqin, L. Jianyan, *Huaxue Fence*, **36**, 370 (2000); *CA*, **133**, 275617.
14. G. Ancheng, Z. Youxian, L. Tao, Z. Xiaoen, Z. Mingjun, Z. Wenyan, L. Jianyan, *Huaxue Fence*, **36**, 259 (2000); *CA,* **133**, 129291.
15. H.-W. Gao, C.-L. Hong, S.-R. Shi, *Asian J. Chem.*, **13**, 1071 (2001).
16. V. A. Lemos, S. L. C. Ferreira, *Anal. Chim. Acta*, **441**, 281 (2001).
17. E. Y. Hashem, M. S. Abu-Bakr, S. M. Hussain, *Spectrochim. Acta, Part A*., **59**, 761 (2003).
18. A. S. Amin, *Quim. Analitica*, **20**, 145, (2001).
19. S.-L. Zhao, X.-Q. Qiao., J.-D. Guangpu, *Shiyanshi*, **19**, 512 (2002).
20. E. Y Hashem, M. S. Abu-Bakr, S. M. Hussain, *Spectrochim. Acta, Part A.,* **59**, 761 (2003).
21. C. Lu, X. Zhang, *Fenxi Ceshi Xuebao*, **23**, 96 (2004); *CA*, **144**, 456735.
22. V. A. Lemos, J. S. Santos, P. Baliza, *J. Braz. Chem. Soc*., **17**, 30 (2006).
23. H. R. Snyder (ed.), Organic Synthesis, John Wiley and Sons, London, 1948, p. 89.
24. Von Theodor Papenfuchs, *Angew. Chem. - Suppl.*, **21**, 1155 (1982).
25. D. Held, USA Patent 5374737 (1994).

СИНТЕЗ И СПЕКТРОФОТОМЕТРИЧНИ ИЗСЛЕДВАНИЯ НА НЯКОИ БЕНЗОТИАЗОЛИЛАЗО-БАГРИЛА – ОПРЕДЕЛЯНА НА МЕД, ЦИНК, КАДМИЙ, КОБАЛТ И НИКЕЛ

К. Шанталакшми*, С. Л. Белагали

Департамент за научни изследвания на околната среда, Университет на Майсур, Майсур 570006, Карнатака, Индия

Постъпила на 5 януари 2009 г.; Преработена на 6 май 2009 г.

(Резюме)

Синтезирани са 4-(2-бензотиазолилазо)-2-амино-3-хидроксипиридин и производните му 4-(4-метил-2-бензотиазолилазо), 4-(6-хлоро-2-бензотиазолилазо) и 4-(6-бромо-2-бензотиазолилазо)-2-амино-3-хидроксипиридини. Всички тези багрила са много чувствителни хромогенни реагенти за определяне на мед, кадмий, цинк, кобалт и никел. Реагентите взиамодействат с металните йони с образуване на пурпурно оцветен комплекс (λ_{max} 540−570 nm) във воден разтвор на ацетон с pH в областта 2.8–4.6. Медта може да бъде определена селективно при pH 2.8 и повечето от металните йони не пречат освен за никел и кобалт. Кадмий, цинк, кобалт и никел могат да бъдат определени при pH 4–5. Тяхното взаимно пречене може да бъде елиминирано с използване на подходящи маскиращи реагенти. Допълнително предимство на метода е че процедурата на екстракция не е необходима и процедурата за анализ е много опростена.

Bulgarian Chemical Communications, Volume 41, Number 4 (pp. 385–390) 2009

Degradation mechanism of diazo dyes by photo-Fenton-like process: Influence of various reaction parameters on the degradation kinetics

L. G. Devi*, K. S. A. Raju, K. E. Rajashekhar, S. G. Kumar

Department of Post Graduate Studies in Chemistry, Central College Campus, Dr. B. R. Ambedkar Veedi, Bangalore University, Bangalore-560 001, India

Received January 19, 2009; Revised May 7, 2009

The degradation of diazo dyes Brilliant Yellow (BY) and Bismark Brown (BB) was investigated by the photo-Fenton-like process Fe^{2+}/ammonium persulphate (APS)/UV in acidic pH medium. The influence of various reaction parameters like pH, concentration of Fe^{2+} ions/APS, structure of the dye and effect of radical scavenger on the degradation kinetics is reported. The rate constant (k), catalytic efficiency (k_c) and process efficiency (Φ) are evaluated at different concentrations of Fe^{2+} ions. It was found out that the BB degrades at a faster rate than BY. The degradation process was followed by GC-MS technique. The results show that the initial step in the degradation of BB involves direct oxidation of azo chromophore, while in the case of BY the initial step is oxidation of azo group followed by the oxidation of ethylenic chromophore. Based on the obtained intermediates, probable degradation mechanism has been proposed. The results show that photo-Fenton-like process could be a useful and efficient technology for the mineralization of diazo dyes at lower concentrations of iron in acidic medium.

Key words: photo-Fenton-like process, ammonium persulphate, diazo dyes, GC-MS analysis.

INTRODUCTION

The textile industry produces large quantities of effluents that contain significant concentrations of organic matter. The coloured waste water is directly discharged into the rivers and other water ways. Traditional methods like adsorption on activated carbon, liquid-liquid extraction, ion-exchange, air or stream stripping, *etc*., are ineffective on refractory and non-volatile pollutants and have another dis-advantage as they simply transfer the pollutants from one phase to another. Hypochlorite oxidations and UV/H_2O_2 or UV/O_3 processes are found to be efficient methods for decolourisation, but they are not desirable due to the high cost of equipment and the secondary pollution arising from the residual chlorine, which further complicates the process. Photo-Fenton process is considered as a promising method for the treatment of wastewater containing dyes [1−5]. It is based on the reaction of Fe^{2+} ions and H_2O_2 under UV illumination for the generation of hydroxyl radicals *in situ*. Hydroxyl radicals are strongly potent oxidizing agent that can mineralize all organic contaminants to CO_2 and H_2O. However, the removal of sludge, containing iron ions, at the end of wastewater treatment is costly and requires large amount of chemicals and manpower [6]. Although H_2O_2 is extensively used as an oxidant in the classical photo-Fenton process, little attempt is made for the use of peroxy disulphate as oxidant. In view of this, the present research work highlights the utility of peroxy disulphate, which is termed as photo-Fenton-like process for the degradation of diazo dyes Brilliant Yellow (BY) and Bismark Brown (BB) at low iron concentration. Azo dyes are not biodegradable by aerobic treatment process [7]. Under anaerobic conditions, they can be decolorized by the reduction of azo bond [8] and the resulting fragment is aromatic amines, which are potentially carcinogenic [9]. Therefore, its mineralization by photo-Fenton-like process is simple, cost effective and important.

MATERIALS AND METHODS

Materials

BY, BB, ammonium persulphate (APS), methyl alcohol, ferrous oxalate, sodium hydroxide and sulphuric acid were supplied from S D Fine Chemicals, Bombay, India and were used as received. The molecular formulae of BB and BY are $C_{18}H_{20}Cl_2N_8$ {(4,4-(1,3-phenylene-bis(azo))bis-1,3-benzenediamine dihydrochloride} and $C_{26}H_{18}N_2Na_2O_8S_2$ {2,2[1]-(1,2-ethenediyl)-bis[5-[(4-hydroxyphenyl)azo}-benzene sulphonic acid disodium salt} respectively. The structures of the dyes are given in the Schemes 1 and 2.

* To whom all correspondence should be sent:
E-mail: gomatidevi_naik@yahoo.co.in

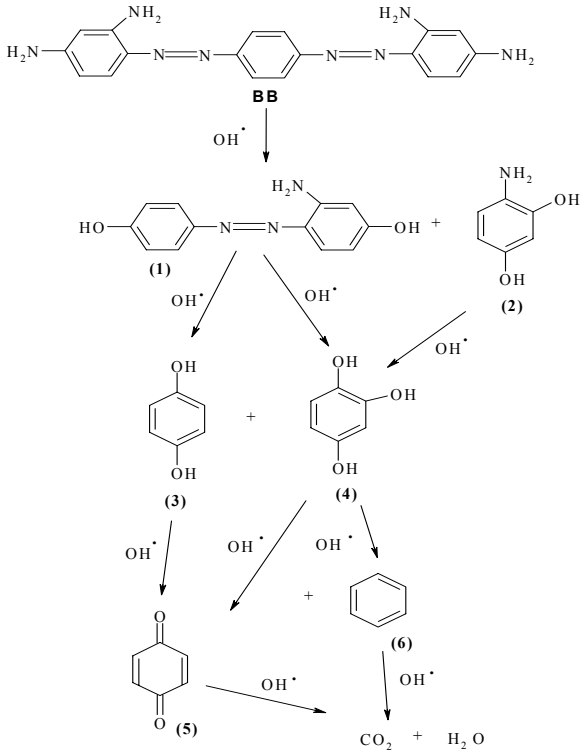

Scheme 1. Probable degradation pathway for BB.

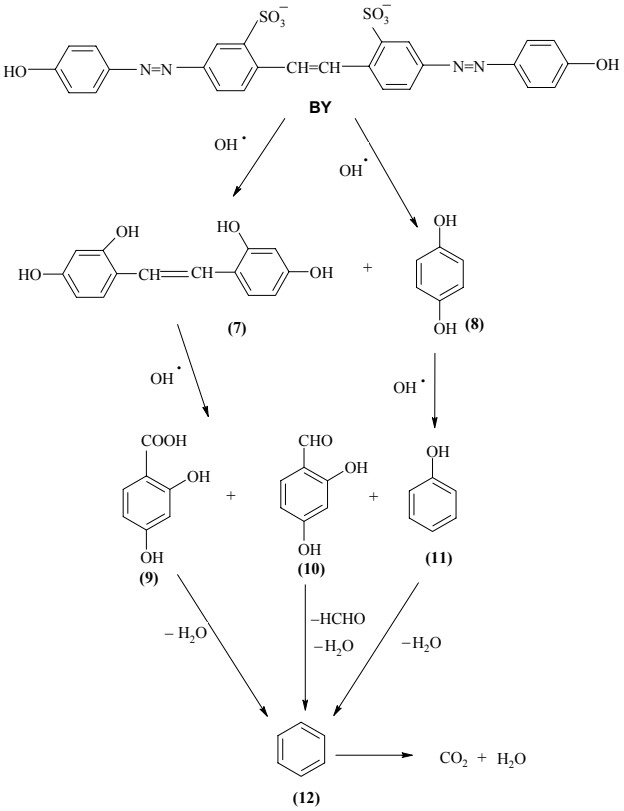

Scheme 2. Probable degradation pathway for BY.

Experimental setup

Artificial light source of 125 W medium pressure mercury vapour lamp with a photon flux of 7.75 mW/cm^2 (as determined by ferrioxalate actinometry) is used whose wavelength of emission is around 350–400 nm**.** In a typical experiment, 10 ppm dye solution is placed in a glass reactor whose surface area is 176 cm^2 and the required concentration of Fe^{2+} ions and APS are added. The light is directly focused on the solution at a distance of 29 cm in the presence of atmospheric oxygen as it is shown in Fig. 1.

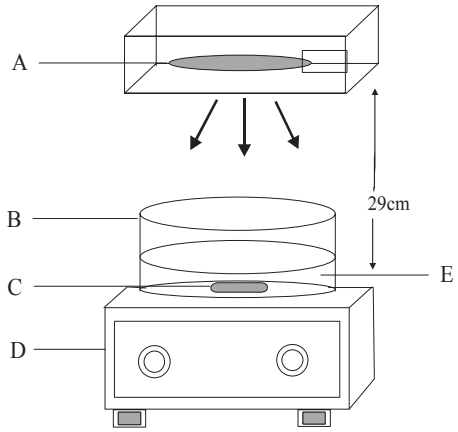

Fig. 1. Schematic illustration of experimental setup used for UV irradiation.
A - Medium pressure mercury vapour lamp; B - glass reactor; C - magnetic bit; D - magnetic stirrer; E - dye solution.

The pH value of the solution is adjusted either by adding dilute NaOH or H_2SO_4.

Analytical methods

Sample solutions (5 ml) were taken out of the reactor at definite time intervals and centrifuged. The centrifugates were analyzed by UV-visible spectroscopic technique using Shimadzu UV-1700 Pharmaspec UV-visible spectrophotometer. The centrifugates were extracted into non-aqueous medium and 1 μL was subjected to GC-MS analysis (using GC-MS-QP-5000 Shimadzu) and Thermo Electron Trace GC Ultra, coupled to a DSQ mass spectrometer, equipped with an Alltech ECONO-CAP-EC-5 capillary column (30 m, 0.25 mm i.d., 0.25 mm film thickness) was used. Pure helium was used as the carrier gas at a flow rate of 1.2 ml/min. The injector/transfer line/trap temperatures were kept at 220/250/200°C respectively. Electron impact ionization was carried out at 70 eV.

RESULTS AND DISCUSSION

Photo-Fenton reaction of Fe^{2+} with $S_2O_8^{2-}$

Ferrous ions react with persulphate anion resulting in the formation of sulphate anion and sulphate radical are oxidized to ferric ions [10].

$$Fe^{2+} + S_2O_8^{2-} \rightarrow Fe^{3+} + SO_4^{2-} + SO_4^{-\bullet} \quad (1)$$

Ferric ion can also react with persulphate ion generating two sulphate radicals, being reduced to ferrous ion:

$$Fe^{3+} + S_2O_8^{2-} \rightarrow 2SO_4^{-\bullet} + Fe^{2+} \quad (2)$$

The sulphate radicals, produced in the above reactions, can react with water molecules to generate the highly oxidative hydroxyl radicals:

$$SO_4^{-\bullet} + H_2O \rightarrow SO_4^{2-} + OH^{\bullet} + H^+ \quad (3)$$

This cyclic process leads to a continuous generation of free radicals, which activates the degradation mechanism. To compare the efficiency of photo-Fenton-like process with the real Fenton process, the experiments were conducted in the dark. Only 12 and 4% of BB and BY respectively were degraded in the dark with Fe^{2+} ions as the catalyst and APS as an oxidant. The complete mineralization could be achieved in 60 and 90 minutes by photo-Fenton-like process under UV illumination for BB and BY respectively. This is due to the fact that Fe^{2+} ions can be oxidized to Fe^{3+} in the presence of APS even in the dark. But the reverse reduction process of Fe^{3+} ion is slow and rate determining step in the dark, which limits the efficiency of the process. Under UV light, the reverse photoreduction of Fe^{3+} ions takes place at a faster rate as it is shown in Equation (4) [5]. The photoreduced Fe^{2+} ions can participate actively in the cyclic Fenton reactions generating excess oxidative free radicals enhancing the degradation rate.

$$Fe^{3+} + h\nu \leftrightarrow Fe^{2+} \quad (4)$$

Direct photolysis of the oxidants additionally contributes to the overall enhancement of the process.

Effect of pH

The pH of the solution plays a significant role for the effective mineralization of pollutants by the Fenton's reagent. Kang *et al*. reported that photo-Fenton process is efficient and can degrade pollutants effectively only under acidic conditions [11], since higher pH values are reported to be unsatisfactory [12]. The degradation of the dye was carried out in the pH range 1.0−9.0 by maintaining constant concentration of Fe^{2+} ions and APS. At lower pH 1.0, the degradation rate is reduced due to the presence of excess H^+ ions in the solution, which can act as hydroxyl radicals scavenger according to Eqn. (5) [13].

$$H^+ + OH^{\bullet} + e^- \rightarrow H_2O \quad (5)$$

When the pH of the medium is increased from 1.0 to 3.0 complete mineralization of both dyes was achieved. This is due to the fact that at pH 3, half of the iron species exist as Fe^{3+} ions and the other half as complex ion $Fe[OH]^{2+}(H_2O)_5$. Both are dominant photo active species that possess highest light absorption coefficient and give high yield of hydroxyl radicals along with Fe^{2+} ions in the wavelength range of 280−370 nm [14]. The change in this optimum pH leads to the decrease in the concentration of $Fe[OH]^{2+}$ complexes and it can also result in the precipitation of ferrous ion as oxy-hydroxides. The various photoactive species of iron, formed under different pH conditions, are $Fe[H_2O]_6^{3+}$ (pH 1−2), $Fe[OH][H_2O]_5^{2+}$ (pH 2−3) and $Fe[OH]_2[H_2O]_4^+$ (pH 3−4) [15]. Beyond this optimum pH (pH ≈ 3), the degradation rate decreases. This inefficiency at higher pH values may be due to the instability of Fe^{2+}/Fe^{3+} ions, since they precipitate as iron oxy-hydroxide, which reduces the concentration of hydroxyl radicals in the solution thus affecting the degradation rate.

Effect of Fe^{2+} dosage

The influence of Fe^{2+} ion on the degradation kinetics is investigated by maintaining the other reaction parameters constant. When the concentration of Fe^{2+} ions is increased from 5 to 15 ppm, due to the excess generation of hydroxyl radicals the rate constant of the degradation increases for both dyes (Tables 1 and 2). With further increase in the concentration (30 ppm) the degradation rate decreases. This is because excess of Fe^{2+} ions, produced by the photo reduction of Fe^{3+} ions in the solution, compete for the hydroxyl radicals along with the dye molecules and act as hydroxyl radical scavenger [13].

$$Fe^{2+} + OH^{\bullet} \rightarrow Fe^{3+} + OH^- \quad (6)$$

The above process reduces the concentration of hydroxyl radicals in the solution and hence the degradation rate also decreases. Moreover, it is better to optimize the photo-Fenton's process at lower iron concentration in order to avoid the sludge production resulting from the iron complexes.

The efficiency of the catalyst is calculated by the term catalytic efficiency (k_c), which is a kinetic parameter, calculated using Eqn. (7):

$$k_c = \frac{k^1 - k_0}{[Fe^{2+}]^n} \quad (7)$$

Where k_c is the catalytic efficiency, k^1 is the rate constant of the reaction in the presence of catalyst, k_0 is the rate constant of the reaction in the absence

of catalyst, n is the order of the reaction (n = 1) and $[Fe^{2+}]$ is the concentration of the catalyst used.

Table 1. Rate constant, catalytic efficiency and process efficiency at different concentrations of Fe^{2+} ions for the degradation of BB.

$[Fe^{2+}]$, ppm	Rate constant (k) from $-\log(C/C_0)$ vs. time plot, $(\times 10^{-2})$ min^{-1}	Catalytic efficiency (k_c), $ppm^{-1} \cdot min^{-1}$	Process efficiency (Φ), $(\times 10^{-12})$ ppm $Einstein^{-1}$
5	1.1	1.05	16.5
10	1.7	1.67	24.3
15	0.96	0.94	17.4
20	0.7	0.68	13.3
30	0.52	0.51	9.8
0 (k_0)	0.26	-	

Table 2. Rate constant, catalytic efficiency and process efficiency at different concentrations of Fe^{2+} ions for the degradation of BY.

$[Fe^{2+}]$, ppm	Rate constant (k) from $-\log(C/C_0)$ vs. time plot, min^{-1}	Catalytic efficiency (k_c), ppm^{-1} min^{-1}	Process efficiency (Φ), $(\times 10^{-12})$ ppm $Einstein^{-1}$
5	0.64	0.58	8.4
10	1.12	1.09	16.2
15	0.78	0.76	8.8
20	0.48	0.46	5.2
30	0.36	0.35	3.6
0 (k_0)	0.26	-	

The effectiveness of the process is calculated by process efficiency (Φ). Φ is defined as the change in concentration divided by the amount of energy in terms of intensity and exposure of surface area per unit of time.

$$\Phi = \frac{C_0 - C}{t.I.S} \quad (8)$$

C_0 is the initial concentration of the dye and C is the concentration at moment t and (C_0–C) denotes the concentration of the dye degraded in ppm. I is the irradiation intensity [I = Einstein/$m^2 \cdot s = 8.36 \times \lambda$ (nm) × Power (Watt)] (where λ is 370 nm and Power is 125 W). S denotes the solution irradiated plane surface area in cm^2 and t represents the irradiation time interval in minutes. The values obtained for k, k_c and Φ suggests that the present experimental conditions, used for the degradation, are efficient at lower concentration of iron. The rate constant calculated for the degradation of BB under optimized conditions is 1.5 times higher than that of BY degradation. This is due to the presence of four bulky aromatic rings and the ethylenic chromophore, which takes longer time interval for complete mineralization.

Effect of oxidizing agent

The present study investigates the application of peroxy disulphate ($S_2O_8^{2-}$), which is a symmetrical peroxide and it can be a potential oxidant in the light induced reaction processes. Persulphate can also generate free radicals like sulphate and hydroxyl radicals, which enable free radical mechanism similar to hydroxyl radical pathways generated in the classical Fenton's chemistry. Sulphate radical is one of the strongest oxidizing species in aqueous media with an oxidation potential of 2.6 V. It is inferior only to the hydroxyl free radical, whose oxidation potential is 2.8 V. When the concentration of APS was increased from 10 to 20 ppm, the degradation rate increased (Fig. 2).

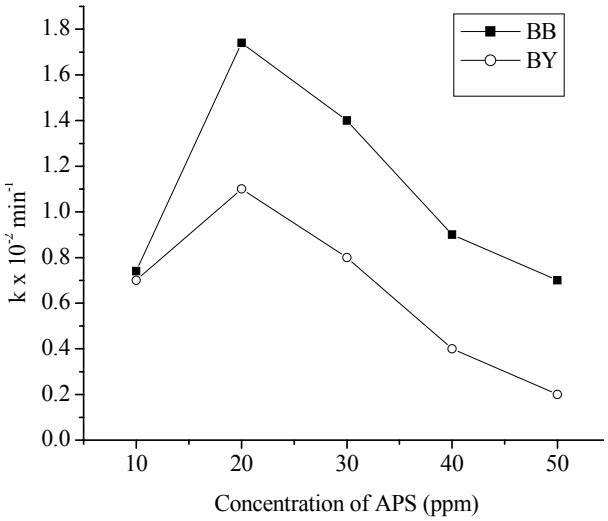

Fig. 2. Dependence of rate constant on concentration of APS (ppm) for both BB and BY.

This is due to the generation of excess sulphate radicals, which in turn can produce higher number of hydroxyl radicals during reaction with water molecules (Eqn. (3)). Upon further increase in the concentration of APS the degradation rate decreases. The excess hydroxyl radicals generated might undergo recombination reaction or may take part in the unwanted reaction pathways:

$$OH^{\bullet} + OH^{\bullet} \rightarrow H_2O_2 \quad (9).$$

Further APS generates protons, along with the hydroxyl radicals, as it is shown in the Eqn. (3). Since the reaction was carried out in acidic pH medium, the generated protons further lower the pH of the reaction medium, which exerts negative effect on the degradation rate (Eqn. 6). Hence, the rate constant decreases at higher concentration of APS.

Effect of hydroxyl radical scavenger

The role of hydroxyl radicals in the degradation mechanism of the photo-Fenton process is confirmed by carrying out the experiment in the presence of hydroxyl radical scavenger like methyl alcohol. Methyl alcohol is known to deactivate hydroxyl radical and its derivatives [10]. Methanol reacts with hydroxyl radical and to a smaller extent with hydrogen radical, whose second order rate constants are 9.7×10^8 $mol^{-1}\cdot sec^{-1}$ and 2.6×10^6 $mol^{-1}\cdot sec^{-1}$, respectively (Eqns. (10), (11)).

$$CH_3OH + {}^{\bullet}OH \rightarrow CH_3O^{\bullet} + H_2O \quad (10)$$

$$CH_3OH + {}^{\bullet}H \rightarrow CH_3O^{\bullet} + H_2 \quad (11)$$

When the concentration of methyl alcohol is increased from 0.05 to 0.125 M, the rate constant decreases gradually and then it remains constant (Fig. 3). This is due to the inability of methyl alcohol to deactivate sulphate radicals. The sulphate radical produced in the case of APS shows the following possible reaction mechanisms in the process of mineralization: (i) Abstraction of hydrogen atom from the saturated carbon. (ii) The former is capable of adding to the unsaturated compounds. (iii) It can remove an electron from anions and neutral molecules [10, 16]. This provides evidence for the role of hydroxyl radical in the photodegradation process.

GC-MS analysis

Degradation of BB. The BB solution containing Fe^{2+} ions and APS on UV irradiation for 15 minutes showed two m/z peaks at 229 and 125 corresponding to the formation of 2-amino-4,4^1-dihydroxyazobenzene (**1**) and 4-aminocatechol (**2**). This suggests that the degradation of BB proceeds through the cleavage of one azo group and the hydroxylation of a terminal amine group ($-NH_2$). The solution after 30 minutes of irradiation shows two m/z peaks of 110 and 142 due to the formation of hydroquinone (**3**) and 1,2,4-benzenetriol (**4**). The attack of hydroxyl radical on the site of C–N bond and substitution of $-NH_2$ by –OH group in the intermediate (**1**) leads to the formation of (**3**) and (**4**). The intermediate (**2**) can also result in (**4**) upon the replacement of $-NH_2$ group by –OH. After 45 minutes of illumination, the mass spectra showed m/z peaks at 108 and 78 of high intensity due to the formation of *p*-benzoquinone (**5**) and benzene (**6**). The subsequent dehydroxylation of intermediates (**3**) and (**4**) can result in the formation of benzene (**6**). The oxidation of intermediates (**3**) results in compound (**5**). The other peaks of lower intensity 101, 94, 74, 56 and 43 were not accounted. After 60 minutes, no characteristic m/z peak of any functional group appeared, which confirms the complete mineralization.

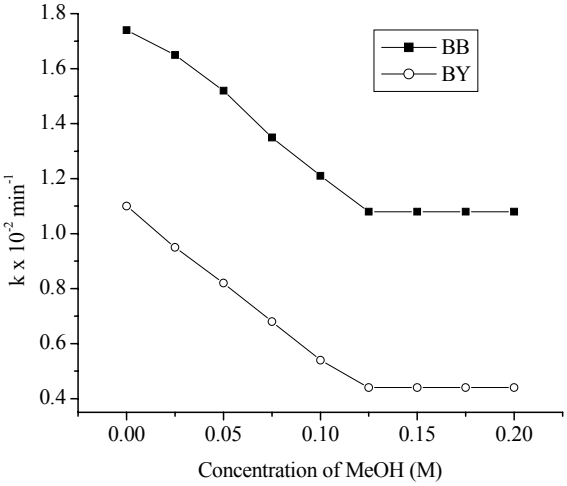

Fig. 3. Dependence of rate constant on concentration of MeOH (Molar) for both BB and BY.

Degradation of BY. The BY solution containing Fe^{2+} ions and APS on UV irradiation for 30 minutes showed m/z peaks at 244 and 110, corresponding to the formation of 2,4,2^1,4^1-tetrahydroxy stilbene (**7**) and hydroquinone (**8**). This indicates that the initial mechanism in the degradation of BY involves the cleavage of two azo groups since the C-N bond is more susceptible to free radicals attack, compared to the C-C bond. The sulphonate group moiety might be eliminated as sulphuric acid. After 60 minutes of irradiation, m/z peaks at 154, 138 and 94 appear which correspond to the formation of 2,4-dihydroxy benzoic acid (**9**), 2,4-dihydroxy bezaldehyde (**10**) and phenol (**11**). This suggests that the degradation at the later stages involves the oxidation of ethylenic chromophore to aldehyde and carboxylic acid respectively. The dehydroxylation of intermediate (**8**) results in compound (**11**). After 75 minutes of irradiation mass spectra showed intense m/z peak at 78 corresponding to the formation of benzene (**12**). The loss of substituent groups in the intermediates (**9**), (**10**) and (**11**) might result in the formation of benzene as it is shown in Scheme 2. At 90 minutes of UV irradiation, no characteristic peaks are observed in mass spectra confirming the complete mineralization of BY.

CONCLUSION

The degradation of two diazo dyes BB and BY was carried out using photo-Fenton-like process under acidic pH 3 and optimum conditions of the experiment. The rate constant, catalytic efficiency and process efficiency for both degradation processes have been calculated. The decrease in the

rate constant in the presence of methanol confirmed the role of hydroxyl radicals in the degradation mechanism. The degradation was followed by GC-MS technique. The results show that the initial step in the degradation of BB involves direct oxidation of azo chromophore, while in the case of BY, the oxidation of the azo group is followed by oxidation of ethylenic chromophore. A probable degradation mechanism has been proposed based on the obtained intermediates.

***Acknowledgements**: Financial assistance by UGC Major Research Project (2007-2010) is greatly acknowledged.*

REFERENCES

1. N. Daneshvar, A. R. Khatee*, J. Environ. Sci. Health, Part A*., **41**, 31 (2006).
2. X.-K. Zhao, G.-P. Yang, Y.-J. Wang, X.-C. Gao, *J. Photochem. Photobiol., A.,* **161**, 215 (2004).
3. H. Kusic, N. Koprivanac, A. L. Bozic, I. Selanec, *J. Hazard. Mater.,* **136**, 632 (2006).
4. H. Katsumata, S. Kawabe, S. Kaneco, T. Suzuki, K. Ohta, *J. Photochem. Photobiol. A.,* **162**, 297 (2004).
5. K. Ntampegliotis, A. Riga, V. Karayannis, V. Bontozoglou, G. Papaolymerou, *J. Hazard. Mater*., **136**, 75 (2006).
6. I. Muthuvel, M. Swaminathan, *Catal. Commun.,* **8***,* 981 (2007).
7. U. Pagga, D. Brown, *Chemosphere,* **15**, 479 (1986).
8. D. Brown, B. Hamburger, *Chemosphere,* **16**, 1539 (1987).
9. G. L. Baughman, E. J. Weber*, Environ. Sci. Technol.,* **28**, 26 (1994).
10. L. G. Devi, S. G. Kumar, K. M. Reddy, C. Munikrishnappa*, J. Hazard. Mater*., **164**, 459 (2009).
11. S. F. Kang, C. H. Liao, M. C. Chen, *Chemosphere,* **46**, 923 (2002).
12. S. F. Kang, C. H. Liao, S. Po, *Chemosphere,* **41**, 1287 (2000).
13. K. Barbusinski, J. Majewski, *Pol. J. Environ. Stud.,* **12**, 151 (2003).
14. H. J. Benkelberg, P. Warneck, *J. Phys. Chem.,* **99**, 5214 (1995).
15. M. Neamtu, A. Yediler, I. Siminiceanu, A. Kettrup, *J. Photochem. Photobiol., A.,* **161**, 87 (2003).
16. P. Neta, V. Madhavan, H. Zemel, R. W. Fessemdem, *J. Am. Chem. Soc.,* **99**, 163 (1977).

МЕХАНИЗЪМ НА ФОТОХИМИЧНО РАЗЛАГАНЕ НА ДИАЗОБАГРИЛА ПО РЕАКЦИЯ НА ФЕНТЪН: ВЛИЯНИЕ НА РАЗЛИЧНИ РЕАКЦИОННИ ПАРАМЕТРИ ВЪРХУ КИНЕТИКАТА НА РАЗЛАГАНЕ

Л. Г. Деви, К. С. А. Раджу, К. Е. Раджашекар, С. Г. Кумар

Департамент по химия, Колеж Д-р Б. Р. Амбедкар Вееди, Университет на Бангалор, Бангалор 560001, Индия

Постъпила на 19 януари 2009 г.; Преработена на 7 май 2009 г.

(Резюме)

Изследвано е фотохимично разлагане на диазобагрила Брилятно жълто (BY) и Бисмарково кафяво (BB) по реакцията на Фентън Fe^{2+}/амониев персулфат (APS) в кисела среда. Представено е влиянието на различни реакционни параметри като pH, концентрация на Fe^{2+}/APS, структура на багрилото и ефекта от улавяне на радикалите върху кинетиката на разлагане. Определени са скоростната константа (k), каталитичната ефективност (k_c) и ефективността на процеса (Φ) при различни концентрации на Fe^{2+} йони. Намерено е, че Бисмарково кафяво (BB) се разлага с по-голяма скорост от Брилятно жълто (BY). Процесът на разлагане е изследван с газова хроматография и масспектрален анализ. Резултатите показват, че началния стадий в разлагането на (BB) включва пряко окисление от азохромофора докато при BY началният стадий е окисление на азо-групата последвано от окисление на етиленовия хромофор. Предложен е вероятен механизъм на разлагане на основата на получените междинни прозукти. Резултатите показват, че фотохимичния процес по реакцията на Фентън може да бъде полезна и ефикасна технология за минерализация на диазобагрила при ниски концентрации на желязо в кисела среда.

Bulgarian Chemical Communications, Volume 41, Number 4 (pp. 391–396) 2009

Analysis of oxycellulose obtained by partial oxidation with different reagents

Sv. M. Diankova*, M. D. Doneva

Institute of Cryobiology and Food Technologies, 53 Cherni Vrah Blvd., 1407 Sofia, Bulgaria

Received February 24, 2009; Revised April 21, 2009

The object of the present work was to study the possibilities for activating of dressings of cellulose and synthetic fibre by a partial oxidation with sodium hypochlorite, hydrogen peroxide and sodium periodate and to investigate the effect of the reaction parameters on the quantitative content of aldehyde groups in the obtained product.

Textile dressings of cellulose and synthetic fiber were treated with oxidizing solutions of sodium hypochlorite, hydrogen peroxide and sodium periodate with an aim to modify the material and form aldehyde groups in the cellulose molecule. The highest values of the copper number and content of aldehyde groups indexes were obtained for pure cellulose treated with sodium periodate solutions. The obtained textile materials could be used as carriers for immobilization of proteolytic enzymes to achieve a biologically active dressing.

Key words: cellulose, copper number, aldehyde groups, oxidation, dressings.

INTRODUCTION

Cellulose, probably the most abundant biopolymer in the world, is present in all higher plants and exists in its purest form in cotton fiber. The materials of natural cellulose fibre still have a major application in medicine as conventional linters and textile dressings that provide for a passive protection of wounds and have a number of advantages: mechanical strength, high absorption capacity, accessibility with respect to sources and price, good physiological endurance and others. The disadvantages that are known: adhering to the wound surface and injuring of the newly formed epithelium when changing the dressings, lack of therapeutic effect for stimulation of the wound healing process, lack of hemostatic and antibacterial action, can be eliminated by structural or chemical modification of the cellulose materials.

The modification of the cellulose materials allows the obtaining of new products from natural cellulose materials. An example of a structural modification is the microcrystalline cellulose widely applied in the food and pharmaceutical industries. Variety of products with different properties and application can be obtained by chemical modification of the cellulose – nitro derivatives, cellulose esters, acetates, xanthogenates and others. The diethylaminoethylcellulose (DEAE-cellulose) and the carboxymethylcellulose (CMC) are widely used in the laboratory practice as ion-exchange substances.

In the case of dressings, a certain percentage of functional groups can be introduced by chemical modification, without disruption of the fibre structure and with preservation of the basic structural-mechanical properties and characteristics of the material. The activated textile materials are fit to be used as carriers of different biologically active components - enzymes, stimulators of the regeneration and epithelization or antibacterial agents [3, 11]. In such a way, the conventional dressings acquire new properties and as a result of this they effectively improve the wound microenvironment and create favourable healing conditions [12]. The immobilization of proteolytic enzymes, (trypsin, chymotrypsin, collagenases, lysozyme, plasmin, papain, bromeline, microbial proteases and others) on the dressing material has a favourable effect for debridement of the wounds [2, 4]. There are different methods for immobilization of the enzymes on cellulose or its derivatives: adsorption on cellulose derivatives with ion-exchange properties (*e.g.* DEAE-cellulose); formation of chelate complexes with cellulose or cellulose derivatives, activated by metal ions; covalent connection [1]. The activating of the carrier prior to the covalent bonding immobilization can be realized in different ways: interaction of the cellulose with cyanogen bromide, through glutaraldehyde and aminoethylcellulose; by using of triazine method; by azide method with carboxymethylcellulose, and others.

In view of its chemical structure the cellulose represents β-1,4-D-glucan. The native cellulose is a typical linear homopolysaccharide consisting β-(1→4) linked D-glucose units *n* (Fig. 1). In the

* To whom all correspondence should be sent:
E-mail: svetla.diankova@ikht.bg

native fibres *n* is from 10 000 to 14 000 and in the purified cellulose it is from 1000 to 3000. The polyanhydroglucose chain is sensitive to certain influences and it is partially interrupted in the process of purification. A multitude of hydrogen bond connections between the separate polymer chains in the cellulose fibrils determines the high stability, tensile strength and low solubility of the cellulose.

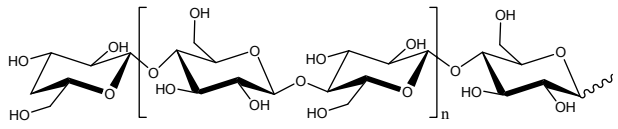

Fig. 1. Chemical structure of cellulose.

The cellulose content in the cotton fibres is 90−98%. After purifying, defatting, bleaching and deviling the raw material a product with all the basic properties of cellulose is obtained, the most important property, with an application in medicine, being its great hygroscopic capacity. The cotton can absorb water and liquids exceeding several times its own weight that justifies its usage as a dressing material and styptic for small wounds. The cotton-based dressings drain the wound, absorb toxins, protect the wound surface from infection and prevent the unnecessary loss of moisture, and after chemical modification and activation, they can serve as carriers of biologically active substances. The choice of the method of activation depends on the structure and the texture of the material, thickness and number of the filament doublings, textile density and other factors.

The partial oxidation of the hydroxyl groups is one of the most widely used methods for activation of cellulose materials. In the process of oxidation aldehyde, ketone and carboxyl groups can be formed, depending on the nature of the oxidizer and the parameters of the process. The sodium hypochlorite, for example, is a non-specific oxidizer and the relative content of the obtained aldehyde, ketone and carboxyl groups depends on pH of the reaction medium [6]. The chloric acid oxidizes the aldehyde groups to carboxyl, with no impact on the hydroxyl groups, while the selective oxidation using nitrogen (IV) oxyde gives carboxyl group at C6. The oxidizing effect of the hydrogen peroxide on cellulose is comparatively weaker, but still induces a transformation of part of the cellulose molecules into oxycellulose [10]. The alkaline salts of the periodic acid oxidize specifically the cellulose through a disruption of the glucopyranose ring at C2-C3 position forming two aldehyde groups per monomer unit [2]. A highly reactive product – dialdehyde cellulose is obtained. However, the introducing of a higher percentage of aldehyde groups in C2-C3 position increases the propensity to hydrolysis in an alkaline medium and decreases the degree of polymerization of the cellulose molecules (Fig. 2).

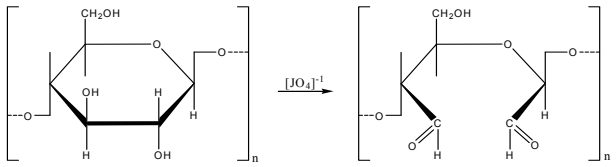

cellulose dialdehydecellulose

Fig. 2. Obtaining of dialdehyde cellulose.

Activated textile and other cellulose materials, containing aldehyde groups, have been used as carriers for covalent immobilization of biologically active components, incl. enzymes [3]. It has been assumed that the forming of covalent bond occurs between the aldehyde groups and the amino groups of the polypeptide chain.

The object of the present work was to study the possibilities for activating of dressings of cellulose and synthetic fibre, by oxidation with sodium hypochlorite, hydrogen peroxide or sodium periodate and to investigate the effect of the reaction parameters on the content of reactive aldehyde groups in the obtained product.

EXPERIMENTAL

Materials

Experiments with three types of textiles were carried out: gauze compresses and knitted bandage, containing pure cotton fibres and unwoven textile of viscose/polyester. All reagents and chemicals used were of p.a. quality (Merck).

Activation of the textile carriers

The textile materials were preliminary treated with a 14% NaOH solution. Sodium periodate, sodium hypochlorite in slightly acidic or alkaline solutions, and hydrogen peroxyde (Table 1) were used as activating agents.

Analyses of the activated textile

Spectrophotometric determination of copper number. Method according to Chai X. et al. [5]. Copper number is commonly defined as the number of grams of metallic copper (as Cu_2O) resulting from the reduction of $CuSO_4$ by 100 g of the cellulose fibres. The method is based on the reaction between reducing groups (mainly CHO) in the cellulose molecule and copper ions (Cu^{2+}).

Table 1. Options of treatment of textile materials.

No	Activating agent	Parameters			
		Concentration	pH	Temperature, °C	Time, h
I	Sodium hypochlorite solution	2 mg Cl/ml	9.0	20	24
	Sodium hypochlorite solution	5 mg Cl/ml	9.0	20	24
	Sodium hypochlorite solution	11 mg Cl/ml	9.0	20	24
II	Sodium hypochlorite solution	2 mg Cl/ml	5.5	20	24
	Sodium hypochlorite solution	3 mg Cl/ml	5.5	20	24
	Sodium hypochlorite solution	5 mg Cl/ml	5.5	20	24
III	Hydrogen peroxyde solution	4 .0%	9.5	90	24
	Hydrogen peroxyde solution	8.0%	9.5	90	24
	Hydrogen peroxyde solution	12.0%	9.5	90	24
IV	Sodium periodate solution	0.5%	3.0	20	7
	Sodium periodate solution	0.5%	3.0	20	24
	Sodium periodate solution	0.5%	3.0	20	42

Content of aldehyde groups in the oxidized cellulose – Iodometric method (according to TAPPI, T430). The method is based on the oxidation of aldehyde groups to carboxyl groups by iodine in alkaline media. In order to achieve a specificity of the reaction it is necessary to use a buffer solution with pH 9.3 to 9.5.

RESULTS AND DISCUSSION

The preliminary treatment of the textile materials with 14% sodium hydroxide solution results in hydrating and swelling of the cellulose fibres, which helps the oxidizing interaction of the material with the activating agent. Solutions of sodium hypochlorite, hydrogen peroxide and sodium periodate were used as activated agents. The technological parameters of the process and the oxidizer concentrations were varied in 4 sample series (Table 1).

The rate of oxidation of the experimental series activated textile and the content of the introduced aldehyde groups were analyzed in two ways: through spectrophotometric determination of copper number and by iodometric titration of the free aldehyde groups.

There are different methods for determining of carbonyl groups and parts of them are based on chemical reactions: oxidation, reduction and condensation. The oxidation by solutions of chlorous acid and iodine allows determining only the aldehyde groups in oxycellulose. The ketone groups do not react under these conditions. Under the reaction conditions mentioned in the Experimental section, the iodometric method is specific for aldehyde groups and it can be used for quantitative determination in oxycellose products.

In Tables 2–5 the experimentally established data of copper number and aldehyde groups content are shown for each separate type of textile material, after treating by the respective oxidizer.

It is known, that the copper number for the purified cotton is below 0.4−0.5. From the results in Tables 2 and 3 it is seen, that after a partial oxidation by sodium hypochlorite in acidic media, this index increases up to 18.93. The applied oxidizers (sodium hypochlorite and hydrogen peroxide) transform part of the hydroxyl groups in the cellulose fibres into carbonyl groups (aldehydes or ketones). In contrast to the sodium hypochlorite and the hydrogen peroxide, the sodium periodate is a strongly specific oxidizer for the cellulose that disrupts the glucopyranose ring at C2-C3 position and forms two aldehyde groups per monomer unit (Fig. 2). Because of this reason, the values for copper number in this series are higher and reach up to 24.74. The reaction intensity and the degree of oxidation depend on the type of the reagent and the parameters of the process.

Higher values of copper number are accounted for gauze compresses and knitted bandages, which are made of cellulose fibres. The results, obtained for unwoven textile, which contains a mixture of regenerated cellulose (viscose) and synthetic fibres, are much lower. In spite of the identical chemical composition, there are differences in the physical structure (degree of polymerization, location and orientation of the macromolecules) and in the physical-mechanical properties of the textile fibres from natural and regenerated cellulose. These differences appear also on the electronic microscope photos (Fig. 4).

In unwoven textile, the percentage of the cellulose component is much lower than that in the other investigated textile materials. These are the reasons that can explain the considerably weaker interaction of this material with all applied oxidizers.

The results in Table 2 and Table 3 show that the reaction of cellulose with sodium hypochlorite is strongly influenced by the pH. At the same con-

centration of free chlorine – 5.0 mg/ml, the copper number of the samples of cotton gauze increases from 3.53 (pH 9.0) to 18.93 (pH 5.5), *i.e*. the content of reducing groups in oxycellulose, obtained by oxidation in slightly acidic medium, is higher.

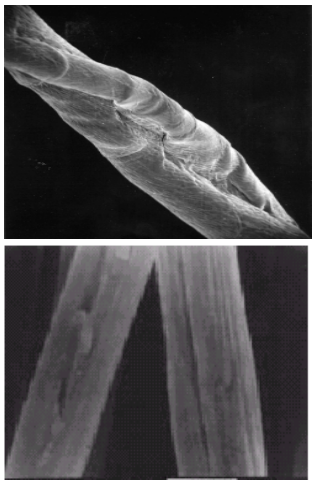

Fig. 4. Structure of textile fibers SEM: a - cotton; b - viscose.

Similar conclusions have been reached by Nevell and Singh who have also established that the reaction of hypochlorite oxidation of cellulose is influenced to the greatest extent by pH, than by the duration of the process [8].

The results from the analysis of the samples, treated by solutions of hydrogen peroxide in alkaline media are presented in Table 4. The copper number is much lower compared to the samples oxidized by sodium hypochlorite. The hydrogen peroxide is a non-specific oxidizer that attacks a lot of organic compounds and it is widely applied in the textile industry as a bleaching agent. Levin and Ettinger have studied the reaction between H_2O_2 and purified cotton fibres [7]. They have observed the action of the hydrogen peroxide in relation to pH and have established that in alkaline solutions a perhydroxyl radical is formed that oxidizes part of the hydroxyl groups at position C2 or C3. The obtained oxycellulose contains aldehyde and ketone groups, which are in β-position with respect to the glycoside bond.

Table 2. Copper number (g/100 g) and aldehyde groups (mmol/100 g) with different kinds of textile materials – oxidizer sodium hypochlorite, pH 9.0.

NaClO (pH 9.0) concentration	Gauze compress		Knitted bandage		Unwoven textile	
	Cu number g/100 g	CHO mmol/100 g	Cu number g/100 g	CHO mmol/100 g	Cu number g/100 g	CHO mmol/100 g
2 mg Cl /ml	2.78 ± 0.24	2.83 ± 0.07	0.47 ± 0.034	1.44 ± 0.09	0.209 ± 0.019	0.05 ± 0
5 mg Cl/ml	3.53 ± 0.46	3.62 ± 0.12	1.44 ± 0.072	2.10 ± 0.26	0.83 ± 0.027	0.11 ± 0
11 mg Cl /ml	5.67 ± 0.53	5.86 ± 0.18	4.14 ± 0.065	4.24 ± 0.21	1.09 ± 0.033	0.12 ± 0.01

Table 3. Copper number (g/100 g) and aldehyde groups (mmol/100 g) with different kinds of textile materials – oxidizer sodium hypochlorite, pH 5.5.

NaClO (pH 5.5) concentration	Gauze compress		Knitted bandage		Unwoven textile	
	Cu number g/100 g	CHO mmol/100 g	Cu number g/100 g	CHO mmol/100 g	Cu number g/100 g	CHO mmol/100g
2 mg Cl /ml	3.309 ± 0.53	4.52 ± 0.08	3.020 ± 0.032	3.97 ± 0.11	0.170 ± 0.02	0.06 ± 0.01
3 mg Cl/ml	11.910 ± 0.72	8.97 ± 0.22	9.980 ± 0.045	8.48 ± 0.18	0.960 ± 0.012	0.09 ± 0.01
5 mg Cl /ml	18.930 ± 0.36	16.14 ± 0.13	17.050 ± 0.48	15.14 ± 0.12	1.20 ± 0.042	0.17 ± 0.01

Table 4. Copper number (g/100 g) and aldehyde groups (mmol/100 g) with different kinds of textile materials – oxidizer hydrogen peroxyde, pH 9.5.

H_2O_2 (pH 9.5) concentration	Gauze compress		Knitted bandage		Unwoven textile	
	Cu number g/100 g	CHO mmol/100 g	Cu number g/100 g	CHO mmol/100 g	Cu number g/100 g	CHO mmol/100 g
4.0%	0.779 ± 0.046	1.0 ± 0.07	0.810 ± 0.067	0.86 ± 0.03	0.091 ± 0.03	0
8.0%	1.588 ± 0.019	1.28 ± 0.03	1.705 ± 0.057	1.24 ± 0.06	0.611 ± 0.019	0
12.0%	1.068 ± 0.038	1.66 ± 0.17	0.98 ± 0.028	1.62 ± 0.07	0.207 ± 0.024	0.14 ± 0.01

Table 5. Copper number (g/100 g) and aldehyde groups (mmol/100 g) with different kinds of textile materials – oxidizer sodium periodate.

$NaIO_4$ (pH 3.0) time, h	Gauze compress		Knitted bandage		Unwoven textile	
	Cu number g/100 g	CHO mmol/100 g	Cu number g/100 g	CHO mmol/100 g	Cu number g/100 g	CHO mmol/100 g
7	10.11 ± 0.30	36.20 ± 1.07	9.20 ± 0.23	33.82 ± 0.9	0.53 ± 0.021	1.16 ± 0.01
24	16.54 ± 0.11	43.82 ± 0.44	15.41 ± 0.29	40.39 ± 0.3	0.96 ± 0.015	1.45 ± 0.02
42	24.74 ± 0.30	51.31 ± 0.18	23.84 ± 0.51	49.17 ± 1.24	1.7 ± 0.031	2.34 ± 0.01

In the process of oxidation, the content of the ketone groups increases more rapidly, compared to the aldehyde and carboxyl groups, and the product of cotton oxidation at pH 9.5 is ketocellulose. According to Lewin and Ettinger the forming of ketone groups occurs predominantly at C3 atom of the anhydroglucoside monomer. The rate of oxidative interaction between the cellulose and the hydrogen peroxide is lower than 10%, while for the sodium hypochlorite it reaches up to 40%.

The weaker interaction, as well as the forming of predominantly ketone groups, explains the lower values for copper number in the third group of samples.

The copper number is highest for cellulose oxidized by sodium periodate (Table 5), which can be explained by the mechanism of the oxidation reaction and forming of two aldehyde groups per monomer unit (Fig. 3).

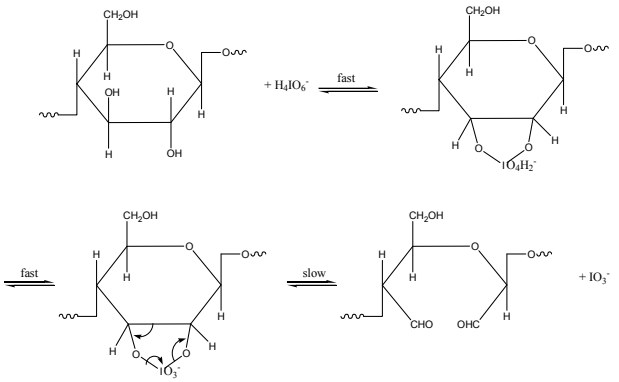

Fig. 3. Mechanism of the reaction of cellulose with sodium periodate.

It is assumed that concentrations of sodium periodate above 0.1 M lead to a much higher degree of cellulose oxidation, to a decrease of the stability of the glycoside connections and respectively to a deterioration of the structural and sorption characteristics of the tissue. For that reason we used sodium periodate with concentration 0.025 M with the purpose to achieve a partial oxidation of cellulose and to form reactive aldehyde groups without destructive changes. The copper number increases upon increasing the duration of the process at one and the same concentration of sodium periodate and pH.

The results, obtained for the content of aldehyde groups in the samples, correlate with the values for copper number. The aldehyde groups introduced into cellulose molecule have a capacity to interact with free groups of enzymes and other biologically active substances, thus achieving an immobilization of the biological component on the textile carrier.

According to literature data, the presence of reactive aldehyde groups with content from 0.06 to 3.1 mg/g textile allows the achievement of a covalent immobilization of collagenase on cellulose carrier. Immobilization of trypsin or alkaline protease has been carried out by similar methods [2–4].

CONCLUSION

Textile materials of cellulose and synthetic fibres can be activated by oxidation with solutions of sodium hypochlorite, hydrogen peroxide and sodium periodate, thus introducing reactive aldehyde groups into them. From the investigated textile materials, highest content of aldehyde groups was established for the samples, containing pure cellulose and those treated by sodium periodate. The obtained activated textile materials are appropriate as carriers for immobilization of proteolytic enzymes with the aim to achieve a biologically active wound dressing.

REFERENCES

1. S. Afaq, J. Iqbal, *Elect. J. Biotech*., **4**, 1 (2001).
2. A. A. Belov, N. F. Kazanskaya, V. N. Filatov, Y. N. Belova, *Vestn. MGU Ser. 2: Khimiya*, **47**, 87 (2006).
3. BG Patent 51438 (A3), 5/1993.
4. N. D. Burkhanova, S. M. Yugai, M. Y. Yunusov, G. V. Nikonovich, T. I. Usmanov, *Chem. Nat. Compd.*, **33**, 488 (1997).
5. X. Chai, D. Zhang, Q. Hou, S. Yoon, *J. Ind. Eng. Chem*., **13**, 597 (2007).
6. M. Lewin, A. Ettinger, *J. Polym. Sci*., 58, 1023 (1962).
7. M. Lewin, A. Ettinger, *Cellul. Chem. Tech.,* **3**, 9 (1969).
8. T. P. Nevell, O. P. Singh, *Text. Res. J*., **56**; 270 (1986).

9. TAPPI Official Test Method T430, TAPPI Press, Atlanta, revised 1994, p. 1.
10. T. Topalovic, V. A. Nierstrasz, L. Bautista, D. Jocic, M. Warmoeskerken, A. Navarro, *Cellulose*, **14**, 385 (2007).
11. US Patent 5098417.
12. T. N. Yudanova, I. V. Reshetov, *Pharm. Chem. J.*, **40**, 430 (2006).

ОХАРАКТЕРИЗИРАНЕ НА ОКСИЦЕЛУЛОЗА ПОЛУЧЕНА СЛЕД ЧАСТИЧНО ОКИСЛЕНИЕ С РАЗЛИЧНИ РЕАГЕНТИ

Св. М. Дянкова*, М. Д. Донева

Институт по криобиология и хранителни технологии, бул. „Черни връх“ № 53, 1407 София

Постъпила на 24 февруари 2009 г.; Преработена на 21 април 2009 г.

(Резюме)

Целта на настоящата работа бе да се проучат възможностите за активиране на превързочни материали от целулозни и синтетични влакна, чрез частично окисление с натриев хипохлорит, водороден пероксид и натриев перйодат и да се изследва влиянието на параметрите на реакцията върху количественото съдържание на реакционноспособни алдехидни групи в получения продукт.

Текстилни превързочни материали от целулозни и синтетични влакна бяха третирани с разтвори на окислители: натриев хипохлорит, водороден пероксид и натриев перйодат, с цел модифициране на материала и формиране реакционноспособни алдехидни групи в целулозната молекула. Най-високи стойности на показателите медно число и съдържание на алдехидни групи бе отчетено при пробите, съдържащи чиста целулоза и обработени с разтвори на натриев перйодат. Получените активирани текстилни материали биха могли да се използват като носители за имобилизация на протеолитични ензими с цел получаване на биологично активно превързочно средство.

Bulgarian Chemical Communications, Volume 41, Number 4 (pp. 397–403) 2009

Synthesis and characterization of carbon foam by low pressure foaming process using H_2SO_4 modified pitch as precursor

B. Tsyntsarski[1]*, B. Petrova[1], T. Budinova[1], N. Petrov[1], A. Popova[1], M. Krzesinska[2], S. Pusz[2], J. Majewska[2]

[1] *Institute of Organic Chemistry, Bulgarian Academy of Sciences, Acad. G. Bonchev St., Block 9, 1113 Sofia, Bulgaria*
[2] *Centre of Polymer and Carbon Materials, Polish Academy of Sciences, Marii Curie-Skłodowskiej 34, PL-41819 Zabrze, Poland*

Received February 24, 2009; Revised May 22, 2009

Carbon foams with anisotropic texture and good mechanical strength were obtained, using coal tar pitch modified by thermal oxidation treatment with H_2SO_4. The investigations on the relation between precursor properties and structure of obtained foam show that the composition and softening point of the pitch precursor significantly affect the foaming process and foam structure. The mechanical strength of carbon foam is found to be related not only to the foam cell structure, but also to the composition of the foaming precursors.

The compositions of the modified and synthetic pitches allow foam formation at relatively low pressure and fast heating of the precursor during foaming process without any stabilization treatment.

Key words: carbon foam, coal tar pitch, optical microscopy, SEM, mechanical properties.

INTRODUCTION

Carbon foam is a sponge-like carbon material, representing cellular ligament microstructure, and it is distinguished by certain features, such as light weight, high temperature tolerance in inert atmosphere, high strength, large external surface area and adjustable thermal and electrical conductivity. As new materials carbon foams have essential advantages, such as low cost, enhanced structural properties, fire resistance, radar cross-section, corrosion susceptibility.

These unique properties, which mainly depend on the precursors' features and synthesis conditions, make carbon foams ultra-high performance engineering materials, and determine their many potential applications in numerous industries [1, 2]: shipbuilding – living space modules, above deck structures, bulkheads; aerospace – aerospace structures, optical benches and lightweight mirrors, rocket nozzles and motors, thermal protection systems, composite tooling, heat transfer systems, radar adsorbing and antennae systems; energy – fuel cells, battery electrodes, nuclear shields, rods for nuclear reactors; automotive catalytic converters, brakes, bumpers; defense-related – insensitive munitions, shields and body lightweight armor; medical – bone surgery material, tooth implants; architecture – insulation, fire-proof blocks, shields and coatings, safe rooms, heating and cooling units; abrasives – for polishing of glass and metals, for paint removal, in cosmetics; filters for hazardous conditions; electronics – processor radiators, radio frequency shields. Carbon foam is used as a core to build fireproof radio frequency sheltered composite structures with superior lightning protection [2].

Klett et al. [3] have synthesized carbon foam sample with specific thermal conductivity about 6 times greater than that of Cu and approximately 5 times greater than that of Al – it is possible to use it in CPU coolers and heat sinks.

Due to their distinctive physical and high-temperature properties, carbon foams appear to be ideal materials for advanced thermal protection systems. Carbon foams, as well as other carbon and graphite materials, have high emissivity, low coefficient of thermal expansion, and they are self-supporting in low and high temperature regimes [1]. In the absence of oxygen these materials can be heated up to about 3000°C without melting or softening and they have high thermal shock resistance and dimensional stability [2]. These characteristics permit utilization of both thermal insulating and conducting properties, respectively, within a thermal management system [3–6]. Thus specific carbon foam is a component of the thermal protection used on the solid rocket booster of the Space Shuttle [2].

* To whom all correspondence should be sent:
E-mail: goriva@orgchm.bas.bg; boykotsyntsarski@yahoo.com

Carbon foams are excellent materials for acoustic absorbing applications in the shipbuilding, aerospace, and automotive industries. Carbon foam absorbs almost 100% of sound waves, depending on their frequency [2]. Pore structure of carbonized foams had a darkroom effect on microwave absorbability, which made the carbon foams a promising radar absorber [7, 8]. They are used for advanced radar antenna construction, due to their specific physical (very important - stable towards vibrations) and electrical properties. Carbon foam can be manufactured with desired electrical resistance, dielectric constant, and radar reflection coefficient. The material can be produced with physical dimensions suitable for antenna assembly [2, 7].

Carbon foam, due to its unique combination of high compressive strength and considerable impact absorption capacity, is an attractive material for enhanced performance bumper systems. At the same time, carbon foam is a good material for the construction of advanced electrodes because of its large surface area, high electrical conductivity, and chemically inertness. Additionally, carbon foam can be readily coated with a number of active materials to form either anode or cathode [2, 9].

Carbon foam is relatively inert even at high temperatures and radiation – it is an ideal candidate for use as a filter for filtration of aggressive solvents and molten metals [2], as well as nuclear shields and rods for nuclear reactors [1, 2, 10]. The inertness and mechanical strength of carbon foam makes it also suitable for bone surgery material, prosthetics, tooth implants [1, 2, 11, 12]. Some researchers and engineers consider carbon foam to be one of the next-generation material systems and components – maybe soon carbon foam is going to replace some of the conventional materials such as wood, ceramics, plastics, glass, rubber, metals [2, 13].

Initially, carbon foam was fabricated by carbonization of polymeric foam [14-21]. The development of carbon foam on the basis of coal tar pitch [22–24], petroleum pitch [22, 23, 25], synthetic pitch from organics [3, 4, 23, 26–31] or biomass – melanine [9], cork [32], olive stones [33], and raw coal [22, 34–36] – provides an economical way for the production of lightweight carbon material. The effect of the precursor on structure and properties of the obtained foam is of great importance and it is under extensive investigations [3, 21]. The properties of synthetic pitch can be adjusted to obtain suitable foaming precursor, which can be foamed directly without any pretreatment. The commercial coal tar pitch needs to be pretreated before foaming. The major problem is that its plastic properties usually do not meet the foaming process requirements for precursors. The well known pretreatments are air blow and thermal treatment in order to control the viscosity and degree of anisotropy of the foaming precursors [37–39].

When starting material is mesophase pitch, the final product is carbon foam with cellular graphitic ligament microstructure, similar to that in high-tech carbon fibers [1, 3, 26, 27, 40–44], ensuring isotropic material properties – high stiffness and high thermal conductivity graphitic foams [43, 45].

Therefore for preparation of high-strength structural carbon foam the desired foaming precursor should be isotropic in nature. On the contrary for the highly thermal and electrical conductive carbon foam, an anisotropic pitch precursor is required [45–55]. Pitch based carbon foam can be either mechanically strong foam or highly conductive.

The aim of the present investigations is to adjust by appropriate modification the composition and the properties of commercial coal tar pitch. The subject of this paper is developing of carbon foams from modified coal tar pitches using relatively simple and low pressure process without any stabilization step. The foaming process of pitch-based carbon foam, the pretreatment of the precursors, and the properties of resultant foams are discussed in this paper.

EXPERIMENTAL

Foaming precursors and pretreatment

Most petroleum and coal-derived pitches need to be pretreated (under various conditions – with different chemical reagents and temperature regimes) before foaming. The plastic properties of these precursors usually do not meet the foaming process requirements. The pretreatments usually involve the polymerization/condensation of pitch by thermal treatment in order to control the viscosity of the foaming precursors.

The precursors used in this work include pitches obtained after thermal oxidation treatment with H_2SO_4 (at 120°C) of commercial coal tar pitch. Details of the thermal oxidation treatment process are available elsewhere [37].

Precursor characterization

An exhaustive extraction is carried out consecutively by Soxhlet apparatus with petroleum ether to extract maltenes and with toluene to extract asphaltenes. After distilling off the solvent the extracts were dried in vacuum and separated as it is shown elsewhere [37].

The elemental analysis was performed on Carlo Erba 1106-type equipment for C, H and N content. Sulphur content was determined by Eshka's method

[56]. Oxygen was determined by the difference.

Softening point of pitches are determined by the Ring and Ball's method using stainless steel balls of diameter 20 mm. For each measurement an average of three readings is taken. The variation is found to be within ±4°C.

Foaming method

Foaming was carried out in a stainless steel pressure vessel by heating the pitch precursor up to 500°C in a N_2 atmosphere at pressure up to 1 MPa. The resultant "green" foams were calcinated at 1000°C in N_2 atmosphere to increase the mechanical strength and to remove further the volatiles.

Foam characterization

Bulk porosity. Both apparent and true densities were measured to determine the bulk porosity of the sample. The apparent density was determined based on the values of the weight and the volume – the latter was calculated using sample dimensions. The true density was measured using a helium gas displacement pycnometer type 1305 Micromeritics®. The porosity was calculated using an expression:

$$P(\%) = 100\times((\rho_t - \rho_a)/(\rho_t)) \quad (1)$$

where P is the porosity, ρ_t and ρ_a are the true and apparent densities of the sample respectively.

Ultrasonic velocity and dynamic elastic modulus. In samples with pores in the 1nm –100 μm range, the acoustic wavelengths for frequencies up to about 20 MHz are considerably larger than the pore diameters [57]. Since scattering of ultrasonic waves on pores as defects does not occur at the above frequencies, carbon foams studied may be treated as homogeneous materials in this frequency range and the following equation can be applied to the determination of dynamic elastic moduli [57]:

$$E = \rho v^2 \quad (2)$$

where v is the velocity of the stress wave propagation through a homogeneous material, E – the dynamic elastic modulus and ρ – the density of the material.

The dynamic elastic moduli for three mutually perpendicular directions (along the three coordinate axes of a sample) were determined using an ultrasonic velocity measurements. The velocity of longitudinal ultrasonic wave of 100 kHz frequency was measured along every one of the three basic axes of monolithic cube-formed sample using an ultrasonic tester (Tester CT1, Unipan-Ultrasonic, Poland) based on the pulse transmission method. The ultrasonic tester serves to determine the time interval of transition of ultrasonic wave throughout a sample. Velocity was derived from the transition time interval (τ) and length of path, i.e., thickness of a sample, measured with a slide caliper. Elastic anisotropy was cal-culated from a relationship v_{max}/v_{min} , where v_{max} is the maximal value among the three velocity values determined for the three mutually perpendicular directions of a cube-formed sample.

Optical parameters. Optical texture and reflectance values of carbon foams were determined with a reflected light microscope Axioskop MPM 200 (Opton-Zeiss, Germany), using monochromatic linearly polarized light with λ = 546 nm, in air. Maximum reflectance (R_{max}) values were automatically measured during rotation of the microscopic stage in several points (15–25), each in various locations on the sample.

RESULTS AND DISCUSSION

Foaming procedure

A lot of factors influence the foaming process, but temperature and pressure are the most critical aspects of the process [3, 13, 27, 29, 54, 55]. Pressure and pressure drop time influence pore structure, density and compressive strength of the carbonized foams. More interconnected open-cellular porous structure is formed for shorter pressure drop times [29].

In this paper the softening point and composition of the pitch precursors, which are connected with the viscosity and volume swelling, are used as important factors influencing the foaming process.

Conventional foaming procedure includes foaming step, oxidation-stabilization step, carbonization step and graphitization step [26]. In order to reduce time and energy consumption, we decided to obtain carbon foam by technology, similar to that of Mehta *et al*. [26], but without stabilization step. Instead of this final stabilization step, a special method for thermal oxidative modification of pitch precursor was developed and carried out as preliminary step.

Foaming precursors and pretreatment

Commercially available pitches are not suitable for producing carbon foam directly. The key problem is that the viscosity is too low to preserve the foam cell shape. Therefore, the pitch properties of these materials were adjusted to meet the foaming requirements. For this aim initial pitch was subjected to thermal oxidative modification with H_2SO_4. Data in Table 1 show increase of the oxygen content in modified pitches. According to data in Table 1, the thermal oxidation treatment with H_2SO_4 lead to the formation of oxygen-containing struc-

tures. Simultaneously condensation reactions with formation of higher molecular weight substances are occurring and the softening point of the pitch increases.

Table 1. Selected properties of studied pitches.

Sample	C, wt.%	H, wt.%	N, wt.%	S, wt.%	O, diff.	C/H
P	90.60	5.25	0.90	0.50	2.75	1.44
M H_2SO_4	83.90	4.24	0.82	2.62	8.42	1.64
M* H_2SO_4	91.20	3.83	0.80	2.12	2.05	2.01

P - initial pitch; M $_{H_2SO_4}$ - coal-tar pitch, modified by oxidation treatment with H_2SO_4; M* $_{H_2SO_4}$ - modified pitch heated up to 350°C.

Heat treatment of pitch up to 350°C in N_2 induces polymerization and condensation reactions through de-hydrogenation of polyaromatic molecules. This treatment results in the formation of larger condensed and more planar molecules in pitch. Thus the viscosity and softening temperature of treated pitch are increased. Table 2 lists the properties of pitch sample before and after thermal treatment at 350°C under N_2 atmosphere.

Table 2. Solubility class separation of the pitches determined by sequential Soxhlet extraction.

Sample	PES, %	PEI-TS %	TI %	QI %	Softening point, °C
P	38.00	34.69	27.31	-	72
M H_2SO_4	33.72	45.04	17.74	3.50	140
M* H_2SO_4	9.19	32.40	45.30	13.11	210

P - initial pitch; M $_{H_2SO_4}$ - coal-tar pitch, modified by oxidation treatment with H_2SO_4; M* $_{H_2SO_4}$ - modified pitch heated up to 350°C; PES - petroleum ether soluble; PEI-TS - petroleum ether insoluble-toluene soluble; TI - toluene insoluble; QI - quinoline insoluble fraction.

Thermal treatment significantly increases the softening temperature and the content of quinoline insoluble (QI), which implies the increase of molecular weight and the degree of polymerization and condensation of the pitch. As a result of occurring of condensation reactions with oxygen containing structures, a considerable decrease of oxygen content in heated pitch is observed (Table 1). An increase of softening temperature reflects an increase in viscosity of the pitches. In addition, thermal treatment increases the thermal stability of the pitch, and thus decreases the weight loss in the foaming stage. This is relevant to the formation of bubbles, because the amount of bubbling agent is related to the weight loss, caused by the evolving volatiles in foaming stage. Therefore, the size of foam cells could also be controlled by the amount of volatiles. The properties and composition of modified coal tar pitches can be controlled by the temperature of thermal oxidation treatment and amount of added acid. In this way, by adjusting the conditions of treatment (temperature and amount of added acid) of tars from agricultural wastes, the properties of the synthetic pitch could be controlled.

Carbon foam properties

Main properties. Table 3 shows the general properties of carbon foam, derived from modified pitch heated up to 350°C. The bulk density of the obtained foam is about 0.5 g/cm^3. The prepared carbon foam has over 90% open cell structure with porosity >69% according to helium pycnometry.

Mechanical strength. Table 3 also summarizes the compressive strength of the carbon foam obtained. The strength of pitch-based foam depends not only on the foam structure, but also on the properties of the precursor. Data in Table 2 and Table 3 show that carbon foam, obtained from modified pitch, containing QI and relatively low amount of PES, has good compressive strength. The results confirm that the composition of the modified pitch allows proceeding of polymerization and polycondensaion reactions with formation of larger condenced molecules during foaming process.

The cellular structure (thickness of cell-wall, t, and the length of the cell edge, l) affects the foam strength. For a regular foam, t and l are corelated with the relative density ρ / ρ_t, where ρ is the bulk density; ρ_t is the true density of foam [58]. It is difficult to measure t and l of the foam, but the relative density is easy to be determined. Although obtained carbon foams do not have perfect and regular cell structure, as a first approximation, relative density is still used to describe the foam cellular structure.

Table 3. General properties of the carbon foam.

Foam precursor	Bulk density g/cm^3	Porosity %	Open-cell, %	Relative density	Compressive strength, MPa
Modified pitch heated up to 350°C	0.52	73.4	92.1	0.27	11.9

The data show that obtained carbon foam is distinguished by high relative density, and high compressive strength, respectively. High relative density implies presence of thicker cell walls and shorter cell edges, which promote higher compressive strength [4].

Carbon foam texture. Figure 1 shows the optical texture of the carbon foam under polarized light in the optical microscope. Microscopical observations showed that the carbonization product is a distinctly

porous material, where mesopores (visible under optical microscopy) have various, irregular shapes and strongly diversified diameters from less than 1 μm to more than several hundreds μm.

The internal structure of the sample is similar to cokes from coal-tar or petroleum pitch, or from very good coking coals. They look like coarse mosaics, domain or flow type according to classification of optical textures of cokes [59]. Maximum reflectance values of the samples are also similar to cokes. The presence of QI in pitch precursor prevents the coalescence of the mesophase spheres during the thermal treatment, hence optical textures of carbon foam are generally anisotropic.

Highly anisotropic textures are dominant. The possible reason for this is the higher content of QI. Lower anisotropic textures transform into higher anisotropic gradually, but some sharp borders between them also exist.

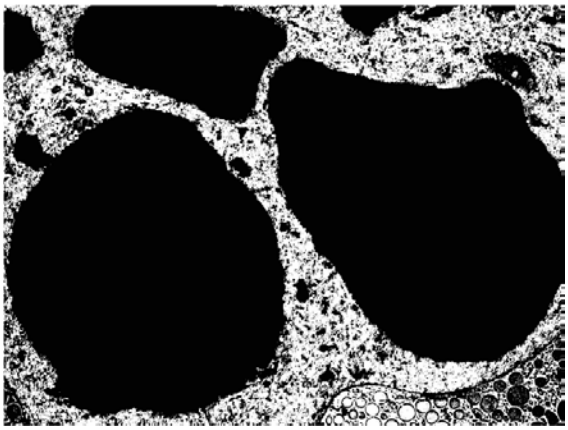

Figure 1. Optical texture of carbon foam derived from pitch, modified with H_2SO_4 (magnification 80x, in air).

SEM observation of carbon foam structure. Figure 2 shows the SEM image of the obtained carbon foam. The foam cell is mainly open with size around 300-350 μm and some cell membranes. The SEM image clearly shows that there are cracks in the samples. These cracks mainly occur between the layers aligned parallel to the cell surfaces, especially in the junction area of the foam cells. However, no major cracks are found on the cell membranes of obtained foams. Carbon foam has small anisotropic domain due to the high content of QI, which prevents the coalescence of the mesophase spheres during thermal treatment.

Ultrasoinic velocity, dynamic elastic modulus and elastic anisotropy. The ultrasonic velocity (Table 4) has considerably high values in (a), (b) and (c) directions. High stiffness corresponds to considerably high values of ultrasonic velocities [57]. This confirms suitable arrangement of the layers in carbon foam, due to considerably high content of QI, which leads to formation of highly orientated structure of the well condensed crystallites, what is indicated by the high ultrasonic velocity.

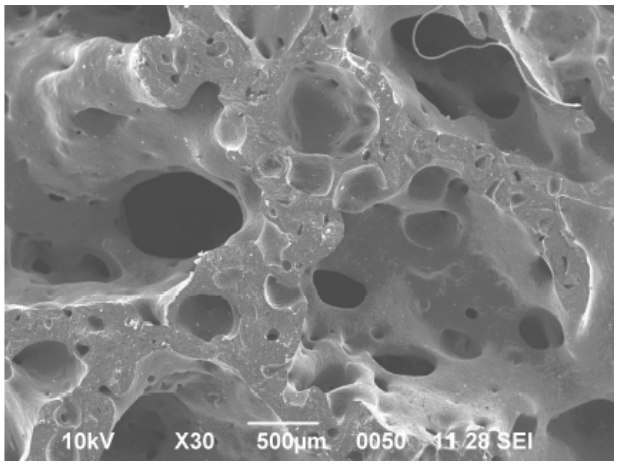

Figure 2. SEM image of carbon foam derived from pitch, modified with H_2SO_4.

Table 4. Values of ultrasonic velocity of obtained carbon foams.

Physical parameter	Pitch treated with H_2SO_4
Ultrasonic velocity: direction a, v_{max} (m/s)	1948
Ultrasonic velocity: direction b, v_{mid} (m/s)	1931
Ultrasonic velocity: direction c, v_{min} (m/s)	1846
Elastic modulus: direction a, E_{max} (GPa)	1.98
Elastic modulus: direction b, E_{mid} (GPa)	1.95
Elastic modulus: direction c, E_{min} (GPa)	1.78
Elastic anisotropy, v_{max}/v_{min}	1.06

CONCLUSIONS

Thermal oxidation modification of commercial coal tar pitch with H_2SO_4 is appropriate treatment to adjust its plastic properties before the foaming process. The properties of modified coal tar pitches can be controlled by thermal oxidation treatment conditions - temperature and amount of added acid. The obtained pitch is suitable foaming precursor and it can generate anisotropic carbon foam with good mechanical strength. The low content of PES and high content of QI in the pitch, treated with H_2SO_4, lead to formation of small crystallites, and respectively carbon foam with high porosity and considerably high strength.

It is important to note that the composition of the obtained modified pitches allows foam formation at relatively low pressure and fast heating of the precursor during foaming process, and without any stabilization treatment.

***Acknowledgement**: This work was supported by the National Science Fund of Bulgaria (Project MU01-0149).*

REFERENCES

1. M. Inagaki, New Carbons: Control of Structure and Functions, Elsevier, 2000.
2. D. Rogers, J. Plucinski, P. Stansberry, A. Stiller, J. Zondlo, in: Proc. Int. Symp. Soc. Adv. Mater. Proc. Eng., 2000; p. 293.
3. J. Klett, R. Hardy, E. Romine, C. Walls, T. Burchell, *Carbon*, **38**, 953(2000).
4. N. C. Gallego, J. W. Klett, *Carbon*, **41**, 1461 (2003).
5. Q. Yu, A. G. Straatman, B. E. Thompson, *Appl. Thermal Eng*., **26**, 131 (2006).
6. D. Gaies, K. T. Faber, *Carbon*, **40**, 1137 (2002).
7. J. Yang, Z. Shen, Z. Hao, *Carbon*, **42**, 1882 (2004).
8. Zh. Fang, Ch. Li, J. Sun, H. Zhang, J. Zhang, *Carbon*, **45**, 2873 (2007).
9. M. Kodama, J. Yamashita, Y. Soneda, H. Hatori, K. Kamegawa, *Carbon*, **45,** 1105 (2007).
10. N. C. Gallego, T. D. Burchell, J. W. Klett, *Carbon,* **44**, 618 (2006).
11. P. I. Zolkin, *Metallurgy*, **40**, 2 (1996).
12. L. M. Mathieu, T. L. Mueller, P.-E. Bourban, D. P. Piolettic, R. Muller, J.-A. E. Manson, *Biomaterials*, **27**, 905 (2006).
13. T. Beechem, K. Lafdi, A. Elgafy, *Carbon*, **43**, 1055 (2005).
14. W. D. Ford, US Patent, 3121050 (1964).
15. W. J. McMillan, US Patent 3342555 (1967).
16. J. Googin, J. Napier, M. Scrivner, US Patent 3345440 (1967).
17. F. C. Cowlard, J. C. Lewis, *J. Mater. Sci*., **2**, 507 (1967).
18. M. Inagaki, T. Morishita, A. Kuno, T. Kito, M. Hirano, T. Suwa, K. Kusakawa, *Carbon*, **42**, 497 (2004).
19. Ya. Chen, B. Chen, X. Shi, H. Xu, Y. Hu, Y. Yuan, N. Shen, *Carbon*, **45,** 2132 (2007).
20. M. Liu, L. Gan, F. Zhao, X. Fan, H. Xu, F. Wu, Z. Xu, Z. Hao, L. Chen, *Carbon*, **45**, 3055 (2007).
21. G. Harikrishnan, T. Umasankar Patro, D. V. Khakhar, *Carbon*, **45**, 531 (2007).
22. C. Chen, E. Kennel, A. Stiller, P. Stansberry, J. Zondlo, *Carbon*, **44**, 1535 (2006).
23. Z. Min, M. Cao, Sh. Zhang, X. Wang, Y. Wang, *New Carbon Mater*., **22**, 75 (2007).
24. X. Wang, J. Zhong, Y. Wang, M. Yu, *Carbon*, **44**, 1560 (2006).
25. M. Wang, Ch. Wang, T. Li, Z. Hu, *Carbon*, **46**, 84 (2008).
26. R. Mehta, D. P. Anderson, J. W. Hager, *Carbon*, **41**, 2159 (2003).
27. J. W. Klett, A. D. McMillan, N. C. Gallego, T. D. Burchell, C. A. Walls, *Carbon*, **42**, 1849 (2004).
28. T. Li, Ch. Wang, B. An, H. Wang, *Carbon*, **43**, 2030 (2005).
29. A. Eksilioglu, N. Gencay, M. F. Yardim, E. Ekinci, *J. Mater. Sci*., **41**, 2743 (2006).
30. S. Li, Q. Guo, Ya. Song, Zh. Liu, J. Shi, L. Liu, X. Yan, *Carbon*, **45**, 2843 (2007).
31. C. M. Leroy, F. Carn, R. Backov, M. Trinquecoste, P. Delhaes, *Carbon*, **45**, 2317 (2007).
32. R. D. Klett, US Patent 3914392 (1975).
33. R. V. R. A. Rios, M. Martinez-Escandell, M. Molina-Sabio, F. Rodriguez-Reinoso, *Carbon*, **44**, 1448 (2006).
34. D. M. Spradling, R. A. Guth, *Adv. Mater. Proc*., **161**, 29 (2003).
35. M. Calvo, R. Garcia, A. Arenillas, I. Suarez, S. R. Moinelo; *Fuel*, **84**, 2184 (2005)
36. M. Calvo, A. Arenillas, R. Garcia, S. R. Moinelo, *Fuel*, **88**, 46 (2009).
37. B. Petrova, T. Budinova, N. Petrov, M. F. Yardim, E. Ekinci, M. Razvigorova, *Carbon*, **43**, 261 (2005).
38. Y. Duk, Y. Korai, I. Mochida, *J. Mater.Sci*., **21**, 424 (1986).
39. B. Rhee, E. Fitzer, M. Ileym, *High Temp. High Press.*, **8**, 307 (1997).
40. D. P. Anderson, K. E. Gunnison, J. W. Hager, in: Proc. Mater. Res. Soc. Symp., 1992, p. 47.
41. J. W. Hager, D. P. Anderson, in: Proc. 21st Biennial Conf. Carbon, Buffalo, NY, USA, 1993, p. 102.
42. J. W. Hager, M. L. Lake, in: Proc. Mater. Res. Soc. Symp., 1992, p. 29.
43. J. W. Hager, in: Proc. Mater. Res. Soc. Symp., 1992, p. 41.
44. E. Bruneton, C. Tallaron, N. Gras-Naulin, A. Cosculluela, *Carbon*, **40**, 1919 (2002).
45. S. S. Sandhu, J. W. Hagar, in: Proc. Mater. Res. Soc. Sym., 1992, p. 35.
46. I. Tanahashi, A. Yoshida, A. Nishino, *Carbon*, **28**, 477 (1990).
47. S. Biniak, B. Dzielendziak, J. Siedlewski, *Carbon*, **33**, 1255 (1995).
48. E. Frackowiak, F. Beguin, *Carbon*, **39**, 937 (2001).
49. D. Lozano-Castello, D. Cazorla-Amoros, A. Linares-Solano, S. Shiraishi, H. Kurihara, A. Oya, *Carbon*, **41**, 1765 (2003).
50. H.-Y. Liu, K.-P. Wang, H. Teng, *Carbon*, **43**, 559 (2005).
51. K. Xia, Q. Gao, J. Jiang, J. Hu, *Carbon*, **46**, 1718 (2008).
52. J. L. White, P. M. Sheaffer, *Carbon*, **27**, 697 (1989).
53. J. H. Aubert, in: Proc. Mater. Res. Soc. Symp., 1990, p. 117.
54. T. Beechem, K. Lafdi, *Carbon*, **44**, 1548 (2006).
55. G. Rosebrock, A. Elgafy, T. Beechem, K. Lafdi, *Carbon*, **43,** 3075 (2005).
56. Annual Book of ASTM Standards, part 26, D3177-75, Total Sulfur in the analysis sample of coal and coke, 1977.
57. M. Krzesinska, A. Celzard, B. Grzyb, J. F. Mareche, *Mater. Chem. Phys*., **97**, 173 (2006).
58. L. J. Gibson, M. F. Ashby, Cellular solids, Cambridge University Press, New York, 1997.
59. H. Fujita, M. Hijiriyama, S. Nishida, *Fuel,* **62**, 875 (1983).

СИНТЕЗ И ОХАРАКТЕРИЗИРАНЕ НА ВЪГЛЕРОДНА ПЯНА ПОСРЕДСТВОМ ПЕНООБРАЗУВАНЕ ПРИ НИСКО НАЛЯГАНЕ С ИЗПОЛЗВАНЕТО НА ПЕК МОДИФИЦИРАН СЪС H_2SO_4 КАТО ПРЕКУРСОР

Б. Цинцарски[1]*, Б. Петрова[1], Т. Будинова[1], Н. Петров[1], А. Попова[1], М. Кжешинска[2], С. Пуш[2], Ю. Майевска[2]

[1] *Институт по органична химия, Българска академия на науките, ул. „Акад. Г. Бончев“, бл. 9, 1113 София*
[2] *Център по полимерни и въглеродни материали, Полска академия на науките, ул. „Мария Кюри-Склодовска“ 34, PL-41819, Забже, Полша*

Постъпила на 24 февруари 2009 г.; Преработена на 22 май 2009 г.

(Резюме)

Получени бяха образци от въглеродни пени с анизотропна текстура и добра механична якост, на базата на каменовъглен пек, модифициран чрез термоокислителна обработка със H_2SO_4. Изследвана бе зависимостта между свойствата на прекурсора и структурата на получената въглеродна пяна и беше показано, че химичния състав и точката на омекване на изходния пек оказват значително влияние върху процеса на пенообразуване и върху порьозната структура на въглеродната пяна. Установено бе, че механичната якост на въглеродната пяна зависи не само от порьозната структура на въглеродната пяна, но и от състава на прекурсора.

Химичния състав на модифицираните и синтетичните пекове позволява образуване на въглеродна пяна при относително ниски налягания и бърз режим на нагрявяне на прекурсора по време на процеса на пенообразуване, като се избягва етапа на стабилизационна обработката.

Bulgarian Chemical Communications, Volume 41, Number 4 (pp. 404–408) 2009

Determination of antimony in gunshot residues (GSR) by electrothermal atomic absorption spectrometry

N. F. Fidan[1], B. İzgi[2,*]

[1] *Turkish National Police Head Office, Department of Bursa Criminal Police Laboratory, Bursa, Turkey*
[2] *Uludag University, Science and Art Faculty, Department of Chemistry, 16059 Bursa, Turkey*

Received March 9, 2009, Revised May 4, 2009

Simple and fast analytical procedure for antimony determination in gunshot residues by electrothermal atomic absorption spectrometry (ETAAS) is described. The sampling method of swab was tested by using adhesive tapes and both cotton rod and bandaged cotton moistened with boric acid. The optimal instrumental parameters for ETAAS measurements are defined: the maximum loss free pretreatment temperature found was 700ºC and the optimum atomization temperature was 1800ºC. Experiments performed with various modifiers (Pd, Ni, ascorbic acid, boric acid) showed that 5% (m/v) of boric acid is the most suitable modifier for Sb ensuring interference free ETAAS measurements. Linear analytical curve is ranging from 5 $\mu g \cdot L^{-1}$ to 40 $\mu g \cdot L^{-1}$ ($R^2 = 0.9998$, n = 3). Limit of detection (LOD) and limit of quantification (LOQ) calculated under optimum conditions are 0.4 $\mu g \cdot L^{-1}$ and 1.3 $\mu g \cdot L^{-1}$, respectively. The degree of interferences from matrix elements like Na, K, Ca, Fe, Pb, Ba, Ag, Cl, SO_4 and PO_4 was investigated and evaluated. Recoveries in the range 70–88% were achieved.

Key words: Antimony, ET-AAS, Zeeman correction, interference, gunshot residues.

INTRODUCTION

The gunshot residues (GSR) are essential samples in the forensic science for the identification of suspected persons. A small part of GSR is smeared on an index finger, back of the thumb and on palm of the person, who has fired the gun. Determination of GSR substances gives some information about the person who fired or touched the gun and about the firing distance [1, 2]. GSR substances could include lead styphnate as an explosive initiator, barium in nitrate form in small-arms and antimony sulphide fuel in primers, calcium silicide, zinc, zirconium, magnesium, titanium, trace amount of chloride, iron, potassium, sodium, phosphorus and also some organic compounds such as nitroglycerin, 2,4-dinitrotoluene and others. [3–5]. The quantities of these elements are affected by some factors such as type of weapon, burning process of powder, firing time and distance, personal hygiene, environmental conditions.

The GSR detection methods are based on analysis of the chemical residues, produced from discharge of cartridge. Several techniques have been used to determine the GSR; each one has advantages and disadvantages as usual. Sampling of GSR is very important to get accurate and reliable results. It is mentioned in the literature that level of GSR components is very low even after three hours of firing [6]. It is also well known that the amount of GSR on the hands could be cleaned out by some activities such as washing/rubbing/wiping of the hands, placing the hands in pockets, characteristics of perspiring of the person, etc. Therefore, sample collection must be done in a fast and proper way on the crime scene. Nowadays GSR samples are collected by "swab" technique via washing of hands by some acidic solutions or wiping some materials like cotton moistened with diluted acid, EDTA [2, 5, 7]. In the literature adhesive film was used principally for lifting organic compounds of GSR from a firer's hand [5] and lifting the particles via adhesive surface called as "tape lifting" technique [2]. Typically, this sampling could be used for all components determination in GSR. Conventional flame atomic absorption (FAAS) has sufficient sensitivity for the detection of Pb encountered in hand samples but it was inadequate for barium and antimony [4]. ICP-AES is a rapid technique with capabilities for multi-elemental analysis, which is relatively free from interference; however, it lacks the sensitivity required for accurate Sb determination on GSR swab extracts. Inductively coupled plasma mass spectrometry has benefits for GSR analyses due to its accuracy, multi-element capability and low detection limits for swab sampling 0.5 ng of Sb, 0.2 ng of Ba and 1.4 ng of Pb [8]. Few reports have been made on this technique because of relatively high cost of analysis. In recent years a scanning electron microscope (SEM) and its combinations such as

* To whom all correspondence should be sent:
E-mail: belgin@uludag.edu.tr

energy dispersive X-ray analysis (SEM/EDX) was found able to acquire information about the distribution of elements in gunshot residue. The main disadvantage of SEM techniques is its high time and manpower consumption [2]. Nowadays anodic stripping voltammetry is also used for determination of GSR, but the determination of barium has insufficient detection limit. Electrothermal atomic absorption is preferable technique for Sb determination in GSR [9, 10]. It permits measurement of Sb at 10 ng level [11, 12]. The combination of ET-AAS and SEM techniques are mostly used by forensic laboratories [3, 5, 7, 8, 13].

In the present work, we optimize the instrumental parameters for Sb determination by ETAAS. The most appropriate pretreatment and atomization temperatures are defined in the presence of boric acid (BA) as matrix modifier. The degree of matrix interferences due to sodium, potassium, calcium, iron, lead, barium, silver, chloride, sulphate, phosphate and others on the Sb absorbance signal was investigated. Sampling and sample preparation procedures are also optimized; the most suitable acidic mixture is recommended. The adhesive tape and both cotton rod and bandaged cotton moistened with boric acid were used as a sampling from hands.

EXPERIMENTAL

Instrumentation

Varian GTA 120 model AA280Z (with Zeeman background corrector) electrothermal atomic absorption spectrometer was used for analysis. The absorbance values were measured with an antimony hollow cathode lamp, which was operated at 217.6 nm with a bandpass width of 0.5 nm at 10 mA current. Pyrolytically coated tubes were used as atomizers. Sample injections volumes of 20 μL were used. Mechanic shaker GFL-3015 ORG and magnetic stirrers with heating IKA-MS 2 VORTEX and ARE were employed for sample preparation. Yavuz 16 compact model of Turkish gun was used for real sampling.

Reagents

Ortho-phosphoric acid (85%, p.a. Merck), hydrochloric acid (37%, p.a. Merck), sulphuric acid (95–98%, p.a. Merck), nitric acid (65%, p.a. Merck), boric acid (BA) (p.a. Merck), ascorbic acid (AA) (p.a. Merck), sodium nitrate, potassium nitrate (p.a. Merck / Fluka), stock standard solutions of Ag, Ca, Ba, Sb, Pb and Fe 1000 $mg \cdot L^{-1}$ (Merck, BDH Lab. and SCP SCIENCE) were used. Doubly distilled water (J. T. Baker) was used throughout all experiments. Working Sb standard solutions were prepared by appropriate dilution of stock standard solution with 8% of HNO_3. Solutions of 1% (w/v) AA and 5% (w/v) BA were used as matrix modifier solutions. Calibration curve was prepared with 5, 10, 20, 30 and 40 $ng \cdot mL^{-1}$ antimony standards. The effect of different acids and acid mixtures (H_2O_2, HNO_3-H_2O_2 and HNO_3-H_2O_2-HCl) was investigated within the acid concentration range from 2 to 10%. A synthetic model solution was prepared containing from 1 to 400 $\mu g \cdot mL^{-1}$ of Ag, Ba, Pb, Fe, Na, K, Ca, as nitrate salts and SO_4, PO_4 and Cl in acid form to simulate the sampling problems of swab on the venue.

Sampling and sample preparation

The collection of samples from gun shots is typically performed by swabbing technique on the spot of event by police officers, so that sampling must be done easily, fast and accurately. It is well known that the efficiency of sampling is affected by interferences coming from the field of firing conditions and time, type of weapon, human activities of firing person (sweat, saliva *etc*.), personal hygiene and biometrics [5, 9, 13]. Sampling is important for both to get accurate, repeatable results and not to damage the hands of suspected person. In early times, nitric acid solution was used as a GSR's collector [2]. Sampling in the field for GSR generally is taken by adhesive tape. Collected GSRs migrated to bulk solution by acid or acid mixtures. On the other hand, sampling could be done with moistened cotton material. In early works, nitric acid was used for collecting of GSRs from hands although it is well known that nitric acid has corrosive effect on the skin. Because of this reason, less corrosive and injurious solutions and materials are examined such as EDTA and adhesive tape [2, 5, 7]. In this work 5% of BA solution is tested as a moistening solution of cotton. It is also known that median lethal dose (LD_{50}) of BA for mammals are given rating 2.66 $mg \cdot kg^{-1}$ bodies mass. BA is poisonous if taken internally and inhaled [14, 15]. BA is functional and harmless for intact skin. It has also some antibacterial and antiseptic usages [16, 17]. So that swabbing with cotton moistened by BA could be used for sample collection of GSR directly from hands.

Shootings were made by using a Yavuz 16 Compact model of Turkish gun. Samples were collected from palm and backsides of both right and left hands of the person who made the shootings via lifting the residues particles on 5 × 5 cm adhesive tapes kept into polyethylene tubes in field. Collected samples were prepared by adding of 4 ml of 8% HNO_3 and the solution was stirred in mechanical shaker at 50 rpm for 30 minutes. The final solution

was analyzed by ET-AAS under optimum working conditions. On the other hand, swabbing procedure also applied with cotton rods (plastic handled cotton tipped) and bandaged cotton moistened with 1 mL of 5% of BA. Then bulk solution of them was prepared analogously to this with adhesive tape. In our work we mentioned that 5 mL of 8% nitric acid and 30 minutes shaking ensures recoveries of about 90% for the determination of Sb.

RESULTS AND DISCUSSION

Optimization of the ETAAS

Furnace temperature program. The optimal furnace temperature program was defined through the pretreatment and atomization curves prepared with 10 ng·mL^{-1} of Sb standard and summarized in Table 1. Calibration plot obtained under optimal instrumental conditions was calculated by linear regression to fit the equation A = 0.0026[Sb] – 0.0012 and R^2 = 0.9998. Limit of detection (LOD) (3σ) and limit of quantification (LOQ) (10σ) were calculated according to IUPAC rules to be 0.4 μg·L^{-1} and 1.3 μg·L^{-1} in respectively.

Effect of acid and acid mixture in the absence of matrix modifier. The effect of different acid/acid mixtures on the antimony absorbance signal was examined. The results obtained are depicted in Table 2. It is well known that HNO_3 and H_2O_2 have oxidative effect, which will be helpful for the formation of Sb oxides on the tube surface before the atomization step. In general, in the presence of HCl acid negative effect on the Sb absorbance signal could be expected due to the volatile compounds formed with chloride ions. In this way parts of the element could be partially lost before the atomization step. However, experiments performed showed that on the contrary the interference effect observed in the presence of HCl as well as gaseous compounds (Sb, $SbCl_5$, SbH_3, Sb_2, Sb_4 and SbS) and condensed compounds (Sb, $SbCl_3$, SbOCl, SbO_2, Sb_2O_3, Sb_2O_5 and Sb_2S_3) formed was insignificant [18–20]. It could also be explained by entrance of chlorides into the graphite lattice at high temperatures [19, 20]. Because of this reason, there were not big differences in the data obtained in the presence of HNO_3, HCl and H_2O_2. It is also known that acids have both extracting and modifying effect in the heating procedure [8, 13, 18].

*Effect of modifier***.** It is well known that matrix modifier is used for thermal stabilization and for elimination of chemical interferences coming from the matrix. In the literature, Dash *et al*. [21] used boric acid as a modifier for the determination of trace amount of indium in high purity antimony by ET-AAS and they obtained satisfactory results. Therefore, in our work we used for the first time BA as a matrix modifier for the determination of antimony by ETAAS. Synthetic matrix solutions were spiked with Sb and analyzed in the presence of 2% and 5% of BA, 1% of AA, 10 μg Pd and Ni solutions as matrix modifiers. Recoveries obtained are presented in Table 3. When AA was used as a matrix modifier, it had no advantage and did not eliminate matrix interferences. In this study, we observed that 5% boric acid used as a matrix modifier has good recovery value compared with AA, Pd and Ni.

Table 1. Optimal temperature program for Sb with modifier.

Step	Temperature, ºC	Time, s	Gas flow, L·min^{-1}
1	95	5.0	0.1
2	120	25.0	0.3
3	700	30.0	0.3
4	1800	4.0	0.0
5	2300	3.0	0.3
6	40	20.9	0.3

Table 3. Recoveries for Sb in the presence of different matrix modifiers (n = 3).

Matrix modifier	maximum loss free pretreatment temperature, ºC	Optimal atomization temperature, ºC	Recovery in presence of a GSR, %
5% BA	700	1800	80–88
2% BA	700	1800	65–70
1% AA	700	1800	35–40
10 μg Pd	1500	2100	25–40
10 μg Ni	1100	2000	28–45

Table 2. Effect of acid/acid mixture on the Sb atomic absorbance signal as recovery (%).

%	Recovery (compared with 10 ng·mL^{-1} of Sb atomic absorbance signal), %					
	HNO_3	HCl	H_2O_2	HNO_3 + HCl	HNO_3 + H_2O_2	HNO_3 + H_2O_2 + HCl
2	80 ± 7	105 ± 2	86 ± 4	105 ± 3	102 ± 3	93 ± 8
4	84 ± 2	102 ± 5	99 ± 3	104 ± 5	107 ± 1	96 ± 3
6	97 ± 1	99 ± 3	103 ± 4	95 ± 3	107 ± 2	95 ± 4
8	100 ± 3	98 ± 3	104 ± 2	105 ± 2	106 ± 4	102 ± 5
10	101± 5	93 ± 4	111 ± 7	104 ± 2	110 ± 6	99 ± 6

Spectral interference effect could be expected in the presence of more than 1 $g \cdot L^{-1}$ of Pb, Cu and Ni because of their close alternative wavelength coincidence [13]. The interference effect of some metals and inorganic ions such as Na^+, Cl^-, PO_4^{3-} and K^+, which comes from the human perspiration and Pb, Ba, Ag, Fe, Ca and SO_4, which may be contained in the structure of gun and bullet material and the environment on the absorbance signal of Sb was also investigated. Model solutions in the range of 1–400 $mg \cdot L^{-1}$ were prepared and spiked with 10 $ng \cdot L^{-1}$ Sb. The interference effect was evaluated through the recoveries obtained. As it is seen from the results in Table 4 the presences of Cl, PO_4, Ca and Na have no serious effect on the Sb absorbance signal because of Zeeman's background correction. The absorbance signal for Sb decreased upon increasing of Ag, Ba, Pb, Fe, K and SO_4 concentration in the solution. Decreasing of recovery in the range of 61-81 % in the presence of Ag could be explained with amalgam formation [22].

Application of procedure

After every shooting with Yavuz Model of Turkish gun, sampling was performed with adhesive tapes, both cotton rods and bandaged cotton moistened with 5% of BA, according to the sampling procedure given in sampling part. Shooting and sampling were repeated three times for every procedure and also the hands were washed after each shot. Results for Sb from real sampling were obtained according to optimal instrumental conditions defined and summarized in Table 5 as concentration in the solution and distribution of amount on the palm and backside in $mg \cdot cm^{-2}$. Recovery tests were conducted for real sampling by putting on the hands' surface 10–20 $ng \cdot mL^{-1}$ of antimony standard. Recoveries achieved by using adhesive type and moistened cotton (both rod and bandaged) are found in the range of 95–122% and 95–140%, respectively. It could be concluded from recoveries that the swabbing procedure with cotton soaked in 5% BA ensures accurate and reliable results.

It is very difficult to compare and confirm results, obtained in this study with other works in the literature because of differences in gun type, bullet or cartridges, sampling procedure, *etc*. [23]. Another difficulty of such kind of studies is to find certified reference material. In spite of these difficulties, we tried to compare our results with the data for 9 mm parabellum type cartridges (such like our cartridges) with swabbing 2% of EDTA. A swabbing nearly resembles the technique used in this work. Results of Sb swabbing with EDTA are at the average range 3.19–60.70 with 2.30–13.3 standard deviations by ICP-MS technique [24]. Results of this work, seen in Table 5, are comparable with the result of Sarkis *et al*. [24]. It could be said that proposing sampling solution and bandaged cotton give also good results.

Table 4. Interference effects on the Sb atomic absorbance signal as recovery (%) without matrix modifier.

$mg \cdot L^{-1}$	Ag	Ba	Pb	Fe	Na	K	Ca	SO_4	PO_4	Cl
1	88 ± 3	109 ± 4	88 ± 2	96 ± 2	-	-	101 ± 2	-	96 ± 2	-
3	-	-	-	-	84 ± 2	73 ± 3	110 ± 7	81 ± 1	-	-
5	-	-	-	-	81 ± 3	71 ± 2	102 ± 5	76 ± 3	95 ± 2	-
10	76 ± 4	89 ± 2	86 ± 3	80 ± 1	-	-	-	-	95 ± 3	92 ± 1
15	-	-	-	-	83 ± 2	69 ± 4	114 ± 2	79 ± 2	95 ± 3	-
20	-	-	-	-	84 ± 1	68 ± 1	107 ± 2	75 ± 1	-	-
50	68 ± 2	57 ± 4	79 ± 4	65 ± 3		66 ± 2	103 ± 2	69 ± 3	-	91 ± 2
100	66 ± 3	33 ± 5	78 ± 4	61 ± 4		63 ± 4	92 ± 3	46 ± 6	-	89 ± 3
200	-	21 ± 3	71 ± 2	53 ± 8					-	89 ± 4
400									-	86 ± 3

Table 5. Results on antimony content in gunshot residues (n = 3).

	Adhesive band, mean ± s.d		Cotton rod, mean ± s.d		Bandaged cotton, mean ± s.d	
	$ng \cdot mL^{-1}$	$ng \cdot cm^{-2}$	$ng \cdot mL^{-1}$	$ng \cdot cm^{-2}$	$ng \cdot mL^{-1}$	$ng \cdot cm^{-2}$
Left hand						
palm	34.1 ± 0.3	5.5 ± 0.1	20.6 ± 1.4	3.3 ± 0.2	36.6 ± 0.4	5.9 ± 0.2
backside	32.4 ± 0.8	5.2 ± 0.2	19.9 ± 0.4	3.2 ± 0.1	30.5 ± 0.9	4.9 ± 0.2
Right hand						
palm	26.5 ± 0.6	4.3 ± 0.1	20.2 ± 4.1	3.2 ± 0.7	31.4 ± 1.2	5.1 ± 0.2
backside	34.1 ± 1.2	5.4 ± 0.2	20.4 ± 0.9	3.3 ± 0.2	37.5 ± 0.7	6.0 ± 0.2

CONCLUSION

It is known that antimony is an uncommon element and it's a kind of diagnostics of gunshot firing. For this reason concentrations of Sb on the hands are very low, ET-AAS technique can be used very sensitively for its detection. The performed study showed that swabbing with bandaged cotton moistened by 5% of BA could be successfully applied as routine sampling procedure for Sb determination in gunshot residues. BA is an efficient modifier for ETAAS measurement of Sb in this solution. However, improving studies are still necessary such as sole usage of standard bandaged cotton to increase the efficiency, accuracy and to decrease the necessity of skilled personnel for swab sampling.

***Acknowledgement**: Authors would like to thank Bursa Criminal Police Laboratory chief for his permission and also the personnel for their kind help for executing of experiments in the shooting place.*

REFERENCES

1. www.firearmsid.com/A_distanceGSR.htm
2. F. S. Romolo, P. Margot, *Forensic Sci. Int.,* **119**, 195 (2001).
3. L. Garofano, M. Capra, F. Ferrari, G. P. Bizzaro, D. Di Tullio, M. Dell'Olio, A. Ghitti, *Forensic Sci. Int.,* **103**, 1 (1999).
4. E. B. Morales, A. L. R. Vázquez, *J. Chromatogr. A,* **1061**, 225 (2004).
5. H. Meng, B. Caddy, *J. Forensic Sci.,* **42**, 553 (1997).
6. A. Zeichner, N. Levin, *J. Forensic Sci.,* **38**, 571 (1993).
7. L. T. E. Reis, J. E. S. Sarkis, O. N. Neto, C. Rodrigues, M. H. Kakazu, S. Viebig, *J. Forensic Sci.,* **48**, 1 (2003).
8. R. D. Koons, D. G. Havekost, C. A. Paters, *J. Forensic Sci.,* **32**, 846 (1987).
9. I. C. Stone, C. S. Petty, *J. Forensic Sci.,* **19**, 784 (1974).
10. G. D. Renshaw, C. A. Pounds, E. F. Pearson, *At. Absorp. Newslett.,* **12**, 55 (1973).
11. C. A. Woolever, H. D. Dewald, *Forensic Sci. Int.,* **117**, 185 (2001).
12. C. A. Woolever, D. E. Starkey, H. D. Dewald, *Forensic Sci. Int.,* **102**, 45 (1999).
13. W. French, E. Lundberg, A. Cedergen, *Prog. Anal. Atom. Spectrosc*., **8**, 257 (1985).
14. http://dic.academic.ru/dic.nsf/enwiki/41151
15. http://www.epa.gov/NCEA/iris/subst/0410.htm
16. N. Ni, H. Chou, J. Wang, M. Li, C. Lu, P. Thi, B. Wang, *Biochem. Biophys. Res. Commun.,* **369**, 590 (2008).
17. M. M. S. R. Soares, A. E. Cury, *Braz. J. Microbiol.,* **32**, 130 (2001).
18. W. Rüdorff, *Adv. Inorg. Chem.*, **1**, 223 (1959).
19. A. V. Dunaeva, I. V. Arkhangelskya, Y. V. Avdeeva, *Carbon,* **46**, 788 (2008).
20. I. Lopez-Garcia, M. Sanchez-Merlos, M. Hernandez-Cordaba, *Spectrochim. Acta, Part B,* **52**, 437 (1997).
21. K. Dash, S. Thangavel, S. C. Chaurasia, J. Arunachalam, *Talanta,* **70**, 602 (2006).
22. K. F. Cai, C. Yan, Z. M. He, J. L. Cui, C. Stiewe, E. Müller, H., Li, *J. Alloys Compd.,* **469**, 499 (2009).
23. Z. Brožek-Mucha, *Forensic Sci. Int.,* **183**, 33 (2009).
24. J. E. S. Sarkis, O. N. Neto, S. Viebig, S. F. Durrant, *Forensic Sci. Int.,* **172**, 63 (2007).

ОПРЕДЕЛЯНЕ НА АНТИМОН В БАРУТНИ ОСТАТЪЦИ ЧРЕЗ ЕЛЕКТРОТЕРМИЧНА АТОМНО-АБСОРБЦИОННА СПЕКТРОМЕТРИЯ

Н. Ф. Фидан[1], Б. Изги[2,] *

[1] Криминална полицейска лаборатория в Бурса, Главно управление на турската национална полиция, Бурса, Турция

[2] Департамент по химия, Факултет по наука и изкуство, Университет на Улугдаг, 16059Бурса, Турция

Постъпила на 9 март 2009 г.; Преработена на 4 май 2009 г.

(Резюме)

Описана е лесна и бърза аналитична процедура за определяне на антимон в барутни остатъци чрез електротермична атомно-абсорбционна спектрометрия (ETAAS). Тестван е метод на пробовземане с използване на адхезивни ленти, памучни тампони и превързочен памук намокрени с борна киселина. Определени са оптималните инструментални параметри за измерване с ETAAS: максимална температура за нагряване без загуби 700ºC и оптимална температура на атомизация 1800ºC. Експерименти с различни модификатори (Pd, Ni, аскорбинова киселина, борна киселина) показаха, че 5% (m/v) борна киселина е най-подходящ модификатор за Sb осигуряващ свободно от пречене измерване с ETAAS. Аналитичната крива е линейна в областта от 5 $\mu g \cdot L^{-1}$ до 40 $\mu g \cdot L^{-1}$ (R^2 = 0.9998, n = 3). Границата на откриване (LOD) и границата на определяне (LOQ) изчислени при оптималните условия са съответно 0.4 $\mu g \cdot L^{-1}$ и 1.3 $\mu g \cdot L^{-1}$. Изследвана и определена е степента на пречене от матрични елементи като Na, K, Ca, Fe, Pb, Ba, Ag, Cl, SO_4 и PO_4. Получени са аналитични добиви в границите на 70–88%.

Bulgarian Chemical Communications, Volume 41, Number 4 (pp. 409–413) 2009

Synthesis and antibacterial activity of a series of novel dihydrobenzofuranols

T. D. Venu[1], B. S. Sudha[2], S. Satish[3], S. Shashikanth[1], K. A. Raveesha[3]*

[1] *Department of Studies in Chemistry, University of Mysore, Manasagangotri, Mysore 570 006, India*
[2] *Department of Chemistry, Yuvaraja's College, University of Mysore, Mysore 570 005, India*
[3] *Department of Studies in Microbiology, University of Mysore, Manasagangotri, Mysore 570 006, India*

Received April 15, 2008; Revised February 3, 2009

A facile synthesis of solely dihydrobenzofuranols was achieved by irradiation of 2-alkoxy substituted benzophenones in acetonitrile**.** The antibacterial activities of the resulting compounds were studied against 12 human pathogens. All the compounds showed significant growth inhibition at concentration of 50 μg/mL. The halogen substituted compounds were most active whereupon one of the compounds showed stronger inhibition towards all the strains than the antibitiocs bacitracin, ciprofloxacin and gentamicin.

Key words: photochemical synthesis, dihydrobenzofuranols, antibacterial activity.

INTRODUCTION

The chemistry of dihydrobenzofurans has recently drawn considerable attention from chemical, physiological and pharmacological point of view [1−4]. Intramolecular hydrogen abstractions are among some of the best studied reactions in organic photochemistry. The most prevalent example involves abstraction of a γ-hydrogen, *i.e.*, the Norrish Type II reaction [5]. However, a number of cases of both δ- and ε-hydrogen abstraction has also been reported [6]. These reactions are object of recent interest because they provide useful insight into ketone photochemistry and biradical behaviour and have potential synthetic application in the construction of five and six membered rings [7]. One example of a δ-hydrogen abstraction, which has found some applications in synthesis, is the photocyclization of 2-alkoxy substituted benzophenones to dihydrobenzofuranols (Scheme 1).

Literature survey on the structure-activity relationship among dihydrobenzofuranol analogues revealed that no efforts were directed towards the study of their antibacterial activities when different substituents were introduced in the aromatic rings. We supposed that varying the substituents in the aromatic ring might affect the antibacterial activity.

In this communication, we report a facile synthesis of a series of new dihydrobenzofuranols with different combinations of substituents in their aromatic rings and evaluation of their antibacterial activity against 12 human pathogens. The synthesis was based on cyclization of 1,5-biradicals, generated by irradiation of substituted 2-alkoxy benzophenones.

CHEMISTRY

The synthesis of the title compounds is outlined in Scheme 1.

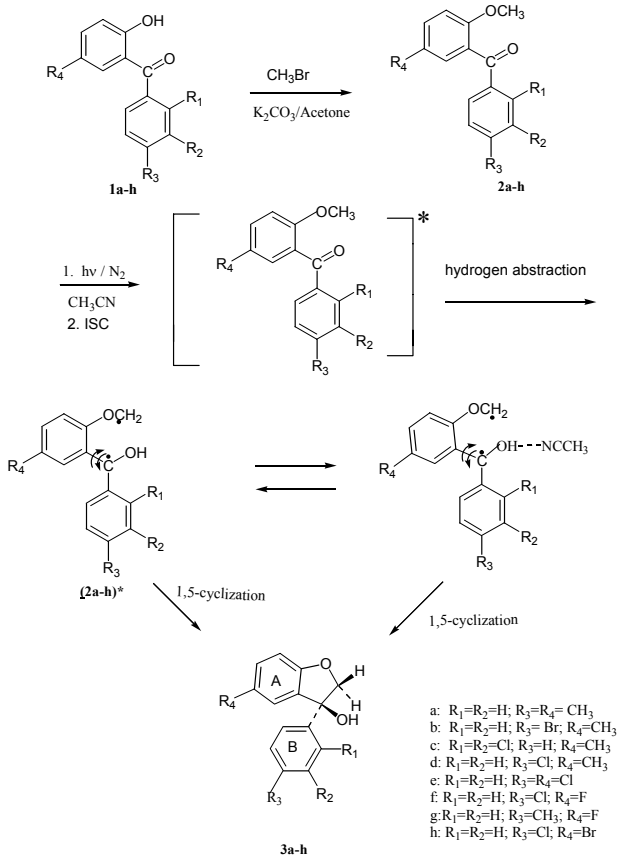

Scheme 1

* To whom all correspondence should be sent:
E-mail: karaveesha@gmail.com

2-Hydroxy substituted benzophenones **1a**–**h**, were synthesized as it was previously described [8]. The substrates for photocyclization, the 2-alkoxy substituted benzophenones **2a**–**h**, were synthesized in good yields by the reaction of **1a**–**h** with methyl iodide in the presence of anhydrous potassium carbonate (Scheme 1). Irradiation of degassed solutions of **2a**–**h** in acetonitrile was conducted at ambient temperatures (~ 33°C) and 365 nm, 400 W high-pressure mercury lamp with Pyrex filter. The products **3a**–**h** were characterized by IRS, NMR and elemental analysis.

RESULTS AND DISCUSSION

Widespread use of antibiotics is thought to have spurred evolutionary adaptations that enable bacteria to survive these powerful drugs. The combat with the bacterial resistance demands a search for alternative newer molecules. For this reason, the eight new dihydrobenzofuranols **3a**–**f** synthesized in this study, were screened in regard to their antibacterial activities. Their growth inhibitory activity was tested against nine Gram-positive and three Gram-negative bacteria (Table 1). Three of the compounds **3e**, **3f** and **3h** were shown to be highly potent antibacterial agents. Their antibacterial activity was much stronger than that of ciprofloxacin, which is a powerful antibiotic used to overcome bacterial infections.

CONCLUSION

Our study shows a strong evidence for the antibacterial activity of halo substituted dihydrobenzofuranols. These compounds exhibited stronger growth inhibitory activity than the reference compounds. The presence of methyl groups in ring A and B was not favourable. The compounds are very good candidates for further investigation on their therapeutic effect for management of bacterial infections.

Table 1. Antibacterial activity measured as zone of inhibition (mm) of eight newly synthesized dihydrobenzofuranols (**3a**–**h**) (50 μg/mL) against human pathogenic bacteria.

Pathogens	**3a**	**3b**	**3c**	**3d**	**3e**	**3f**	**3g**	**3h**	Bacitracin	Ciprofloxacin	Gentamicin
Bacillus subtilis MTCC441	12.50 ± 0.39	18.66 ± 0.22	28.50 ± 0.27	19.50 ± 0.25	29.50 ± 0.27	33.66 ± 0.15	22.66 ± 0.06	28.50 ± 0.25	0.00 ± 0.00	19.62 ± 0.18	12.66 ± 0.12
Escherichia coli MTCC443	15.16 ± 0.22	20.00 ± 0.00	29.50 ± 0.25	26.66 ± 0.66	31.50 ± 0.17	34.50 ± 0.27	28.50 ± 0.27	30.66 ± 0.66	0.00 ± 0.00	10.00 ± 0.00	10.25 ± 0.14
Klebsiella pneumoniae MTCC109	09.50 ± 0.28	17.33 ± 0.16	21.50 ± 0.17	17.50 ± 0.19	23.66 ± 0.15	25.38 ± 0.18	19.83 ± 0.20	22.83 ± 0.20	0.00 ± 0.00	20.25 ± 0.16	11.75 ± 0.16
Proteus mirabilis MTCC1429	18.00 ± 0.00	15.50 ± 0.27	22.66 ± 0.15	19.83 ± 0.14	21.50 ± 0.27	22.16 ± 0.12	21.66 ± 0.25	20.83 ± 0.20	0.00 ± 0.00	18.25 ± 0.16	08.50 ± 0.16
Pseudomonas aeruginosa MTCC1688	10.00 ± 0.00	16.50 ± 0.23	34.50 ± 0.13	17.50 ± 0.25	35.38 ± 0.18	36.50 ± 0.12	19.75 ± 0.16	32.66 ± 0.25	0.00 ± 0.00	34.25 ± 0.16	12.63 ± 0.16
Salmonella paratyphi A MTCC735	11.50 ± 0.18	18.50 ± 0.21	29.50 ± 0.25	20.66 ± 0.66	30.16 ± 0.12	32.66 ± 0.25	22.83 ± 0.14	29.50 ± 0.17	0.00 ± 0.00	27.75 ± 0.16	15.25 ± 0.16
Salmonella typhi MTCC733	18.83 ± 0.14	20.50 ± 0.19	27.83 ± 0.20	22.83 ± 0.20	29.50 ± 0.12	31.83 ± 0.14	24.66 ± 0.15	28.50 ± 0.19	0.00 ± 0.00	20.25 ± 0.16	17.75 ± 0.16
Salmonella typhimurium MTCC98	12.33 ± 0.15	18.50 ± 0.20	25.50 ± 0.27	19.33 ± 0.17	26.66 ± 0.25	28.66 ± 0.06	22.50 ± 0.25	25.66 ± 0.12	0.00 ± 0.00	18.75 ± 0.31	16.00 ± 0.31
Shigella flexneri MTCC1457	10.33 ± 0.16	13.50 ± 0.27	19.66 ± 0.11	14.83 ± 0.20	21.83 ± 0.14	24.50 ± 0.25	18.66 ± 0.66	20.66 ± 0.11	0.00 ± 0.00	27.63 ± 0.18	11.38 ± 0.18
Shigella sonnei MTCC 2957	08.50 ± 0.27	12.66 ± 0.14	21.50 ± 0.17	13.66 ± 0.25	23.66 ± 0.06	29.83 ± 0.14	23.83 ± 0.20	22.50 ± 0.13	0.00 ± 0.00	21.75 ± 0.16	15.25 ± 0.16
Staphylococcus aureus MTCC 737	19.00 ± 0.00	24.00 ± 0.22	35.33 ± 0.18	23.50 ± 0.17	34.50 ± 0.25	35.50 ± 0.13	25.83 ± 0.20	33.66 ± 0.15	26.75 ± 0.84	18.13 ± 0.48	24.63 ± 0.48
Streptococcus faecalis MTCC459	15.50 ± 0.33	21.50 ± 0.30	33.66 ± 0.11	20.66 ± 0.66	32.83 ± 0.14	33.12 ± 0.19	27.66 ± 0.25	31.83 ± 0.14	10.00 ± 0.00	10.00 ± 0.00	12.50 ± 0.00

Zone of inhibition (Mean of six replicates ± standard error). $p < 0.05$.

EXPERIMENTAL

Chemistry

Chemicals were purchased from Aldrich Chemical Co. Thin layer chromatography (TLC) was performed on silica gel plates with visualization under UV-light. Melting points were determined on a Thomas Hoover capillary melting point apparatus with a digital thermometer and were not corrected. The IR spectra were recorded in nujol on FT-IR Shimadzu 8300 spectrometer. ^{1}H NMR and ^{13}C NMR spectra were recorded in $CDCl_3$ at 300 and 100 MHz, respectively. Chemical shifts were in parts per million downfield from tetramethylsilane. *J* constants were in Hz. Elemental analysis data are within 0.4% deviation of the calculated value.

*General procedure for synthesis of substituted 2-alkoxybenzophenones **2a**–**2h***

Bromomethane (1.9 g, 0.02 mol) was added to a solution of (2-hydroxy-5-methylphenyl)-4-methyl phenyl methanone **1a** (5.21 g, 0.02 mol) and anhydrous potassium carbonate (2.8 g, 0.02 mol) in dry acetone (50 ml). The solution was refluxed for 18 h, cooled down and then evaporated to dryness. The residue was treated with ice water to remove potassium carbonate and extracted with (ethyl) ether (3×50 ml). The organic layer was washed with 10% sodium hydroxide solution (3×30ml) and water (3×30 ml), dried over anhydrous sodium sulphate and evaporated. The obtained crude solid was recrystallized from ethanol to give the pure **c**ompounds 2a-2h.

Compound **2a:** [9] yield 83%**,** m.p. 160−162°C; IRS (nujol): 1658 cm^{-1} (C=O); ^{1}H NMR ($CDCl_3$) δ 2.25 (s, 3H, Ar–CH_3), 2.32 (s, 3H, Ar–CH_3), 3.6 (s, 3H, OCH_3), 6.7−7.7 (bm, 7H, Ar–H); ^{13}C NMR ($CDCl_3$): δ 20.9 (q), 56.0 (q), 113.7 (d), 123.3 (s), 128.9 (d), 129.9 (s), 130 (d), 131.8 (d), 133.9 (d), 134.8 (s), 141.4 (s), 160.6 (s), 187.0 (s). Anal. Calcd for $C_{16}H_{16}O_2$ (240); C 80.0; H 6.67%. Found: C 80.12; H 6.63%.

Compound **1a**–**h:** [9] yield 75%, m.p. 55−58°C; IRS (nujol): 1660 cm^{-1} (C=O); ^{1}H NMR ($CDCl_3$) δ 2.23 (s, 3H, Ar–CH_3), 3.55 (s, 3H, OCH_3), 6.65−7.5 (bm, 7H, Ar–H); ^{13}C NMR ($CDCl_3$): δ 20.9 (q), 56.0 (q), 113.7 (d), 123.3 (s), 126.8 (s), 129.7 (s), 131.5 (d), 131.8 (d), 132.3 (d), 133.9 (d), 136.8 (s), 160.6 (s), 187.0 (s). Anal. Calcd for $C_{15}H_{13}BrO_2$ (305); C 59.02; H 4.26; Br 26.23%. Found: C 58.95; H 4.25; Br 26.21%.

Compound **2c:** [9] yield 71%, m.p. 150−152°C; IRS (nujol): 1659 cm^{-1} (C=O); ^{1}H NMR ($CDCl_3$) δ 2.22 (s, 3H, Ar–CH_3), 3.5 (s, 3H, OCH_3), 6.6−7.8 (bm, 7H, Ar–H); ^{13}C NMR ($CDCl_3$): δ 20.9 (q), 56.0 (q), 113.7 (d), 123.3 (s), 127.7 (d), 129.6 (d),129.7 (s), 131.8 (d), 133.9 (s), 133.9 (d), 134.0 (d), 135.8 (s), 139.6 (s), 160.6 (s), 187.0 (s). Anal. Calcd for $C_{15}H_{12}Cl_2O_2$ (295); C 61.02; H 4.07; Cl 24.07%. Found: C 60.89; H 4.02; Cl 24.05%.

Compound **2d:** yield 83%, m.p. 151−153°C; IRS (nujol): 1665 cm^{-1} (C=O); ^{1}H NMR ($CDCl_3$) δ 2.33 (s, 3H, Ar–CH_3), 3.65 (s, 3H, OCH_3), 6.75−7.6 (bm, 7H, Ar–H); ^{13}C NMR ($CDCl_3$): δ 20.9 (q), 56.0 (q), 113.7 (d), 123.3 (s), 128.9 (d), 129.9 (s), 130 (d), 131.8 (d), 133.9 (d), 134.8 (s), 141.4 (s), 160.6 (s), 187.0 (s). Anal. Calcd for $C_{15}H_{13}ClO_2$ (260.72); C 69.10; H 5.03; Cl 13.60%. Found: C 69.12; H 5.01; Cl 13.59%.

Compound **2e:** yield 83%, m.p. 138−141°C; IRS (nujol): 1668 cm^{-1} (C=O); ^{1}H NMR ($CDCl_3$) δ 3.7 (s, 3H, OCH_3), 6.77−7.64 (bm, 7H, Ar–H); ^{13}C NMR ($CDCl_3$): δ 56.0 (q), 115.2 (d), 124.8 (s), 125.8 (s), 128.6 (d), 131.5 (d), 131.6 (d), 133.6 (d), 135.9 (s), 137.5 (s), 161.7 (s), 187.0 (s). Anal. Calcd for $C_{14}H_{10}Cl_2O_2$ (281.13); C 59.81; H 3.59; Cl 25.22%. Found: C 59.79; H 3.63; Cl 25.20%.

Compound **2f:** yield 83%, m.p. 132−134°C; IRS (nujol): 1670 cm^{-1} (C=O); ^{1}H NMR ($CDCl_3$) δ 3.68 (s, 3H, OCH_3), 6.85−7.65 (bm, 7H, Ar–H); ^{13}C NMR ($CDCl_3$): δ 56.0 (q), 115.4 (d), 118.1 (d), 120.2 (d), 125.0 (s), 128.6 (d), 131.5 (d), 135.9 (s), 137.5 (s), 154.1 (s), 159.2 (s), 187.0 (s). Anal. Calcd. for $C_{14}H_{10}ClFO_2$ (264.68); C 63.53; H 3.81; Cl 13.39; F 7.18%. Found: C 63.55; H 3.83; Cl 13.37; F 7.16%.

Compound **2g:** yield 83%, m.p. 143−145°C; IRS (nujol): 1667 cm^{-1} (C=O); ^{1}H NMR ($CDCl_3$) δ 2.3 (s, 3H, Ar–CH_3), 3.67 (s, 3H, OCH_3), 6.71–7.47 (bm, 7H, Ar–H); ^{13}C NMR ($CDCl_3$): δ 20.9 (q), 56.0 (q), 115.4 (d), 118.1 (d), 120.2 (d), 125.0 (s), 128.9 (d), 130.0 (d), 134.8 (s), 141.4 (s), 154.1 (s), 159.2 (s), 187.0 (s). Anal. Calcd for $C_{15}H_{13}FO_2$ (244.26); C 73.76; H 5.36; F 7.78%. Found: C 73.78; H 5.33; F 7.76%.

Compound **2h:** yield 79%, m.p. 149−151°C; IRS (nujol): 1675 cm^{-1} (C=O); ^{1}H NMR ($CDCl_3$) δ 3.6 (s, 3H, OCH_3), 6.7−7.7 (bm, 7H, Ar–H); ^{13}C NMR ($CDCl_3$): δ 56.0 (q), 115.1 (s), 116.0 (d), 125.6 (s), 128.6 (d), 131.5 (d), 134.4 (d), 135.9 (s), 136.5 (d),137.5 (s), 162.6 (s), 187.0 (s). Anal. Calcd for $C_{14}H_{10}BrClO_2$ (325.59); C 51.65; H 3.10; Br 25.54.18; Cl 10.89%. Found: C 51.63; H 3.12; Br 25.55, Cl 10.87%.

General procedure for the synthesis of dihydrobenzofuranols **3a**–**3h**

The starting compounds **2a**–**2h** (15 mmol) were dissolved in acetonitrile (50 mL) and deoxygenated by bubbling nitrogen gas for 1 h and then irradiated

for 4−20 h. After the completion of the reaction (monitored by TLC), the solvent was evaporated under reduced pressure at 40°C. The residue was subjected to column chromatography on silica gel with eluent mixture hexane:chloroform:acetone (7:3:1) to give pure compounds **3a**–**3h**.

Compound **3a:** [9] yield 77%, m.p. 156−157°C; IRS (nujol): 3410 cm^{-1} (OH); ^1H NMR ($CDCl_3$): δ 2.4 (s, 3H, Ar–CH_3), 2.5 (s, 3H, Ar–CH_3), 3.9 (s, 1H, C_2–H), 4.3 (s, 1H, C_2–H), 6.0−6.2 (bs, 1H, OH), 7.2–8.0 (bm, 7H, Ar–H); ^{13}C NMR ($CDCl_3$): δ 20.9 (q), 21.2 (q), 80.5 (t), 88.3 (s), 114.6 (d), 127.3 (d), 128.3 (d), 128.6 (s), 129.7 (d), 129.8 (s), 135.2 (s), 140.0 (s), 155.7 (s). Anal. Calcd for $C_{16}H_{16}O_2$ (240); C 80.0; H 6.67%. Found: C 79.60; H 6.62%.

Compound **3b:** [9] yield 72%, m.p. 155−157°C; IRS (nujol): 3420 cm^{-1} (OH);^1H NMR ($CDCl_3$): δ 2.4 (s, 3H, Ar–CH_3), 3.8 (s, 1H, C_2–H), 4.4 (s, 1H, C_2–H), 6.0−6.2 (bs, 1H, OH), 7.2−8.0 (bm, 7H, Ar–H); ^{13}C NMR ($CDCl_3$): δ 21.2 (q), 80.5 (t), 88.3 (s), 114.6 (d), 120.6 (s), 127.3 (d), 128.3 (d), 128.6 (d), 129.7 (d), 129.8 (s), 155.7 (s). Anal. Calcd for $C_{15}H_{13}BrO_2$ (305); C 59.02; H 4.26; Br 26.23%. Found: C 59.0; H 4.21; Br 26.18%.

Compound **3c:** [9] yield 81%, m.p. 158−159°C; IRS (nujol): 3415 cm^{-1} (OH); ^1H NMR ($CDCl_3$): δ 2.4 (s, 3H, Ar–CH_3), 3.9 (s, 1H, C_2–H), 4.4 (s, 1H, C_2–H), 6.0−6.3 (bs, 1H, OH), 7.2−8.0 (bm, 7H, Ar–H); ^{13}C NMR ($CDCl_3$): δ 21.2 (q), 78.7 (s), 80.0 (t), 88.3 (s), 114.6 (d), 127.3 (d), 127.8 (d), 127.9 (d), 128.5 (d), 128.6 (s), 129.7 (d), 129.8 (s), 134.1 (s), 134.7 (s), 144.8 (s), 155.7 (s). Anal. Calcd for $C_{15}H_{12}Cl_2O_2$ (295); C 61.02; H 4.07; Cl 24.07%. Found: C 61.0; H 4.08; Cl 23.04%.

Compound **3d:** yield 75%, m.p. 160−162°C; IRS (nujol): 3430 cm^{-1} (OH); ^1H NMR ($CDCl_3$): δ 2.35 (s, 3H, Ar–CH_3), 3.8 (s, 1H, C_2–H), 4.2 (s, 1H, C_2–H), 6.1−6.3 (bs, 1H, OH), 7.0−7.8 (bm, 7H, Ar–H); ^{13}C NMR ($CDCl_3$): δ 21.2 (q), 80.5 (t), 88.3 (s), 114.6 (d), 127.3 (d), 128.6 (s), 129.4 (d), 129.7 (d), 129.8 (s), 131.4 (s),141.1 (s), 155.7 (s). Anal. Calcd for $C_{15}H_{13}ClO_2$ (260.72); C 69.10; H 5.03; Cl 13.60%. Found: C 69.35; H 5.01; Cl 13.59%.

Compound **3e:** yield 78%, m.p. 165−167°C; IRS (nujol): 3425 cm^{-1} (OH); ^1H NMR ($CDCl_3$): δ 3.9 (s, 1H, C_2–H), 4.3 (s, 1H, C_2–H), 6.2−6.4 (bs, 1H, OH), 7.3−7.9 (bm, 7H, Ar–H); ^{13}C NMR ($CDCl_3$): δ 80.5 (t), 87.5 (s), 116.1 (d), 125.9 (s), 127.0 (d), 129.4 (d), 129.5 (d), 129.8 (d), 130.1 (s), 131.3 (s), 141.1 (s), 156.8 (s). Anal. Calcd for $C_{14}H_{10}Cl_2O_2$ (281.13); C 59.81; H 3.59; Cl 25.22%. Found: C 59.79; H 3.57; Cl 25.21%.

Compound **3f:** yield 81%, m.p.. 151−153°C; IRS (nujol): 3435 cm^{-1} (OH); ^1H NMR ($CDCl_3$): δ 3.75 (s, 1H, C_2–H), 4.1 (s, 1H, C_2–H), 6.05−6.3 (bs, 1H, OH), 7.2−7.85 (bm, 7H, Ar–H); ^{13}C NMR ($CDCl_3$): δ 80.5 (t), 88.0 (s), 113.6 (d), 116.0 (d), 116.3 (d), 129.4 (d), 129.5 (d), 129.8 (d), 130.3 (s), 131.3 (s), 141.1 (s), 154.2 (s), 154.3 (s). Anal. Calcd for $C_{14}H_{10}ClFO_2$ (264.68); C 63.53; H 3.81; Cl 13.39; F 7.18%. Found: C 63.55; H 3.84; Cl 13.31; F 7.17%.

Compound **3g:** yield 69%, m.p. 147−149°C; IRS (nujol): 3415 cm^{-1} (OH); ^1H NMR ($CDCl_3$): δ 3.85 (s, 1H, C_2–H), 4.3 (s, 1H, C_2–H), 6.0−6.25 (bs, 1H, OH), 7.1−7.8 (bm, 7H, Ar–H); ^{13}C NMR ($CDCl_3$): δ 20.9 (q), 80.5 (t), 88.0 (s), 113.6 (d), 116.0 (d), 116.3 (d), 128.3 (d), 129.7 (d), 130.3 (s), 135.2 (s), 140.1 (s), 154.2 (s), 154.3 (s). Anal. Calcd for $C_{15}H_{13}FO_2$ (244.26); C 73.76; H 5.36; F 7.78%. Found: C 73.73; H 5.38; F 7.76%.

Compound **3h:** yield 67%, m.p. 159−160°C; IRS (nujol): 3420 cm^{-1} (OH); ^1H NMR ($CDCl_3$): δ 3.75 (s, 1H, C_2–H), 4.3 (s, 1H, C_2–H), 6.05−6.3 (bs, 1H, OH), 7.25−8.05 (bm, 7H, Ar–H); ^{13}C NMR ($CDCl_3$): δ 80.5 (t), 87.3 (s), 115.2 (s), 116.9 (d), 129.4 (d), 129.8 (d), 129.9 (d), 130.9 (s), 131.2 (s), 132.3 (d), 141.1 (s), 157.7 (s). Anal. Calcd for $C_{14}H_{10}BrClO_2$ (325.59); C 51.65; H 3.10; Br 24.54; Cl 10.89%. Found: C 51.63; H 3.08; Br 24.56; Cl 10.87%.

Antibacterial activity assay

The antibacterial activity was determined by agar diffusion method. The sterile medium (20 mL) was poured onto a 9 cm Petri plates. The medium was allowed to cool down in a sterile condition and plates were then inculcated with 1×10^5 cfu cultures of the tested bacteria. The concentration of bacterial cells in the suspension was adjusted to a minimum of 1×10^5 cfu/ml in nutrient broth solution. Agar cups of 5 mm diameter were made in the plates. Each test sample was dissolved in dimethyl formamide (DMF), 50 μL of the test solution containing 50 μg/mL of the test compound were placed in each cup. The plates were left to stay for an hour in order to facilitate the diffusion of the drug solution. Negative control samples were prepared using the same solvent (DMF) employed to dissolve the examined compounds [10]. Then the plates were incubated at 37°C for 24 h. The zone of inhibition (if any) against the used bacteria was measured in mm. Bacitracin and ciprofloxacin were used as positive reference to determine the sensitivity of each bacterial strain tested.

Acknowledgements: *The authors express their sincere gratitude to University of Mysore, Mysore, for the laboratory facilities.*

REFERENCES

1. H. Mallesha, N. D. Dinesh, K. S. Rangappa, S. Shashikanth, N. K. Lokanath, M. A. Sridhar, J. S. Prasad, *Indian J. Chem*., Sect. B, **41**, 196 (2002).
2. R. S. Kusurkar, D. K. Bhosale, *Synth. Commun*., **20**, 101 (1990).
3. P. Cagniant, D. Cagniant, in: Advances in Heterogeneous Chemistry, A. R. Katritzky, A. J. Boulton (eds), vol. 18, Academic Press, New York, 1975, p. 338.
4. K. B. G. Torssell, in: Natural Product Chemistry, John Wiley and Sons Ltd., Great Britain, 1983, pp. 127, 155.
5. P. J. Wagner, *Acc. Chem. Res*., **4**, 168 (1971).
6. P. J. Wagner, *Acc. Chem. Res*., **22**, 83 (1989).
7. M. A. Aziz, J. V. Auping, M. A. Meador, *J. Org. Chem.,* **60**, 1303 (1995).
8. S. A. Khanum, S. K. Murari, S. Viswanath, S. Shashikanth, *Bioorg. Med. Chem. Lett*., **15**, 4100 (2005).
9. S. Shashikanth, B. S. Sudha, S. A. Khanum, *Heteroat. Chem*., **16**, 212 (2005).
10. Anonymous, Pharmacopoeia of India (The Indian Pharmacopoeia), 3rd Edn., Government of India, 1996.

СИНТЕЗ И АНТИМИКРОБНА АКТИВНОСТ НА НОВИ СЕРИИ ДИХИДРОБЕНЗОФУРАНОЛИ

Т. Д. Вену[1], Б. С. Судха[2], С. Сатиш[3], С. Шашикант[1], К. А. Равееша[3,*]

[1] *Департамент по химия, Университет на Майсур, Манасаганготри, Майсур 570006, Индия*
[2] *Департамент по химия, Колеж на Ювараджа, Университет на Майсур, Майсур 570005, Индия*
[3] *Департамент по микробиология, Университет на Майсур, Манасаганготри, Майсур 570006, Индия*

Постъпила на 15 април 2009 г.; Преработена на 3 февруари 2009 г.

(Резюме)

Лесна синтеза само на дихидробензофураноли е постигната чрез облъчване на 2-алкокси заместени бензофенони в ацетонитрил. Изследвана е антимикробната активност на получените съединения срещу 12 човешки патогени. Всички съединения показват значително задържане на растежа при концентрация от 50 μg/mL. Халоген-заместените съединения са по-активни, докато едно от съединенията показа по-силно инхибиране към всичките форми от антибиотиците бацитрацин, ципрофлоксацин и гентамицин.

Bulgarian Chemical Communications, Volume 41, Number 4 (pp. 414–421) 2009

Control of production campaigns with optimal loading of the power systems during multipurpose and multiproduct batch chemical plants operation

B. B. Ivanov*, K. I. Mintchev

Process Systems Engineering Laboratory, Institute of Chemical Engineering, Bulgarian Academy of Sciences, Acad. G. Bonchev St., Block 103, 1113 Sofia, Bulgaria

Received September 19, 2008; Revised June 3, 2009

The paper is devoted to the problem of optimal loading of the joint systems of power supply of multipurpose and multiproduct batch chemical plants (MMBCP) operating in regime of production campaign. Mathematical method is proposed for determining the control independent variables that ensures minimum deviation of the loading characteristics of power demand of the related power systems from the ideal ones. The models developed for power consumption of the individual productions that belong to a production campaign were based on Fourier series. The task of optimum control was formulated as a non-linear mathematical programming one. The method proposed is verified by a test example.

Key words: multipurpose and multiproduct batch chemical plants, optimal loading of the power systems.

INTRODUCTION

Up to 50% of the world industrial units, related to chemical industry, are batch operating ones Stoltze *et al*. [1]. The chemical industry is a large power consumer and its effective use of power is very important. Referring to the continuous systems, the problem of effective use of their power utilization nets is most often seen as reduction of the power demand by effective utilization of the net internal power or introduction of energy-saving technologies. This is realized mainly by process heat integration according to Linnhoff [2]. However, the power bills of the batch processing systems represent only 5−10% of the total production costs per unit of product [3]. The power effectiveness of these systems depends strongly on the optimal load of the external power supply systems that is temporally non-uniform. Characteristic property of their performance is the fact that during simultaneous operation of a set of batch productions it is possible to reach the loading threshold values leading to emergency situations or to experience falls of the effectiveness parameters of the external power supply systems. The occurrence of such problems is characteristic of the operation of this class of systems. They are often met in various industries, such as the food processing, pharmaceutical, oils and paints and fine chemicals processing and they are considered widely in the literature [4, 5].

Referring to available sources, the problem of optimal loading of the various power systems connected with multipurpose and multiproduct batch chemical plants (MMBCP) has two aspects. The first aspect includes problems of shrinking demands of any kind of power by process heat integration [3, 6–8,]. This approach is known to lead to high utilization effectiveness of the systems' internal power, and, while using appropriate schedules and heat integration flow charts, also to loading reduction and therefore to more uniform load of the particular external power system. However, the ideas of heat integration may not be always applicable, as they are intercorrelated with system reconstruction activities that require proofs of economical feasibility. Besides, one may not reach the desirable loading non-uniformity.

Another approach to deal with effective power utilization is referring to development of appropriate production schedules [3, 4, 6, 9–12] that lead to decrease in loading non-uniformity. The latter unilaterally leads to higher performance effectiveness of the relevant power system.

Among the first papers to consider the issue of optimal loading of the power systems during operation of a group of batch productions is the one of Bieler *et al*. [13]. This work proposed a method for assessing the performance conditions of systems including batch production units that leads to a decrease in the peak load of the power systems. The task has been solved by analytical models of power consumption, based on Fourier series, while the optimal operation conditions were found by formulating this task in terms of mathematical programming. The formulation thus proposed by

* To whom all correspondence should be sent:
E-mail: bivanov@bas.bg

Ivanov *et al*. [9] considered the deviation of the instant power of start-up of batch production as a single control variable. In this way, the possibility to achieve optimal load of the power demand systems can be largely limited.

Referring to another work by Badel. *et al*. [14], the issue of optimal loading of multipurpose plant systems has been discussed from the point of view of financial resources. This work assumes operation of the system in a production schedule "follow-up" regime of the type Job Shop Scheduling.

An interesting approach is reported in refs. [13, 15, 16], where mathematical models of power consumption of some charts of batch reactors have been proposed. Nevertheless, the approach of MMBCP operation control considered in this group of works is not enough general to be used.

From the above review of the literature, it becomes clear that the issues related to optimal loading of the power systems during operation of multipurpose and multi-product chemical plants can be resolved following two main directions, namely: 1. Using means and charts allowing maximum utilization of the systems' internal energy by process heat integration, and 2. Creating performance conditions that lead to optimal load of the external power systems by formulation of appropriate schedules of operation and selection of appropriate production technologies for the majority of the products.

In any case, the issue of formulation of appropriate mathematical criteria for evaluation of the power effectiveness as well as effective methods for determination of the control variables leading to optimal loading of the various power systems still remains to be targeted.

PROBLEM DESCRIPTION

Let us consider a multipurpose chemical plant producing simultaneously a given amount of products within a production campaign (Fig. 1). The productions included in the campaign are batch ones with fixed production cycle. Assume that some stages of these productions, related to fixed power types, are power consuming and that they load the relevant external power supply system batchwise during the process stage time. Referring to fixed schedules and vessel parameters, one can determine the amount of power corresponding to any heat carrier required to produce a unit of end product (electrical power, cold, steam, cooling water, *etc*.). The consumption of any power type in the various stages of the process is carried out at constant intensity. During the operation of the set of productions simultaneously within a campaign using the various external power systems, depending on the process arrangement in time one may obtain different loading and often in some time periods it may exceed significantly the allowable threshold level of the external power system.

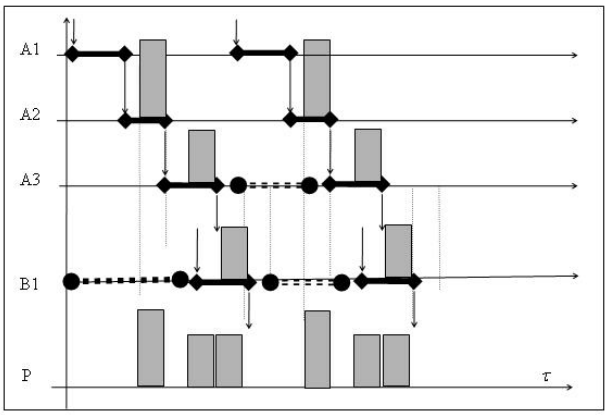

Fig. 1. Gant's chart of a production campaign of two processes.

Considering the operation of such a production system, one may find ways to dislocate the productions themselves in the course of overall production or to delay the start-up of any one of the batches in a series or to change its size. Obviously, using these control variables one can reach optimal load of the relevant power systems.

The aim of the study was to determine, within a campaign and for batch production, the values of the batch size, the delay of production start-up in a campaign, compared to a pre-selected basic production, as well as the waiting time interval among the individual batches - in such a way as to ensure the external power system by type the best loading in terms of a pre-selected criterion. Additionally, the number of batches in each production, pre-determined in order to fulfil the planned overall production program, has to be determined. In order to solve such a task, it is evident that one has to propose appropriate criterion relationships to be able to evaluate the power demand, as well as to formulate appropriate mathematical models, describing the power consumption in time.

The aim of the study was to formulate a mathematical model for evaluation of the control independent variables that ensure pre-determined loading requirements of the power systems during MMBCP operation in a fixed production campaign.

Theory

Basic data. Let us consider the sets of variables, as follows:

Set $I\{i_1, i_2, ..., i_N\}$ – set of products subject to simultaneous production.

Set $J_i\{j_1, j_2, ..., j_N\}$ – set of stages of any separate production process.

Set $P_{ij}\{p_1, p_2, ...p_N\}$ – set of processes within any production stage.

Additionally, also consider the data, as follows:

e_{ijpw} – the amount of power of type *w*, required to produce a unit mass of end product during the *p*-th process of the *j*-th stage and in the *i*-th production line.

The power demand in the case of permanent loading during the process will be:

$$p_{ijpw} = \frac{e_{ijpw} B_i}{\tau_{ijp}}, \text{ respectively,}$$

where τ_{ijp} is the time interval of the relevant process, and B_i is the batch size.

The duration of each stage of a given production will be:

$$\tau_{ij} = \sum_{p_{ij}} \tau_{ijp} \ , \quad \forall i \in I, \forall j \in J \ .$$

The amount of mass of product of any kind for the planning horizon *H* should not be less than the previously fixed value, namely, G_i^{min} .

The cycle time intervals of the productions operating in regime of overlapping cycles is calculated by means of the equation $\tau_i = \boldsymbol{max}_j(\tau_{ij})$, and in the cases where the production arrangement is without overlapping of cycles, the cycle time will be $\tau_i = \sum_j \tau_{ij}$.

It is assumed also that the relationships for determination of the process time intervals as a function of the batch size are known:

$$\tau_{ijp} = F_{ijp}^f(B_i), \quad \forall_i \in I, \forall_j \in J_i, \forall_p \in P_{ij}$$

The *Max* and *Min* batch size are also previously calculated for any product:

$$B_i^{MIN} = MIN_j\left\{\frac{V_{ij}^{MIN}}{s_{ij}}\right\}, \quad B_i^{MAX} = MIN_j\left\{\frac{V_{ij}^{MAX}}{s_{ij}}\right\}, \quad \forall i \in I$$

where $V_{ij}^{MIN}, V_{ij}^{MAX}$ indicate the maximum and the minimum permissible volumes of the vessels used in the relevant production stages, and s_{ij} is the dimension coefficient that determines the vessel's volume required to produce a unit mass of end product corresponding to the *i*-th production *j*-th-stage. Besides, one assumes the maximum permissible average intensity of loading of the relevant power system, P_w^{max} , to be predetermined.

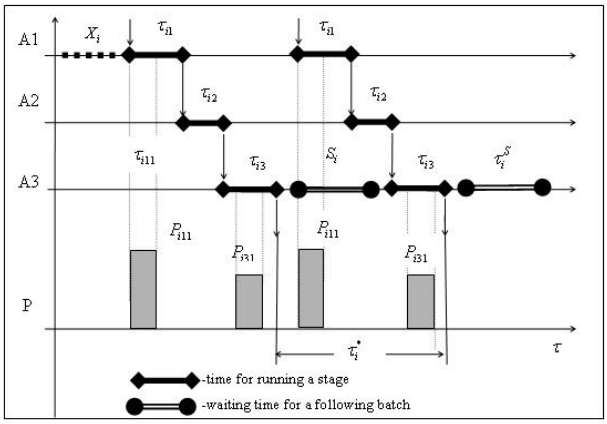

Fig. 2. Gant's chart of a production including three stages.

Control variables. The following sets of continuous control variables are entered:

- Time intreval of dislocation of the start-up of operation of the separate productions X_i , $\forall i \in I$.

- Waiting time interval among the separate production batches S_i , $\forall i \in I$.

- Size of the batch mass produced - B_i , $\forall i \in I$.

The size of the batch mass produced, corresponding to each product, may assume values within the fixed range B_i^{MIN}, B_i^{MAX}, previously calculated and depending on the degree of completeness of the individual batch vessels, engaged in the production of a given product. The intensity of the power demand of given type and/or the time interval of the individual processes are directly related to the size of the production lot.

Constraints. The following sets of inequality constraints are entered:

- Constraints of permissible size of the batch of product:

$$B_i^{MIN} \le B_i \le B_i^{MAX} \ , \quad \forall i \in I \qquad (1)$$

- Constraints for permissible waiting time interval between the batches:

$$0 \le S_i \le \frac{H - N_i \tau_i}{N_i} \ , \quad \forall i \in I \qquad (2)$$

where

$$N_i = \left\lfloor \frac{G_i^{min}}{B_i} \right\rfloor \ , \ \forall i \in I$$

means permissible minimum number of batches that has to be produced in each production process for the planning horizon *H*.

- Constraints for the allowable dislocation time intervals for the start-up of each batch relevant to one basic production process:

$$0 \le X_i \le (\tau_i + S_i), \quad \forall i \in I \tag{3}$$

- Constraints providing for execution of the programme by quantities:

$$G_i^{min} \le \left\lfloor \frac{H}{\tau_i + S_i} \right\rfloor B_i \ , \quad \forall i \in I \tag{4}$$

- Constraints providing for execution of the time programme:

$$(\tau_i + S_i) N_i \le H \ , \quad \forall i \in I \tag{5}$$

- Constraint providing for permissible average power demand during production of the products in the campaign in the course of the planning:

$$\sum_i P_{iw}^{const}(S_i, B_i) \le P_w^{max}, \forall w \in W \tag{6}$$

Mathematical model of power consumption during production campaign

The function of variation of the intensity of power of any type for each process and stage of production can be written analytically by representing the periodical function of loading through Fourier series (Fig. 2):

$$P_{ijpw}(S_i, X_i, B_i, t) = \frac{A_{ijpw}^0}{2} + \\ + \sum_k \left(A_{ijpw}^K \sin\left(\frac{2\pi k}{\tau_i^*}\left(t - \tau_{ijp}^{shift}\right)\right)\right) + \\ + \sum_k \left(B_{ijpw}^K . \cos\left(\frac{2\pi k}{\tau_i^*}\left(t - \tau_{ijp}^{shift}\right)\right)\right) \tag{7}$$

where $\tau_i^* = \tau_i + S_i$,

$$\tau_{ijp}^{shift} = X_i + \sum_{j=1}^{j} \sum_{p \in P_j} \tau_{ijp} + \sum_{p=1}^{P} \tau_{ijp} - \tau_{ij1} - \sum_{p \in P_1} \tau_{i1p}, \\ \forall i, j, p$$

k is the harmonic number of the development in series of Fourier, $A_{ijpw}^0, A_{ijpw}^k, B_{ijpw}^k$ are the Fourier coefficients that can be determined, depending on the loading curve by using analytical relationships reported for the most frequent cases or for arbitrary curves by using numerical methods. The coefficients referring to the cases of permanent loading during some process (which is the most frequent case) depend only on the process time interval and on the constant power -component and they can be written, as shown below:

$$A_{ijpw}^0 = \frac{2\, e_{ijpw}}{\tau_i^*} B_i, \\ A_{ijpw}^k = \frac{e_{ijpw}}{\pi k \tau_{ijp}} B_i \ \boldsymbol{sin}\left(\frac{2\pi k\, \tau_{ijp}}{\tau_i^*}\right), \\ B_{ijpw}^k = \frac{e_{ijpw}}{\pi k \tau_{ijp}} B_i \ \boldsymbol{cos}\left(\frac{2\pi k\, \tau_{ijp}}{\tau_i^*}\right) \tag{8}$$

Based on the Fourier transformation of the separate processes, one can write the analytical equations of the stages, of the productions and of the campaign, as follows:

- The capacity of power demand of any kind in stage *j* of a given production *i* is described as:

$$P_{ijw}(S_i, X_i, B_i, t) = P_{ijw}^{const}(S_i, B_i) + \\ + P_{ijw}^{var}(S_i, X_i, B_i, t), \quad \forall i \in I, \forall j \in J, \\ \forall w \in W \tag{9}$$

where

$$P_{ijw}^{const}(S_i, B_i) = \sum_p \frac{A_{ijpw}^0}{2}, \\ \forall i \in I, \forall j \in J, \forall w \in W \tag{10}$$

$$P_{ijw}^{var}(S_i, X_i, B_i, t) = \\ = \sum_p \left\{ \begin{array}{l} \sum_k \left(A_{ijpw}^K \sin\left(\frac{2\pi k}{\tau_i^*}\left(t - \tau_{ijp}^{shift}\right)\right)\right) + \\ + \sum_k \left(B_{ijpw}^K \cos\left(\frac{2\pi k}{\tau_i^*}\left(t - \tau_{ijp}^{shift}\right)\right)\right) \end{array} \right\} \tag{11}$$

- Capacity of power demand of any type for production *i* is described as:

$$P_{iw}(S_i, X_i, B_i, t) = P_{iw}^{const}(S_i, B_i) + \\ + P_{iw}^{var}(S_i, X_i, B_i, t), \forall i \in I, \forall w \in W \tag{12}$$

where

$$\boldsymbol{P}_{iw}^{const}(S_i, B_i) = \sum_j \boldsymbol{P}_{ijw}^{const}(S_i, B_i), \\ \forall i \in I, \forall w \in W \tag{13}$$

$$\boldsymbol{P}_{\mathrm{iw}}^{\boldsymbol{var}}\left(S_{\mathrm{i}},X_i,B_i,t\right)=\sum_j \boldsymbol{P}_{\mathrm{ijw}}^{\boldsymbol{var}}\left(S_{\mathrm{i}},X_i,B_i,t\right), \quad \forall i\in I,\forall w\in W \tag{14}$$

- Capacity of power demand of any type for the whole campaign is described as:

$$P_{\mathrm{w}}\left(\mathrm{S},X,B,t\right)=P_{\mathrm{w}}^{const}\left(S,B\right)+P_{\mathrm{w}}^{\boldsymbol{var}}\left(S,X,B,t\right) \tag{15}$$

where:

$$\boldsymbol{P}_{\mathrm{w}}^{const}\left(S,B\right)=\sum_i \boldsymbol{P}_{\mathrm{iw}}^{const}\left(S_{\mathrm{i}},B_i\right),$$

$$\boldsymbol{P}_{\mathrm{w}}^{\boldsymbol{var}}\left(S,X,B,t\right)=\sum_i \boldsymbol{P}_{\mathrm{iw}}^{\boldsymbol{var}}\left(S_{\mathrm{i}},X_i,B_i,t\right).$$

The constant component of the capacity of the power demand P_{w}^{const} does not depend on time and it is considered to be the ideal value that should be targeted as a result of the control of the production campaign based on criterion of minimum oscillation. The variable component $P_w^{\boldsymbol{var}}$ shows the power variance around the permanent component. This function can be used for assessing the degree of deviation of the real curve compared to the ideal one.

The variable component is determined by the relationship:

$$\int_0^H P_w^{\boldsymbol{var}}\left(S,X,B,t\right)dt=0. \tag{16}$$

Objective function. The deviation of the real curve with respect to the ideal one is evaluated by the relationship:

$$J_w=\frac{\int_0^H \left| P_w^{\boldsymbol{var}}\left(S,X,B,t\right)\right| dt}{H\ P_w^{const}}100\%. \tag{17}$$

Formulation of the problem of optimal control ensuring minimum variance of the power demand

The problem of optimal control of a given production campaign providing for minimum deviation of the curve of the power loading with regard to the ideal curve can be formulated as a non-linear progamming task with continuous independent variables, as follows: the values of the sets of control variables (*S*, *X*, *B*) are found in such a way as to ensure minimum of the objective function (Eqn. (17)) conforming to the set of inequality constraints (Eqns. (1) through (6)). Thus formulated, the task can be solved by using some of the known NLP techniques [17].

Example problem. An example represents the production process of three different products, carried out simultaneously in one production campaign. The workshop, involved in producing the three products, contains three reaction units with similar vessels of different operating volumes.

Table 1 contains the data related to the vessels.

Table 1. Data related to the vessels.

Vessels type P	Work volume (min/max)	Vessels type V	Work volume (min/max)	Vessels type D	Work volume (min/max)
P1	300/300	V1	300/300	D1	140/140
P2	250/250	V2	400/400	D2	160/160
P3	250/250	V3	250/250		

Table 2 contains the time intervals of the production stages in terms of products.

Table 2. Time intervals of the production stages in terms of products.

Stage	Production A	Production B	Production C
Stage 1	30 min.	30 min.	30 min.
Stage 2	240 min.	240 min.	240 min.
Stage 3	30 min.	30 min.	

The size coefficients (indicating the required operating volumes for production of unit of end product) by individual stages and productions are presented in Table 3.

Table 3. Size coefficients by individual stages and productions.

Stage/Product	Stage 1	Stage 2	Stage 3
Product A	1.2	1.96	6.3
Product B	1.2	1.23	7.3
Product C	1.2	1	

The power required to produce a unit of end product by individual stages and productions is given in Table 4.

Table 4. Power required to produce an end product unit by individual stages and productions.

No	Power required for production of a unit product in stage		
	Stage 1, kW	Stage 2, kW	Stage 3, kW
Product A	0.24	0	0.092
Product B	0.295	0	0.11
Product C	0.029	0	

The planning horizon of this production campaign is $H = 100$ hours.

Table 5 describes the vessels for production of products “A”, “B” and “C”.

The task was solved by using software package ECAM performing a NLP task.

Table 6 contains the optimal values of the control variables.

Figures 3, 4 and 5 illustrate the curves of variation of the power demand, corresponding to the individual productions and the total loading of the power system.

Table 5. List of the vessels relevant to separate productions.

Production process	Stage 1	Stage 2	Stage 3	Planned amount
Product A	P1	V1	D1	400
Product B	P2	V2	D2	250
Product C	P3	V3		3000

Table 6. Optimal values of the control variables.

Production	Time of starting-up, h	Time of cycle and waiting time between batches, h	Optimum size of a batch and total amount produced in the horizon, kg	Maximum peak power, kW	Mean power in the planning horizon, kW	Process variability, %
A	0	5.47/1.47	22.22/406.2	10.56	1.34	11.17
B	1.06	7.33/3.33	21.91/298.9	13.2	1.21	67.5
C	2.52	6.909/2.909	208.33/3015	12.1	0.87	52.5
A+B+C				25.01	3.433	16.325

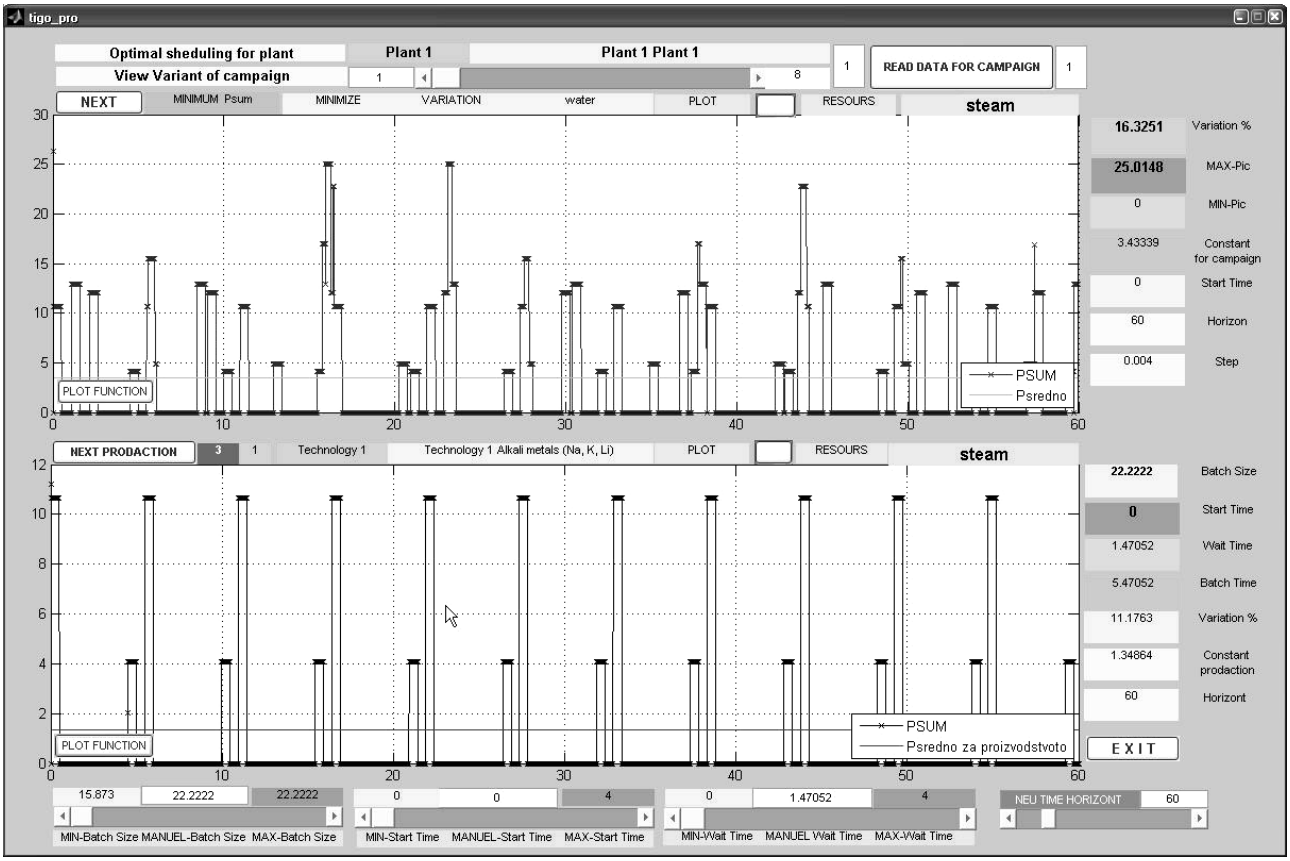

Fig. 3. Loading of the power system at optimal dislocation (arrangement) of the start-up of productions "B" and "C" with regard to production "A". Upper curve – overall loading of the power system during operation of the three production processes; Lower curve – loading due to production process "A".

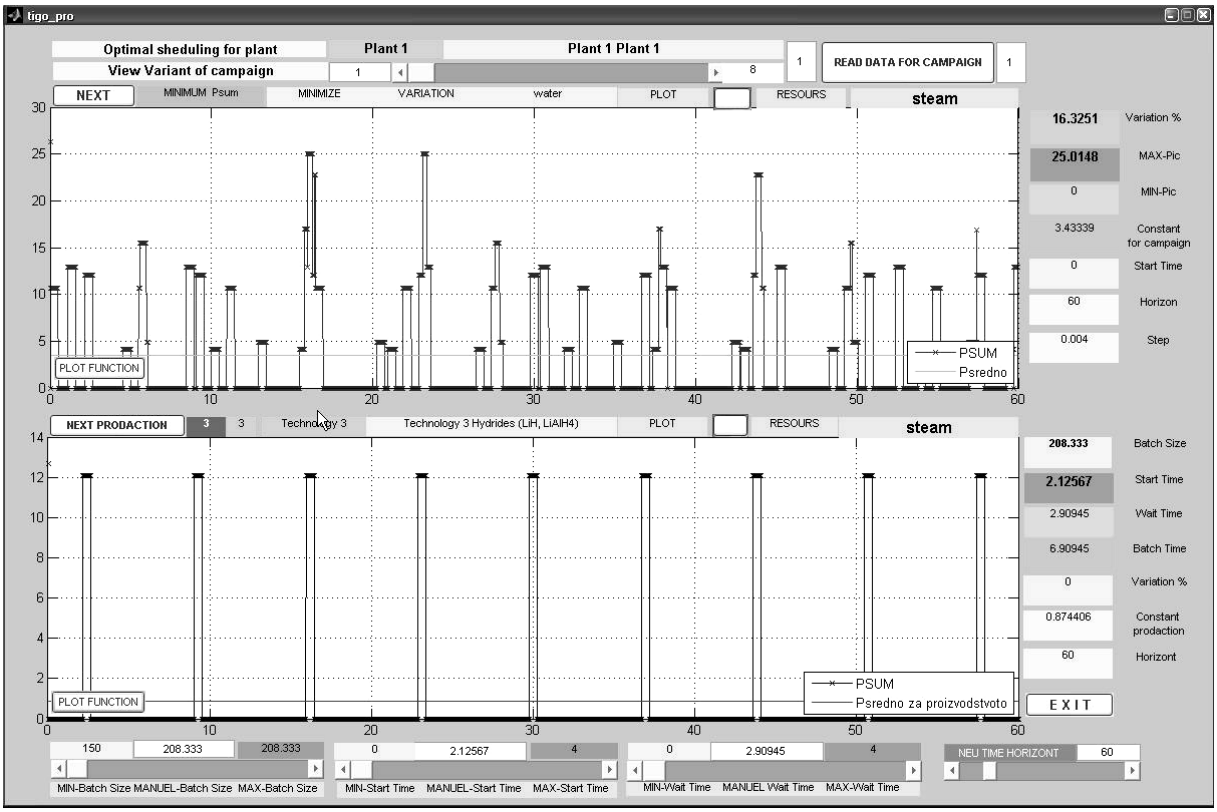

Fig. 4. Loading of the power system at optimal dislocation (arrangement) of the start-up of productions "B" and "C" with regard to production "A". Upper curve – overall loading of the power system during operation of the three production processes; Lower curve – loading due to production process "B".

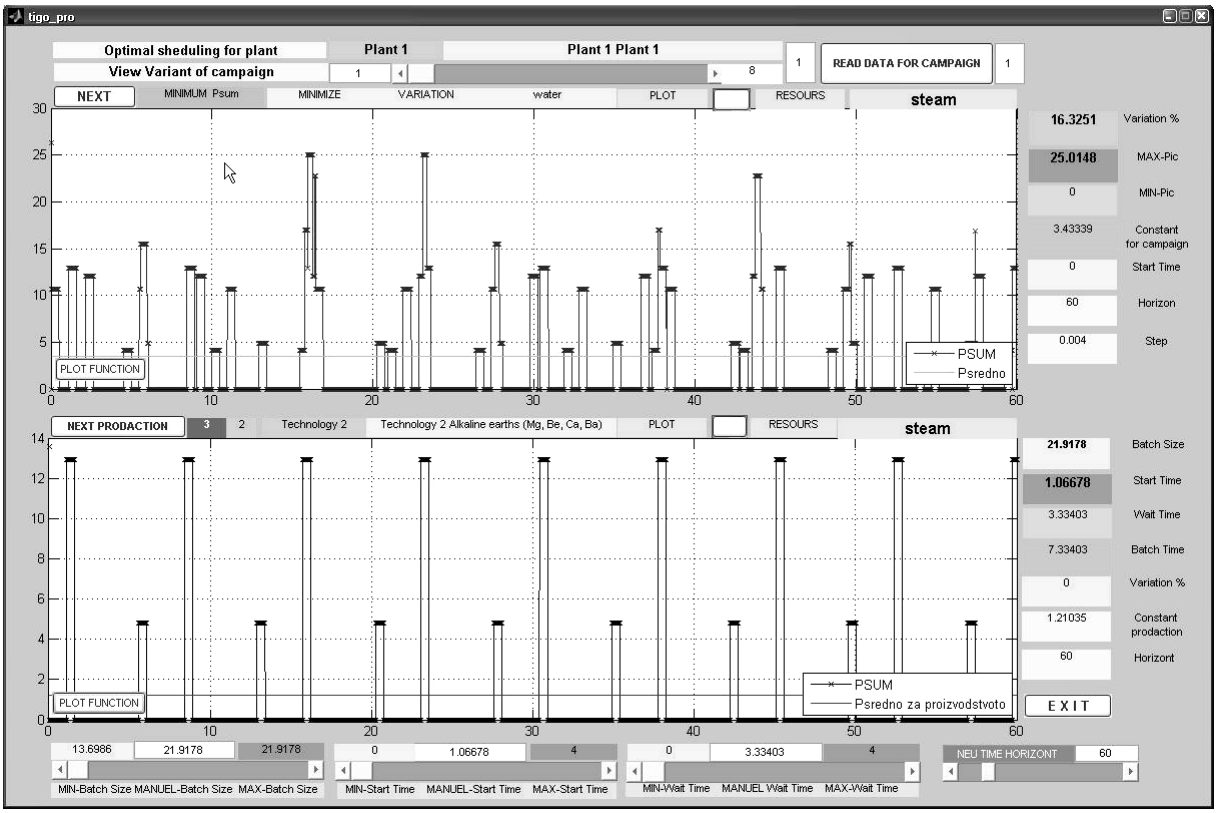

Fig. 5. Loading of the power system at optimal dislocation (arrangement) of the start-up of productions "B" and "C" with regard to production "A". Upper curve – overall loading of the power system during operation of the three production processes; Lower curve – loading due to production process "C".

CONSLUSIONS

Based on the analysis of production campaigns involving power supply systems in MBCP operation, the following conclusions could be drawn:- A mathematical model of the general problem of controlling the production campaigns of MBCP operation, while accounting for the power loading of the external power supply systems, is proposed.

- The control problem is formulated as a task of the non-linear mathematical programming methodology.

- The theory proposed is verified by an example problem solved by using software package ECAM.

REFERENCES

1. S. Stoltze, J. Mikkelsen, B. Lorentzen, P. M. Petersen, B. Qvale, *J. Energy Resources Technol.; Trans. ASME*, **117**, 142 (1995).
2. B. Linnhoff, *Trans. IChemE, Part A*, **71**, 503 (1993).
3. N. Vaklieva-Bancheva, B. B. Ivanov, N. Shah, C. C. Pantelides, *Comput. Chem. Eng*., **20**, 989 (1996).
4. D. C. A. Muller, F. M. A. Marechal, T. Wolewinski, P. J. Roux, *Appl. Therm. Eng*., **27**, 2677 (2007).
5. D. W. T. Rippin, *Comput. Chem. Eng*., **17**, Suppl., S1 (1993).
6. Z. Calderón, R. Grau, A. Espuña, L. Puigjaner, *Hung. J. Ind. Chem*., **28**, 31 (2000).
7. K. C. Furman, N. V. Sahinidis., *Ind. Eng. Chem. Res*., **41**, 2335 (2002).
8. C. Jiménez-González, M. R. Overcash,. *J. Chem. Technol. Biotechnol*., **75**, 983 (2000).
9. B. Ivanov, N. Vaklieva-Bancheva, Chr. Boyadjiev, *Hung. J. Ind. Chem.*, **18**, 55 (1990).
10. I. Cho, B. Lee, I. B. Lee, E. S. Lee, *Hwahak Konghak*, **36**, 601 (1998).
11. N. G. Vaklieva-Bancheva, E. G. Shopova, B. B. Ivanov, *Hung. J. Ind. Chem.,* **30**, 199 (2002).
12. J. M. Pinto, I. E. Grossmann, *Comput. Chem. Eng.,* **21**, 801 (1997).
13. P. S. Bieler, U. Fischer, K. Hungerbühler, *Ind. Eng. Chem. Res*., **42**, 6135 (2003).
14. M. Badell, J. Romero, L**.** Puigjaner, *Int. J. Production Economics*, **95**, 359 (2005).
15. P. S. Bieler, ETH Zürich, Swiss Federal Office of Energy, Final Report, March 2004.
16. P. S. Bieler, U. Fischer, K. Hungerbühler, *Ind. Eng. Chem. Res.,* **43**, 7785 (2004).
17. A. Brooke, D. Kendrick, A. Meeraus, R. Raman**,** GAMS: A User's Guide, GAMS Development Corporation, Washington, 1998.

УПРАВЛЕНИЕ НА ПРОИЗВОДСТВЕНИ КАМПАНИИ, ОСИГУРЯВАЩО ОПТИМАЛНО НАТОВАРВАНЕ НА ЕНЕРГОСИСТЕМИТЕ ПРИ РАБОТАТА НА МНОГОЦЕЛЕВИ ЗАВОДИ

Б. Иванов*, К. Минчев

Лаборатория Инженерно-химична системотехника, Институт по инженерна химия, Българска академия на науките, ул. „Акад. Г. Бончев”, бл. 103, 1113 София

Постъпила на 19 септември 2008 г.; Преработена на 3 юни 2009 г.

(Резюме)

Работата е посветена на проблема за оптималното натоварване на общите системи за енергозахранване на многоцелеви заводи, работещи в режим на производствени кампании. Предложен е математичен метод за определяне на управляващите независими променливи, осигуряващи минимално отклонение на кривите на натоварването на съответните енергосистеми от идеалните такива. За описание на моделите на потребление на енергия на отделните производства и производствената кампания са използувани редове на Фурие. Задачата за оптимално управление е формулирана като задача на нелинейното математичното програмиране. За потвърждение на предлагания метод е предложен тестов пример.

Bulgarian Chemical Communications, Volume 41, Number 4 (pp. 422–426) 2009

Synthesis and antimicrobial activity of 2,10-dichloro-6-substituted amino acid ester-12*H*-dibenzo[d,g][1,3,2]dioxaphosphocin-6-oxides

B. S. Kumar[1], M. V. N. Reddy[2], G. C. S. Reddy[2], A. B. Krishna[2], C. S. Reddy[2,*]

[1] *Department of Nanomaterials, Graduate School of Science and Technology, Shizuoka University, Hamamatsu, Japan - 432-8561*

[2] *Department of Chemistry, Sri Venkateswara University, Tirupati, India - 517502*

Received September 29, 2008; Revised February 10, 2009

A new class of 2,10-dichloro-6-substituted amino acid ester-12*H*-dibenzo[d,g][1,3,2]dioxaphosphocin-6-oxides have been synthesized in good yields via the condensation of 2,10-dichloro-6-chloro-12*H*-dibenzo[d,g][1,3,2]dioxaphosphocin with various amino acid esters in the presence of triethylamine. The title compounds were characterized by elemental analysis, IRS, NMR (^{1}H, ^{13}C and ^{31}P) and mass spectral studies and found to exhibit moderate antimicrobial activity.

Key words: Dioxaphosphocin-6-oxides, amino acid esters, spectral studies, antimicrobial activity.

INTRODUCTION

Phosphoramide compounds substituted with amino acid esters are important class of rationally designated therapeutics especially with antineoplastic properties. Phosphate triester derivatives of nucleotides have been prepared as the memberane-soluble prodrug of the bio-active nucleotides and were found to contain good activity against HIV-1 in-vitro [1]. The aryloxyphosphoramidates were found to exhibit enhanced activity against HIV-1 and HIV-2 in cellular culture, compared to their parent ddN's with full retention of activity in thymidine kinase – deficient cell lines [2,3]. This type of nucleosides have been shown to be potent inhibitors of HIV and to display reduced toxicity in progenitorcells [4-6]. Exhaustive modifications to the amino acid moiety in aryloxyphosphoramidate have established L-alanine to be optimal for antiviral activity [7]. Hence synthesis of the title compounds were contemplated and accomplished. They have been characterised by elemental analysis, IRS, multi NMR and mass spectral analysis.

EXPERIMENTAL

Melting points were determined in open capillary tubes on a Mel-Temp apparatus and were uncorrected. IR spectra (ν_{max} in cm^{-1}) were recorded in KBr pellets on Perkin Elmer 1000 unit. The ^{1}H, ^{13}C and ^{31}P NMR spectra were recorded on Varian Gemini 300 and Varian AM X 400 MHz NMR spectrometer operating at 300 or 400 MHz for ^{1}H, 75.46 or 100.57 MHz for ^{13}C and 121.7 MHz for ^{31}P. All the compounds were dissolved in DMSO-d_6 and chemical shifts were referenced to TMS (^{1}H and ^{13}C) and 85% H_3PO_4 (^{31}P). Micro analytical data were obtained from Central Drug Research Institute, Lucknow, India.

RESULT AND DISCUSSION

The synthetic route (Scheme 1) involves the cyclocondensation of 5,5'-dichloro-2,2'-dihydroxy biphenyl methane (**1**) with phosphorus oxychloride at 0°C under inert and anhydrous conditions in dry toluene to afford the 2,10-dichloro-6-chloro-12*H*-dibenzo[d,g][1,3,2]dioxaphosphocin-6-oxide (**3**) and its subsequent condensation with various amino acid esters in the presence of triethylamine in dry tetrahydrofuran at room temperature. The final products were purified by column chromatography using hexane, ethyl acetate as step gradient mixtures as eluents.

IR spectra of **4a**–**i** showed absorption bands at 3383–3333, 1759–1733 and 1241–1219 cm^{-1} for NH [8], C=O and P=O [9, 10], respectively (Table 1). Their ^{1}H NMR spectra gave complex multiplets at δ 6.72–7.91 for aromatic protons (Table 2). The splitting pattern of bridged methylene protons showed their non-equivalance [11]. One of the bridging protons appeared as doublet of doublet in the region 4.21–4.41 (dd, $^2J_{HH}$ = 12.9–13.9 Hz and $^5J_{PH}$ = 3.5–4.3 Hz) due to the germinal coupling with the another bridging proton and long range coupling with the phosphorus. Second bridging proton resonated as doublet in the region δ 3.57–3.65 ($^2J_{HH}$ = 13.6–14.9 Hz) due to germinal coupling with

* To whom all correspondence should be sent:
E-mail: csureshsvu@yahoo.com

germinal proton and its arrangement masked it from coupling with phosphorus.

The dioxaphosphocin ring in all these compounds appeared to exist in boat like configuration, in which one of the bridging protons protruded away from the phosphorus. The NH proton resonated as a broad singlet in the region δ 3.82–5.43.

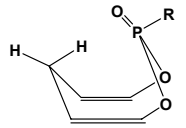

Table 1. Infrared spectral data of compounds **4a–i**.

Comp.	IR band maximum, cm^{-1}		
	N–H	C=O	P=O
4a	3351	1751	1231
4b	3374	1736	1238
4c	3333	1749	1230
4d	3371	1742	1231
4e	3342	1752	1239
4f	3356	1746	1224
4g	3364	1759	1241
4h	3383	1733	1237
4i	3341	1742	1219

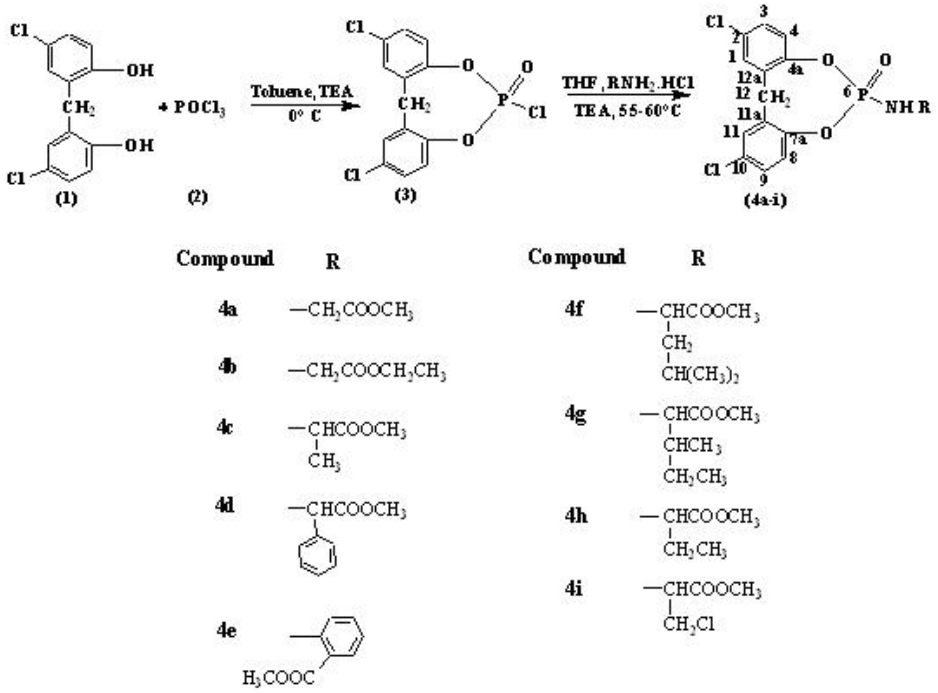

Scheme 1.

Table 2. ^{1}H NMR spectral data[a,b] of compounds **4a–i**.

Comp.	Ar-H	CH_2	N-H	Amino acid ester
4a	6.82–7.74 (m, 6H)	4.33 (dd, *J* = 13.2, 3.9 Hz), 3.61 (d, *J* = 13.5 Hz)	3.92 (brs, 1H)	4.47 (s, 3H, OCH_3), 3.87 (s, 2H, CH_2)
4b	6.89–7.86 (m, 6H)	4.25 (dd, *J* = 13.4, 3.5 Hz), 3.63(d, *J* = 13.8 Hz)	4.12 (brs, 1H)	4.39 (q, *J* = 7.1 Hz, 3H, OCH_2), 3.79 (s, 2H, CH_2), 3.12 (t, *J* = 6.9 Hz, 3H, CH_3)
4c	6.72–7.79 (m, 6H)	4.21 (dd, *J* = 13.7, 4.1 Hz), 3.65 (d, *J* = 13.9 Hz)	4.62 (s, 1H)	4.29 (s, 3H, OCH_3), 3.40 (m, 1H, CH), 1.41 (d, *J* = 7.9 Hz, 3H, CH–C<u>H</u>$_3$)
4d	7.02–7.93 (m, 11H)	4.23 (dd, *J* = 12.9, 3.5 Hz), 3.61 (d, *J* = 13.2 Hz)	4.45 (s, 1H)	4.79 (s, 1H, CH), 4.40 (s, 3H, OCH_3)
4e	6.97–7.82 (m, 10H)	4.22 (dd, *J* = 13.2, 3.6 Hz), 3.64 (d, *J* = 13.2 Hz)	5.43 (s, 1H)	4.11 (s, 3H, OCH_3)
4f	6.93–7.91 (m, 6H)	4.24 (dd, *J* = 13.5, 4.2 Hz), 3.59 (d, *J* = 14.2 Hz)	-	4.32 (s, 3H, OCH_3), 3.41 (t, 1H, –C<u>H</u>–CH_2), 1.78–1.73 (m, 2H, –CH–C<u>H$_2$</u>–$CH(CH_3)_2$), 1.51–1.45 (m, 1H, –CH–CH_2–C<u>H</u>$(CH_3)_2$), 1.09–0.96 (m, 6H)
4g	7.03–7.88 (m, 6H)	4.31 (dd, *J* = 13.9, 3.7 Hz), 3.57 (d, *J* = 13.8 Hz)	5.13 (s, 1H)	4.19 (s, 3H, OCH_3), 3.58–3.52 (m, 1H, –C<u>H</u>–$CH(CH_3)$–CH_2CH_3), 2.21–2.25 (m, 1H, –CH–C<u>H</u>$(CH_3)CH_2CH_3$), 1.51–1.48 (m, 2H, $CHCH(CH_3)CH_2CH_3$), 1.09–0.94 (m, 6H)
4h	7.01–7.74 (m, 6H)	4.41 (dd, *J* = 13.2, 4.3 Hz), 3.61 (d, *J* = 13.6 Hz)	3.83 (brs, 1H)	4.24 (s, 3H, OCH_3), 3.51 (m, 1H, C<u>H</u>$(COOCH_3)CH_2$), 2.08–2.02 (m, 2H, C<u>H$_2$</u>–CH_3), 1.02 (t, *J* = 7.4 Hz, 3H, CH_2–C<u>H$_3$</u>)
4i	6.82-7.71 (m, 6H)	4.29 (dd, *J*= 13.5, 3.7Hz), 3.59 (d, *J* = 13.5 Hz)	5.04 (s, 1H)	4.23 (s, 3H, OCH_3), 4.10–3.91 (m, 2H, CH_2Cl), 3.58 (s, 1H, CH)

a - Chemical shifts are in ppm from TMS and coupling constants (*J*) in Hz are given in parenthesis; b - Recorded in DMSO–d_6.

Their ^{13}C chemical shifts were interpreted based on comparison of basic units, present in them. Because of the symmetrical nature of dibenzophosphocin moiety only seven ^{13}C signals were observed for thirteen carbons (Table 3). The oxygen bearing C (4a) and C (7a) atoms gave signals in the down field 149.97–152.41 ppm as a doublet ($^2J_{POC}$ = 6.9–7.3 Hz). The doublets at δ 131.72–132.98 (d, J = 3.7–4.5 Hz) were assigned to the C-11a and C-12a atoms. The chemical shifts in the region 130.98–131.92 ppm were assigned to chlorine bearing C-2 and C-10 atoms. The carbonyl carbon of amino acid ester moiety appeared at δ 169.49–176.2.

^{31}P NMR chemical shifts [12] for all the title compounds were observed in the region 2.13–8.19 ppm (Table 4). The compounds **4a** and **4b** exhibited molecular ion peaks at their respective and relative molecular ion weights in their mass spectrum (Table 5).

Antimicrobial activity

Compounds **4a–i** were screened with respect to their antibacterial activity against *Staphylococcus aureus* (gram positive) and *Escherichia coli*(gram negative) by the disc-fusion method [13, 14] in nutrient agar medium at various concentrations (250, 500 ppm) in dimethyl formamide (DMF). These solutions were added to each filter disc and DMF was used as control. The plates were incubated at 35°C and examined for zone of inhibition around each disc after 24 h. The results were compared with the activity of the standard antibiotic Penicillin (250 ppm) (Table 6).

The antifungal activity of the synthesized compounds was evaluated against *Curvularia lunata* and *Aspergillus niger* at different concentrations (250, 500 ppm) and Griseofulvin was used as the reference compound. Fungal cultures were grown on potato dextrose broth at 25°C and spore suspension was adjusted to 10^5 spore/mL. Most of the compounds showed moderate activity against bacteria and high activity against fungi (Table 7).

Table 4. Synthetic, elemental and ^{31}P NMR spectral data of compounds **4a**–**i**.

Comp.	M. p., °C	Yield, %	Molecular Formula	Elemental analysis, % Found (Calc.)		^{31}P NMR, δ
				C	H	
4a	162–164	72	$C_{16}H_{14}NO_5Cl_2P$	47.89 (47.78)	3.63 (3.51)	6.75
4b	171–173	76	$C_{17}H_{16}NO_5Cl_2P$	49.21 (49.06)	3.98 (3.87)	6.82
4c	149–151	75	$C_{17}H_{16}NO_5Cl_2P$	49.19 (49.06)	3.99 (3.87)	7.81
4d	197–199	71	$C_{22}H_{18}NO_5Cl_2P$	55.39 (55.25)	3.91 (3,79)	7.99
4e	133–135	69	$C_{21}H_{16}NO_5Cl_2P$	55.48 (54.33)	3.61 (3.47)	8.19
4f	204–206	77	$C_{20}H_{22}NO_5Cl_2P$	52.57 (52.42)	4.97 (4.84)	2.13
4g	153–155	74	$C_{20}H_{22}NO_5Cl_2P$	52.59 (52.42)	5.01 (4.84)	4.22
4h	187–189	79	$C_{18}H_{18}NO_5Cl_2P$	50.39 (50.25)	4.38 (4.22)	2.20
4i	146–148	73	$C_{17}H_{15}NO_5Cl_3P$	45.42 (45.31)	3.46 (3.35)	5.44

Table 5. Mass spectral data of compounds **4a** and **4c**.

Compd.	m/z (%)
6	404 [9, $M^{+\bullet}$+2], 402 [28, $M^{+\bullet}$], 369 (11), 358 (24), 343 (22), 325 (17), 314 (27), 268 (19)
7	418 [9, $M^{+\bullet}$+2], 416 [31, $M^{+\bullet}$], 383 (17), 372 (16), 343 (21), 339 (19), 314 (21), 268 (16), 140 (32)

Table **6**. Antibacterial activity of compounds **4a-i**.

Comp.	Zone of inhibition			
	Staphylococcus aureus		*Escherichia coli*	
	250[a]	500[a]	250[a]	500[a]
4a	8	13	12	17
4b	7	11	14	19
4c	7	12	13	18
4d	6	11	15	18
4e	8	11	16	25
4f	7	12	14	22
4g	6	12	13	20
4h	5	10	13	19
4i	6	12	14	20
Penicillin[b]	12		24	

a - Concentration in ppm; b - Standard reference.

Table 7. Antifungal activity of compounds **4a-i**.

Comp.	Zone of inhibition			
	Curvularia lunata		*Asperigillus niger*	
	250[a]	500[a]	250[a]	500[a]
4a	16	27	20	27
4b	14	21	16	20
4c	16	23	19	25
4d	16	22	22	29
4e	14	20	19	26
4f	18	28	23	31
4g	15	27	13	17
4h	15	26	21	29
4i	16	21	15	20
Griseofulvin[b]	23		26	

a - Concentration in ppm; b - Standard reference.

Table 3. ^{13}C NMR spectral data[a,b] of compounds **4a–i**.

Comp.	C(1/11)	C(2/10)	C(3/9)	C(4/8)	C(4a/7a)	C(11a/12a)	C(12)	α	β	γ	Ar-H				C=O	OCH_2/ OCH_3	CH_3
											C-1'	C-2'/6'	C-3'/5'	C-4'			
4a	129.38	131.84	128.62	124.50	150.14 [d, J = 7.1 Hz]	132.98 [d, J = 3.7 Hz]	33.41	54.89 [d, J = 126.2 Hz]	–	–	–	–	–	–	174.90	52.61	–
4b	129.48	131.85	128.67	124.53	150.16 [d, J = 7.2 Hz]	132.87 [d, J = 4.5 Hz]	33.48	54.70 [d, J = 126.2 Hz]	–	–	–	–	–	–	172.91	–	13.22
4c	129.51	131.89	128.61	124.51	150.15 [d, J = 6.8 Hz]	132.85 [d, J = 4.5 Hz]	33.39	54.79 [d, J = 126.2 Hz]	23.23	–	–	–	–	–	172.61	56.92	–
4d	129.11	131.67	128.32	124.47	149.97 [d, J = 7.0 Hz]	132.52 [d, J = 4.1 Hz]	33.12	54.21 [d, J = 126.2 Hz]	–	–	135.21	128.92	127.89	125.4	169.49	56.63	–
4e	129.69	131.53	128.11	124.82	151.31 [d, J = 7.3 Hz]	131.99 [d, J = 4.0 Hz]	34.09	–	–	–	149.62	116.8	132.9	118.12	179.32	53.91	–
4f	129.12	131.92	127.92	124.03	152.11 [d, J = 7.1 Hz]	132.91 [d, J = 4.3 Hz]	34.12	54.13 [d, J = 121.3 Hz]	26.3	15.7 13.3(γ')	–	–	–	–	171.34	54.32	–
4g	128.97	131.62	128.41	124.53	151.31 [d, J = 6.9 Hz]	132.17 [d, J = 3.9 Hz]	33.79	55.03 [d, J = 126.7 Hz]	28.4 14.6(β')	16.2 13.9 (β')	–	–	–	–	172.37	52.31	–
4h	129.32	130.98	128.17	124.32	152.41 [d, J = 7.0 Hz]	131.72 [d, J = 4.0 Hz]	35.31	53.97 [d, J = 120.3 Hz]	29.3	14.1	–	–	–	–	176.20	51.20	–
4i	129.82	131.03	128.47	124.55	150.75 [d, J = 6.9 Hz]	132.11 [d, J = 4.5 Hz]	33.72	55.07 [d, J = 123.7 Hz]	9.3	–	–	–	–	–	173.11	51.37	–

a - Chemical shifts are in ppm from TMS and coupling constants (J) in Hz are given in parenthesis; b - Recorded in DMSO-d^6.

Synthesis of 2,10-dichloro-6-glycene methyl ester-12H-dibenzo[d,g][1,3,2]dioxaphosphocin-6-oxid **4a**. *General Procedure*

To a well stirred solution of 5,5'-dichloro-2,2'-dihydroxy biphenyl methane(**1**, 1.34 g, 0.005 mole) and triethylamine (1.01 g, 0.01 mole) in dry toluene (25 mL) phosphorous oxychloride (0.466 g, 0.005 mole) in dry toluene (15 mL) was added at 0°C. After the addition, the temperature of the reaction mixture was raised slowly and kept at 55–60°C for 2 hours. Completion of the reaction was monitored by TLC analysis. After cooling down to room temperature it was filtered to remove triethylamine hydrochloride and evaporated in rotary evaporator to obtain concentrated solution of 2,10-dichloro-6-chloro-12*H*-dibenzo[d,g][1,3,2]dioxaphosphocin-6-oxide (**3**), which is used for the next step without any further purification.

To the concentrated solution of compound **3** (1.748 g, 0.005 mole)and triethylamine (1.01 g, 0.01 mole) in dry tetrahydrofuran (30 mL), a solution of L-glycine methyl ester (0.698 g, 0.005 mole) was added at room temperature. Progress of the reaction was monitored by TLC analysis. Triethylamine hydrochloride was filtered and the filtrate was evaporated in rotary evaporator. Finally, the residue was purified by column chromatography by using hexane and ethyl acetate mixtures as eluents to yield 1.63 g (72%) m.p. 162–164°C.

Analogous compounds were prepared by adopting the same procedure.

SUMMARY

A new class of phosphomides substituted with aminoacid esters having good anti-microbial activity were synthesized conveniently in good yields.

Acknowledgements: *The authors express their thanks to Prof. C. Devendranath Reddy, Department of Chemistry, Sri Venkateswara University, Tirupati for his academic interaction and Director IISc (SIC), Bangalore for providing the spectral data.*

REFERENCES

1. L. I. Wiebe, E. E. Knaus, *Adv. Drug Delivery Rev.,* **39**, 63 (1999).
2. J. Balzarini, J. Kruining, O. Wedggood, C. Pannecouque, S. Aquro, C. F. Perno, L. Naesen, M. Wifuroun, R. Heijtink, E. Declercq, C. McGuigan, *FEBS Lett*., **410**, 324 (1997).
3. C. McGuigan, D. Cahard, H. H. Sheeka, E. De Clercq, J. Balzarini, *Bioorg. Med. Chem. Lett*., **6**, 1183 (1996).
4. C. McGuigan, D. Cahard, H. H. Sheeka, E. De Clercq, J. Balzarini, *J. Med. Chem.,* **39**, 1748 (1996).
5. C. McGuigan, H. W. Tsang, D. Cahard, S. Turner, S. Velazquez, A. Salgado, L. Bidois, L. Naesens, E. De Clercq, J. Velazquez, *Antiviral Res.,* **35**, 195 (1997)
6. J. Balzarini, G. J. Kang, M. Dala, P. Herdewijn, E. De Clercq, S. Broder, D. G. Johns, *Mol. Pharmacol.,* **32**, 162 (1987).
7. M. Baba, R. Pauwels, P. Hardewifn, E. De Clercq, J. Desmyter, M. Vandeputte, *Biochem. Biophys. Res. Commun*., **142**, 128 (1987).
8. M. M. Mansuri, M. J. M. Hitchcock, R. A. Buroker, C. L. Bergman, I. Ghazzouli, J. V. Descdrio, J. E. Starrett, R. Z. Jr. Sterzycki, J. C. Martin, *Antimicrob. Agents Chemother.*, **34**, 637(1990).
9. W. Kemp, Organic Spectroscopy, Third Edition, Palgrave Publishers Ltd. New York, 1991, p. 83-86.
10. K. A. Kumar, C. S. Reddy, C. D. Reddy, *Phosphorus, Sulfur Silicon*, **177**, 1745 (2000).
11. K. A. Kumar, C. S. Reddy, L. N. Prasad Rao, C. N. Raju, *Heterocyclic Commun*., **7**, 253 (2001).
12. B. S. Kumar, A. U. Ravi Sankar, C. S. Reddy, S. K. Nayak, C. N. Raju, *Arkivoc,* **13**, 155 (2007).
13. J. C. Vincent, H. W. Vincent, *Proc. Soc. Enpt. Biol. Med*., **55**, 162 (1944).
14. H. J. Benson, Microbiological applications, 5th Edn., W. C. Brown Publications, Boston, 1990.

SYNTHESIS AND АСИНТЕЗ И АНТИМИКРОБНА АКТИВНОСТ НА 2,10-ДИХЛОР-6-ЗАМЕСТЕНИ С ЕСТЕРИ НА АМИНОКИСЕЛИНИ-12*H*-ДИБЕНЗО[d,g][1,3,2]ДИОКСА-ФОСФОЦИН-6-ОКСИДИ

Б. С. Кумар[1], М. В. Н. Реди[2], Г. Ч. С. Реди[2], А. Б. Кришна[2], К. С. Реди[2,]*

[1] *Department of Nanomaterials, Graduate School of Science and Technology, Shizuoka University, Hamamatsu, Japan - 432-8561*

[2] *Department of Chemistry, Sri Venkateswara University, Tirupati, India - 517502*

Received September 29, 2008; Revised February 10, 2009

(Резюме)

Синтезирани са с добър добив нов клас 2,10-дихлор-6-заместени с естери на аминокиселини-12*H*-дибензо[d,g][1,3,2]ди-оксафосфоцин-6-оксиди чрез кондензация на 12*H*-дибензо[d,g][1,3,2]диоксафосфоцин с различни естери на аминокиселини в присъствие на триетиламин. Съединенията са охарактеризирани с елементен анализ, ИЧС, ЯМР (^{1}H, ^{13}C и ^{31}P) и масспектроскопия и показват умерена антимикробна активност.

AUTHOR INDEX

SUBJECT INDEX

АВТОРЕН УКАЗАТЕЛ

ПРЕДМЕТЕН УКАЗАТЕЛ

CONTENTS

СЪДЪРЖАНИЕ